

# Self-powered wireless current sensor

Proof of concept: continuous current measurement and energy extraction using one Current Transformer

**R.L. van der Plaats**



# Self-powered wireless current sensor

Proof of concept: continuous current  
measurement and energy extraction using one  
Current Transformer

by

R.L. van der Plaats

to obtain the degree of Master of Science  
at the Delft University of Technology,  
to be defended publicly on Thursday October 27, 2016 at 13:00 AM.

Student number:	4011937
Project duration:	January 1, 2016 – October 27, 2016
Thesis committee:	Prof. dr. ir. P. Bauer, TU Delft, supervisor
	Dr. Ir. H. Polinder, TU Delft
	Dr. M. Cvetkovic, TU Delft
	E. Noordmans, ELEQ Steenwijk
	V. Prasanth, TU Delft

*This thesis is confidential and cannot be made public until December 31, 2017.*

An electronic version of this thesis is available at <http://repository.tudelft.nl/>.



# Summary

Due to changes in the electricity grid, and the awareness of the energy consumption, management of energy flows is an important business. For the management of energy flows, detailed information about the current flow is needed. For the integration of current sensors in the grid there is a need for non-invasive current sensors that are easy to installable.

In this thesis project a non-invasive current sensor based on a Current Transformer (CT) is described. For simple installation, the sensors takes the power required for the electronics in the sensor, from the magnetic field that is created around a cable by a current flowing through the cable. Based on the combination of energy extraction and continuous current measurement a proof of concept self-powered current sensor is designed. The measured data of the current is send wireless to the operators.

A study on current measurement, energy extraction with a CT, and the configuration of a sensor network, is used to create a configuration for a non-invasive current sensor. Based on the configuration a simulation model of the sensor is realized and used as first verification to check if the configuration can be used as current sensor. From the simulation model a prototype is designed and tested.

For simulation of the system and analysis of energy extracting capabilities of a CT, a model is created that is, as long as the core is not saturated, accurate for the analysis in this thesis. Based on accuracy, size, cost and power losses a shunt is used to measure the secondary side current of a CT. The secondary side current is related to the primary side current, the current of which information is wanted, by the turns ratio of the CT.

From the analysis on the energy extracting capabilities of a CT it is concluded that at low primary current the output power of a CT is very low. There are options to increase the energy extracting capabilities of a CT. However, they all have negative influence on the current measurement. To supply the electronic parts in the sensor a AC/DC conversion stage as well as an DC/DC conversion stage are used. All topologies have influence on the measurement. Based on simulation the influence of a Schottky diode full bridge rectifier and a buck/down converter is limited and only visible at small current.

The configuration of multiple measurement sensors to a network, and the communication between sensor nodes are optimized for power consumption and accurate time synchronization between sensors. A local concentrator initiates a time-slotted communication channel to which the sensor nodes are connected. The time synchronization implemented in this project is accurate with a difference in time between initiator and sensor node of about 20  $\mu$ s average.

For the integration of current measurement and energy extraction, isolation of the measurement and active consumption of energy is required. By using a shunt monitor with internal isolation of input and output it is possible to measure the Alternating Current (AC) current with an Analog to Digital Converter (ADC) of a microcontroller. Active energy consumption is used to ensure that almost all available CT current passes the shunt.

Simulation of the complete sensor showed that it is possible to measure current accurately from 10 A to 240 A. Although the accuracy of the measurement with the prototype is not as good as the simulation, it is expected that further development of the configuration will lead to more accurate measurements.

Based on the research in this project it is concluded that the designed configuration can be used for current measurement from 10 A to 240 A. It is furthermore expected that changing some components can lead to current sensors that measure current within other ranges as well. To increase the accuracy some parts need small modifications but the concept of a self-powered wireless current sensor based on one CT is proofed to work.



# Preface

This thesis is written as part of the final assessment for the completion of the master Electrical Engineering (track Electrical Power Engineering) at the TU Delft. In January 2016 the project was started in collaboration with ELEQ Steenwijk. ELEQ is a company that designs and manufactures smart electrotechnical applications for protecting, measuring and connecting electrical energy. ELEQ delivers its products around the world and the products are used in many installations and grids around the world. ELEQ defined a project to do research related to a self-powered wireless current sensor. Within this project there was a lot of freedom to define the final project. The thesis is about the design of a concept demonstrator measuring continuously current and meanwhile power the sensors electronics using a single Current Transformer (CT).

The design of this concept is based on a study on related work and the identified parts included in the design. After an introduction including a motivation for this work, the topics measurement, energy extraction and network structure, in which the sensor is placed, are discussed. Based on the conclusions from these chapters the elements are combined and a simulation model of the system is created. Based on the system configuration a prototype is realized and tested.

During this project many people are involved to make this project possible. First of all I would like to thank the colleagues at ELEQ for their support during this project and especially Ealse Noordmans, my supervisor from ELEQ, and Robert Getreuer for making this project possible. Part of the work is performed at TU Delft and I would like to thank Prasanth for the feedback and tips on my thesis and professor Bauer for the supervision of this project. From my regular meetings with Reinout Getreuer during the first part of this project I received many good ideas and input for this project. Also support, tips and feedback from colleague students helped a lot during this project. Finally I would like to thank my girlfriend and family for their support during my entire study period, and especially during this thesis project.

*R.L. van der Plaats  
Delft, September 2016*



# Contents

<b>Summary</b>	<b>v</b>
<b>Preface</b>	<b>vii</b>
<b>List of Figures</b>	<b>xi</b>
<b>List of Tables</b>	<b>xiii</b>
<b>List of Abbreviations</b>	<b>xv</b>
<b>List of Symbols</b>	<b>xvii</b>
<b>1 Introduction</b>	<b>1</b>
1.1 Motivation . . . . .	1
1.2 Related work . . . . .	2
1.3 Problem statement and research question . . . . .	3
1.4 Thesis structure . . . . .	4
<b>2 CT model &amp; Current measurement techniques</b>	<b>7</b>
2.1 Introduction . . . . .	7
2.2 Current Transformer . . . . .	7
2.2.1 CT Models based on equivalent circuit. . . . .	8
2.2.2 Model verification . . . . .	11
2.3 Current measurement techniques . . . . .	12
2.3.1 Ohm's law . . . . .	12
2.3.2 Faraday's law of induction . . . . .	14
2.3.3 Magnetic field sensors . . . . .	16
2.3.4 Conclusion. . . . .	17
<b>3 Energy extraction and power conversion</b>	<b>19</b>
3.1 Introduction . . . . .	19
3.2 Energy extraction . . . . .	19
3.2.1 Series compensation for reactive currents . . . . .	23
3.2.2 Parallel compensation for reactive currents . . . . .	25
3.2.3 Alternative configuration for compensation of reactive currents . . . . .	27
3.2.4 Conclusion. . . . .	28
3.3 Power conversion . . . . .	29
3.3.1 AC/DC conversion . . . . .	29
3.3.2 DC/DC conversion. . . . .	31
3.3.3 PFC techniques . . . . .	33
3.3.4 Conclusion. . . . .	34
<b>4 Network structure</b>	<b>35</b>
4.1 Introduction . . . . .	35
4.2 Network topology. . . . .	35
4.2.1 Existing gateway far away . . . . .	35
4.2.2 Existing gateway nearby . . . . .	36
4.2.3 Custom gateway . . . . .	37
4.2.4 Conclusion. . . . .	37
4.3 Communication protocol . . . . .	38
4.3.1 Bluetooth . . . . .	38
4.3.2 Zigbee . . . . .	38
4.3.3 6LoWPAN . . . . .	38
4.3.4 Conclusion. . . . .	39

---

4.4	Synchronization of sensor nodes . . . . .	39
4.4.1	Implemented synchronization . . . . .	40
4.4.2	Conclusion. . . . .	43
<b>5</b>	<b>System integration and model of system</b>	<b>45</b>
5.1	Introduction . . . . .	45
5.2	Integration . . . . .	45
5.2.1	Measurement . . . . .	45
5.2.2	Excess energy consumption . . . . .	48
5.2.3	Complete configuration of sensor . . . . .	49
5.3	Simulation model of current sensor. . . . .	49
5.4	Simulation results. . . . .	50
<b>6</b>	<b>Design and measurement results</b>	<b>53</b>
6.1	Introduction . . . . .	53
6.2	Sensor node. . . . .	53
6.2.1	Hardware design. . . . .	53
6.2.2	Software design . . . . .	55
6.3	Concentrator . . . . .	55
6.3.1	Hardware design. . . . .	55
6.3.2	Software design . . . . .	55
6.4	Results of measurement. . . . .	56
<b>7</b>	<b>Conclusions and recommendations</b>	<b>59</b>
7.1	Conclusions. . . . .	59
7.2	Recommendation for further research . . . . .	60
	<b>Bibliography</b>	<b>63</b>

# List of Figures

1.1	Example of situation in which current measurement takes a lot of wiring . . . . .	2
1.2	Setup using two transformers [4] . . . . .	3
1.3	Setup using single CT not measuring actual current [7] . . . . .	3
1.4	Setup using a single CT and switched based solution [2] . . . . .	3
1.5	Top level block diagram of sensor . . . . .	4
2.1	Block diagram of sensor, measurement block is considered in this chapter and an equivalent circuit of the CT is derived . . . . .	7
2.2	Ratio error according to IEC 61869-2 . . . . .	8
2.3	Transformer equivalent circuit . . . . .	9
2.4	Secondary transposed transformer equivalent circuit . . . . .	9
2.5	Simplification of current transformer equivalent circuit . . . . .	9
2.6	Simplification of current transformer equivalent circuit . . . . .	10
2.7	Parameter estimation of TQ40-c with OMICRON CT Analyzer . . . . .	11
2.8	Ratio error of simulation . . . . .	11
2.9	Ratio error of measurement . . . . .	12
2.10	Shunt measurement . . . . .	13
2.11	Rogowski coil . . . . .	14
2.12	Current transformer . . . . .	15
2.13	Hall-effect sensor . . . . .	16
2.14	Magneto resistance effect sensor . . . . .	16
3.1	Block diagram of sensor, energy extraction block is considered in this chapter . . . . .	19
3.2	Current transformer equivalent circuit with load connected . . . . .	20
3.3	Equivalent impedance at different loads . . . . .	20
3.4	Current ratio $\frac{I_s}{I_p}$ at different load resistance values . . . . .	21
3.5	Relation output voltage and magnetizing current . . . . .	21
3.6	Simulated power consumed at variable load . . . . .	22
3.7	Measured power consumed at variable load . . . . .	22
3.8	Series resonance topology . . . . .	23
3.9	Influence of $R_{load}$ on ideal capacitance value . . . . .	24
3.10	Measured power consumed at variable load with series resonance . . . . .	25
3.11	Parallel resonance topology . . . . .	25
3.12	Influence of $R_{load}$ on ideal capacitance value . . . . .	26
3.13	Measured power consumed at variable load with parallel resonance . . . . .	26
3.14	Measured power consumed at 1 $\Omega$ load resistance without resonance and with series and parallel resonance . . . . .	27
3.15	Measured power consumed at 100 $\Omega$ load resistance without resonance and with series and parallel resonance . . . . .	27
3.16	Relation output voltage and magnetizing current with and without air-gap . . . . .	28
3.17	Hybrid series resonance topology . . . . .	28
3.18	Voltage source and current source based rectifiers . . . . .	29
3.19	Waveforms of current source and voltage source rectification . . . . .	30
3.20	Rectification of the output of a CT . . . . .	30
3.21	Voltage-source character of diode, schottky diode and MosFET . . . . .	31
3.22	Walton-Craft voltage doubler circuit[26] . . . . .	32
3.23	Two schematic circuits of Power Factor Correction (PFC) techniques . . . . .	33

4.1	Block diagram of sensor, wireless communication and network structure is considered in this chapter . . . . .	35
4.2	Network structure of LoRa network . . . . .	36
4.3	Network structure with IP router . . . . .	37
4.4	Network structure with custom gateway . . . . .	37
4.5	Proposed network topology . . . . .	39
4.6	Overview of survey [24] . . . . .	41
4.7	Measured delays between initiated beacon transmission and beacon reception . . . . .	41
4.8	Measured delays between time slot initiator and sensor node . . . . .	42
4.9	Time Slotted Channel Hopping (TSCH) based time slots with current and zero-crossing signals . . . . .	43
5.1	Block diagram of sensor, in this chapter the integration of all blocks into a system are considered . . . . .	45
5.2	Location of current shunt, both in AC and Direct Current (DC) path are considered . . . . .	46
5.3	Lifting potential for ADC measurement of AC current . . . . .	46
5.4	Block diagram of sensor with more details on measurement subsystem . . . . .	46
5.5	Differential amplifier with reference voltage . . . . .	47
5.6	Schematic picture of INA282 which is used for monitoring the shunt . . . . .	47
5.7	Block diagram of sensor with more details on energy extraction and subsystem and the location of excess energy consumption . . . . .	48
5.8	Circuit used for the excess energy consumption . . . . .	49
5.9	Detailed block diagram of the self-powered wireless current sensor . . . . .	50
5.10	Ratio error based on simulation results . . . . .	51
5.11	Simulated ADC input, zero-crossing input and DC voltage levels at 100% rated current . . . . .	52
6.1	Detailed block diagram of the self-powered wireless current sensor . . . . .	53
6.2	Designed Printed circuit board (PCB)s for the sensor node . . . . .	54
6.3	PCBs for the sensor node . . . . .	54
6.4	Concentrator node with CC2650 launchpad and ESP8266 WiFi module . . . . .	56
6.5	Measured sensor node accuracy based on ratio error . . . . .	57
6.6	Measured ADC input, zero-crossing input and DC voltage levels at 100% rated current . . . . .	58

# List of Tables

2.1	Ratio error [%] according to IEC 61869-2 . . . . .	8
2.2	Parameters of lumped elements in current transformer equivalent circuit . . . . .	10
2.3	Measurement of current transformer output compared with simulation results and theoretical value . . . . .	12
2.4	Current measurement sensor . . . . .	17
3.1	Parameters of CT . . . . .	24
4.1	Network structure rating . . . . .	38
4.2	Communication protocols rating . . . . .	39
4.3	Synchronization results of beaconing and TSCH . . . . .	43
5.1	Ratio error based on complete system simulation . . . . .	51
6.1	Spreading of measurement and influence on measurement . . . . .	57



# List of Abbreviations

**AC** Alternating Current.

**ADC** Analog to Digital Converter.

**BOM** Bill of material.

**CT** Current Transformer.

**DC** Direct Current.

**EMI** Electromagnetic interference.

**IoT** Internet of Things.

**IPT** Inductive Power Transfer.

**LDO** Low-dropout.

**MR** Magneto Resistance.

**NTP** Network Time Protocol.

**PCB** Printed circuit board.

**PF** Power Factor.

**PFC** Power Factor Correction.

**PWM** Pulse Width Modulation.

**RMS** Root Mean Square.

**SMPS** Switch Mode Power Supply.

**TSCH** Time Slotted Channel Hopping.

**WSN** Wireless Sensor Network.



# List of Symbols

$\mu$	Permeability	$H/m$
$\omega$	Angular frequency	$rad/s$
$\Phi$	Magnetic flux	$Wb$
$\rho$	Resistivity	$\Omega \cdot m$
$\sigma$	Conductivity	$S/m$
$B$	Magnetic flux density	$T$
$C$	Capacitance	$F$
$D$	Electric flux density	$C/m^2$
$E$	Electric field strength	$V/m$
$f$	Frequency	$Hz$
$H$	Magnetic field strength	$A/m$
$I$	Electric current	$A$
$J$	Current density	$A/m^2$
$L$	Inductance	$H$
$V$	Electric potential difference	$V$
$R$	Electrical resistance	$\Omega$





# Introduction

In this introductory chapter of the thesis the motivation for the research project is described. Related work is discussed in order to define a research objective which is covered in the rest of this thesis. The end of this chapter consists of the thesis setup and a brief description of every chapter.

## 1.1. Motivation

The transportation and generation of electric energy is a business that has changed throughout the years. One of the recent changes in the transportation and generation of electric energy, is due to the high greenhouse gas emissions. Greenhouse gas emissions are a growing problem and before the year 2050 the emission of greenhouse gasses should be reduced to almost zero[8, 35].

One of the methods to reduce the emission of greenhouse gasses is to integrate more renewable energy sources in the electricity grid. By integrating more renewables into the electricity grid, the generation of electric energy is no longer centralized but more and more decentralized. The energy generation of most renewable energy sources is not synchronized with the consumption. The difference between demand and usage leads to energy flows in the electricity grid. Consumers become producers and to ensure stable grid operation, the generation at other places needs to be adjusted to compensate for the generation of energy by renewables. To regulate the energy flow, grid operators need detailed information about the energy flow in the grid.

Another change is observed at the consumption side of the grid. More and more devices use electric energy and this leads to increased energy consumption. The increased usage of electric energy leads to increased costs. To keep energy costs low, people are more aware of their energy usage. To reduce the energy consumption, un-used equipment is turned of as much as possible in buildings. Before people start saving energy, they need to know where they consume energy. To observe where energy is consumed in buildings, the monitoring of the current flow is used. By monitoring the flow of current, the energy consumption at particular parts of the building can be determined. With that information devices can be turned off or can be replaced by more efficient devices.

For both grid operators and consumers of energy, information about the energy flow is used to manage the energy flow. Although the scale is different for both parties, the current flow gives information about the energy flow. Current sensors are used to measure the flow of current through a conductor, and voltage sensors are used to measure the voltage. Besides information about the amplitude of the current or voltage, information about the phase is important as well. Combining the information of amplitude and phase of voltage and current measurements, gives information about power flow, power factor and more.

As part of the energy management, a current sensor is considered in this thesis. There are already many different types of current sensors. Some sensors need to be placed in the current path, while other are non-invasive and can be mounted later on. An example of a current sensor which is clamped onto a cable, without interrupting the circuit, is a CT. CTs are sometimes used to drive relays, but in case of current measurement with a CT the current value is analog or digitally presented.

A CT is an instrument transformer designed for current measurement. Instrument transformers and power transformers use the same principle of operation. The application of the transformers is however completely different. In case of power transformers the voltage and current of the primary side are transformed

up or down to the secondary side. The dimensioning and winding configuration is designed in a way that power transfer is efficient. For instrument transformers the voltage or current is transformed to measurable levels, while the dimensioning and winding configuration is designed in a way that it draws almost no power.

A CT on itself is a passive device that transforms primary current down to measurable quantities on the secondary side. For current measurement the output of a CT is connected to a burden resistor in most applications. The voltage drop across the burden is used as measure for the primary current. For energy management this information must be digitalized and send to grid operators or the consumers of energy.

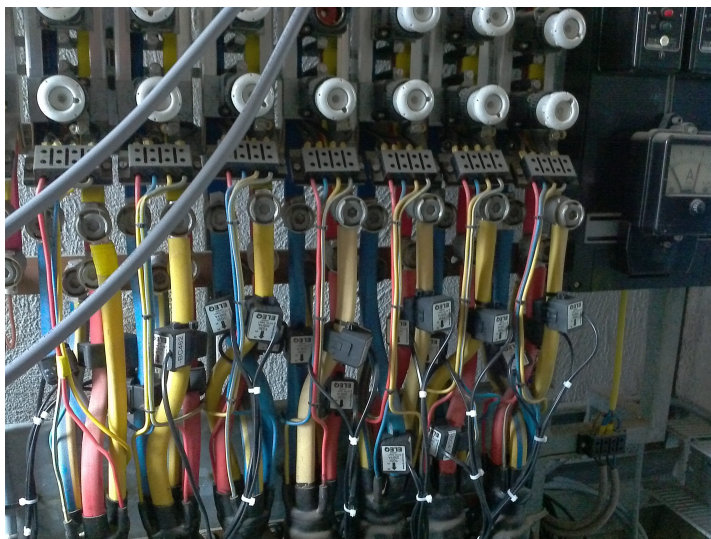


Figure 1.1: Example of situation in which current measurement takes a lot of wiring

The installation of CTs in local distribution cabinets to measure incoming and outgoing current takes a lot of wiring. In figure 1.1 an example is given in which the installation of CT for current measurement is a time consuming business. In this picture there are 7 outgoing lines, each consisting of 3 phases. Each incoming and outgoing phase needs a CT, and connecting the CT output to a concentrator takes a lot of wiring, and is due to the limited space a time consuming job. To reduce installation time and get rid of the wires, a wireless current sensor based on a CT is a solution. For the electronics in these sensors there is however energy needed. Powering every CT removes the advantage of sending data wireless. Removing all wires requires a self-powering current sensor. In this thesis the design of a self-powering current sensor, which send the current readings wireless, is considered.

## 1.2. Related work

At this moment there are already some examples of wireless current sensors, self-powered sensors and self-powered current sensors available. In this section these examples are discussed and some advantages and disadvantages are mentioned.

Campbell and Dutta describe in their paper a wireless power metering sensor that uses a wireless voltage sensor and multiple wireless current sensors to measure power consumption in a house. This current sensor is self-powered and uses two CTs. One CT is used for energy extraction while the other one is used for the measurement [4]. Figure 1.2 shows a schematic overview of this setup [4]. This setup with two CTs is used in other examples as well [6]. Although this particular example is used to monitor current flow inside a house the setup could also be used for energy management applications.

The usage of two CTs adds additional size and costs and a solution using a single CT is more efficient in terms of size and most likely in costs. An example of a self-powered wireless current sensor using a single CT relates the current flowing through the measured conductor with the sending frequency of the sensor node [7]. The actual current is not measured and therefore information about phase is not available and only an indication of the current is given. In figure 1.3 a schematic overview of this setup is given [7].

The examples in which the combination of current measurement and energy extraction is based on a single CT, use a switch to switch between measuring and harvesting [2, 22]. Once there is enough energy harvested with the CT the harvesting circuit is disconnected and the measuring circuit is connected. This

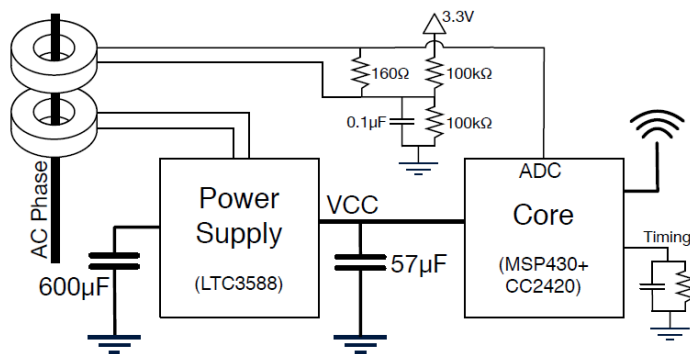


Figure 1.2: Setup using two transformers [4]

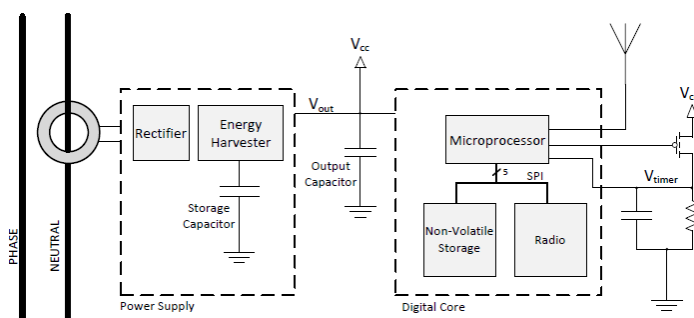


Figure 1.3: Setup using single CT not measuring actual current [7]

method is acceptable if primary currents are high enough to accumulate enough charge for a measurement in a short time. If primary currents are lower, accumulation of charge takes longer, less measurements can be done. A schematic overview of a sensor based on a single CT which switches between measurement and extraction is given in figure 1.4 [2].

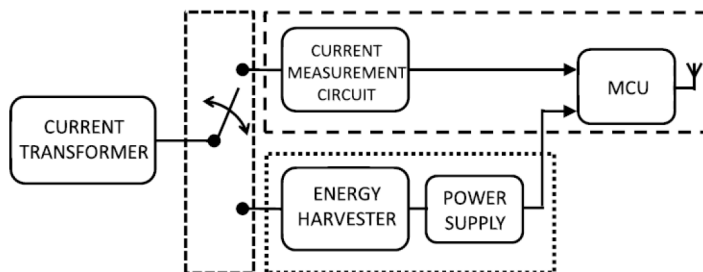


Figure 1.4: Setup using a single CT and switched based solution [2]

The previously mentioned examples of wireless current sensors use energy extraction with a CT as power supply. Studies on energy extraction with a CT mostly describe the optimization of energy extraction with a CT [3, 10, 15, 37]. In most of these research studies, resonance and voltage doubling circuits are used to extract more energy from the primary conductor.

### 1.3. Problem statement and research question

Design of self-powered current sensors based on a CT can be based on one or two CTs and may vary between continuous measurement or measurement during short cycles. As mentioned in the previous sections there are already examples which consider the design of a self-powered current sensor based on two current transformers and measure continuously and designs where they use a single CT but switch between energy extraction and measurement. The disadvantage of the last method is the missing information about the current flow in the periods the sensor need to harvest energy while the other setup using two CTs has

the disadvantage of larger size, cost and higher number of components. To have the advantage of measuring the current continuous and the advantage of using a single CT, the design of a self-powered wireless current sensor, based on a single CT, with continuous current measurement is considered in this thesis project.

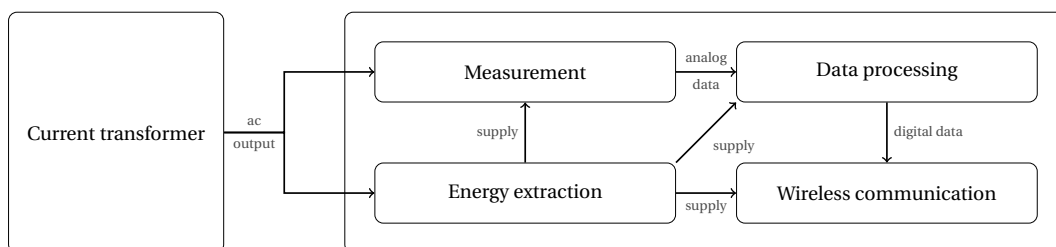


Figure 1.5: Top level block diagram of sensor

The main goal of this thesis is the combination of continuous current measurement and energy extraction using one CT as link between sensor and current carrying conductor. To achieve this goal the project is divided into a few questions.

1. What type of current measurement techniques are currently available and could be implemented in the application of self-powered wireless current sensor?
2. What amount of energy can be extracted with a CT and what influence has the extraction of energy on the normal operation of a CT?
3. How can continuous current measurement be combined with energy extraction?
4. Which network topologies could be used for wireless current sensors and how can accurate time synchronization be achieved?

The project is based on these questions and the integration of the answers to these questions into a self-powered wireless current sensor. A schematic overview of the topics which will be considered in this thesis is provided in figure 1.5. Based on the topics a configuration is defined, simulated and a prototype is created.

Based on research questions and the application area of this sensor there are certain specifications which are set at the beginning of this project to work as guideline and check at the end of the project if these specifications are met. In the list below the specifications are mentioned and shortly described.

- **Primary currents measurable up to 240 A (120 % rated current).** The selected rated current is 200 A and based on the IEC 61869-2 the sensor must give reliable measurement up to 240 A (120 % rated current). The decision for this rated current is based on the range of currents in which energy management is important. Within ELEQ a retro-fit CT was available which is used in this project (TQ40-c).
- **Accuracy class 1.** According to the IEC 61869-2 (see section 2.2) the allowed ratio error of the measurement must be within the given specifications of a class 1. The ratio error is a measure for the accuracy of the measurement.
- **Almost no added space needed.** Compared with the CT as it is now, the TQ40-C, the additional size for the electronics must be kept to a minimum. The only direction in which the current design may be expanded is the bottom side of the CT.
- **Additional cost must be low.** The additional cost of the electronics and other modifications on the standard CT must be low.

## 1.4. Thesis structure

The thesis is divided into several chapters. This first chapter is an introduction in the subject and consists of a motivation for this project, related work and the research question of this project. In figure 1.5 a block diagram is given in which 5 blocks are identified. Based on these blocks the thesis is divided into several chapters. In the first few chapters one or two blocks are considered. When all blocks are discussed a sensor configuration is formed which is used in the rest of the thesis.

In chapter 2 an equivalent circuit of a CT is derived. The derived equivalent circuit is validated by comparing simulation results with measurement. The measurement of current is the other topic considered in that chapter. A review of different current measurement techniques and current sensors based on these techniques is provided.

For the power supply of the electronics in the current sensor, chapter 3 provides an analysis of energy extraction using a CT. Different steps and methods in the power conversion process are discussed as well. The theory in this chapter is supported by simulations and measurements. Besides normal energy extraction with a CT, increased energy extraction with the application of resonance is discussed as well.

Chapter 4 deals with the network topology of the network of sensors in which the current sensor of this research should be integrated. The time synchronization of the sensor nodes with a reference time is the other topic in chapter 4. Network protocols and network structure are discussed briefly. Timing inside a microcontroller and timing between microcontrollers are part of the chapter as well. Measurements on the time delay completes this chapter.

In chapters 2 to 4 all aspects required for a wireless sensor node are described and in chapter 5 the combination of measurement and energy extraction is completed. Based on the complete configuration a simulation model is described and the results of simulations with this simulation model are given.

With the knowledge from chapter 5 the prototype that is realized as part of this thesis project is described. The hardware design as well as a description of the software and the integration in a network is part of chapter 6. In chapter 6 the results of the measurements with the designed sensor node are included and compared with the results of the simulations from chapter 5.

Finally in chapter 7 the conclusions based on the research questions and the rest of the project are given. In chapter 7 also some recommendations are listed which could be used for further research projects or for improvements in the design presented in this project.



# 2

## CT model & Current measurement techniques

### 2.1. Introduction

As a link between primary conductor and the rest of the current sensor a CT is used. For system modeling and other analysis in this thesis, an equivalent circuit is derived and verified in this chapter. CTs for measurement purpose are always defined according to a certain accuracy class. In this chapter this will be shortly discussed. Another important aspect is the method of current measurement in the sensor. Several measurement techniques are discussed. The information in this chapter provides a base for the decision of how the primary current is measured.

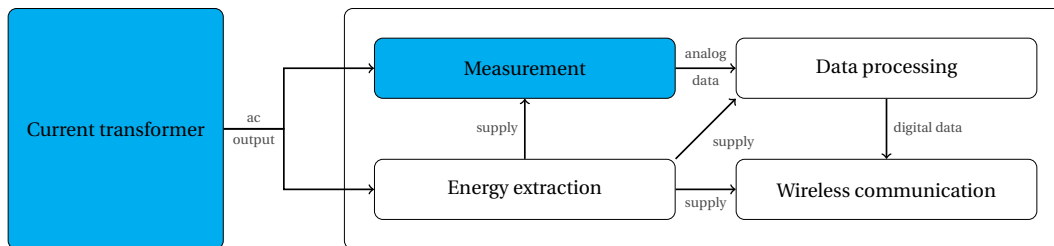


Figure 2.1: Block diagram of sensor, measurement block is considered in this chapter and an equivalent circuit of the CT is derived

The derivation and verification of equivalent circuits, as well as more information about CT in general, is discussed in section 2.2. In section 2.3 different potential current measurement techniques are discussed and reviewed.

### 2.2. Current Transformer

Instrument transformers used for current measurements always have a defined accuracy class. This accuracy class defines for different current levels the maximum ratio error which is allowed within that class. A commonly used standard is the IEC 61869-2[34]. This standard is used for instrument transformers to define accuracy class and more. The ratio error (equation 2.1) and more specifications for different classes are specified within the standard. The ratio error is calculated using equation 2.1. In this equation  $N_p$  and  $N_s$  are the number of primary and secondary turns

$$Ratio\ error = \frac{I_s \frac{N_s}{N_p} - I_p}{I_p} \times 100\% \quad (2.1)$$

In table 2.1 the allowed ratio error in percentage is given for different classes at different percentage of the rated current. In figure 2.2 the different classes are illustrated. A CT has a certain class if for the complete range of specified currents the measurements meet the requirement of the specified class (i.e. ratio error). Although this standard (IEC 61869-2) is used for CT and not for current sensors based on a CT, the standard

Accuracy	at % of rated current				
	5	20	50	100	120
Class 0.1	0.4	0.2		0.1	0.1
Class 0.2	0.75	0.35		0.2	0.2
Class 0.5	1.5	0.75		0.5	0.5
Class 1	3	1.5		1	1
Class 3			3	3	3
Class 5			5	5	5

Table 2.1: Ratio error [%] according to IEC 61869-2

specifies ratings for a CT and therefore it is used to specify the class of the current sensor based on a CT. There are, as far as known, no standards for this type of sensor. Before there is a standard for this type of sensor, the standard for CT is used to specify the class of the current sensor.

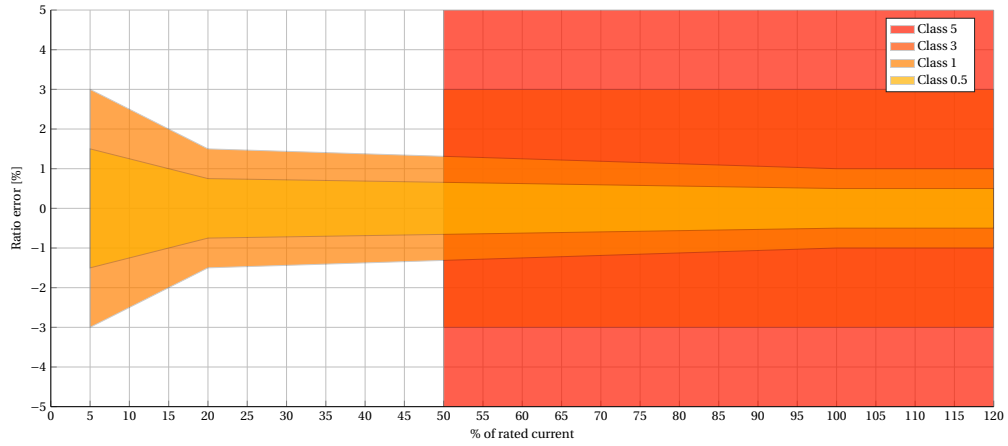


Figure 2.2: Ratio error according to IEC 61869-2

### 2.2.1. CT Models based on equivalent circuit

A CT is an instrument transformer and since instruments transformers are except the dimensions equal to other transformers. Therefore the equivalent circuit of a transformer (figure 2.3) is used as starting point for the derivation of a circuit that is used in this thesis. The model based on the equivalent circuit is used for simulating the current sensors behavior, and for the analysis on the energy extracting capabilities of a CT.

The currents in the primary winding can be very high and to prevent damage to the measurement equipment the CT transforms the current down to measurable quantities. The voltage at the secondary side depends on the load and the size of the transformer but is low as well. Since the current is transformed down by the CT, the voltage is transformed up according to the power balance (equation 2.2). Therefore the voltage across the primary winding is very low. A typical CT has one, or sometimes a few, primary turns and many secondary turns. Most current transformers use an iron core as magnetic conduction path.

$$V_p I_p = V_s I_s \quad (2.2)$$

In figure 2.3 the equivalent circuit of a transformer is given. From this circuit a few simplifications are made in order to create a circuit that is used for simulation purpose. In figure 2.3  $R_p$  and  $R_s$  are the winding losses of primary and secondary turns respectively, and  $L_{\sigma p}$  and  $L_{\sigma s}$  are the leakage inductances of those windings. The primary and secondary are coupled by an ideal transformer with turns ratio  $\frac{N_s}{N_p}$ . The magnetizing inductance and core losses are represented by  $R_m$  and  $L_m$ .

In this project the secondary side of the transformer is considered. Therefore all elements of the circuit of figure 2.3 are transformed to the secondary side of the ideal transformer which results in the circuit of figure 2.4. The primary inductance and resistance are transformed to the secondary side of the circuit and the source of this circuit is the transformed primary current.

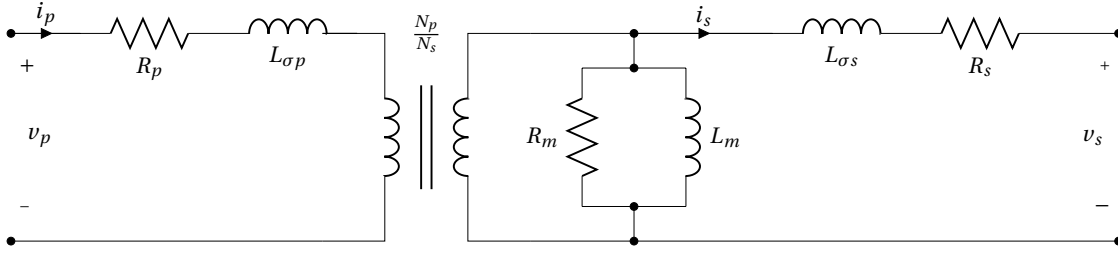


Figure 2.3: Transformer equivalent circuit

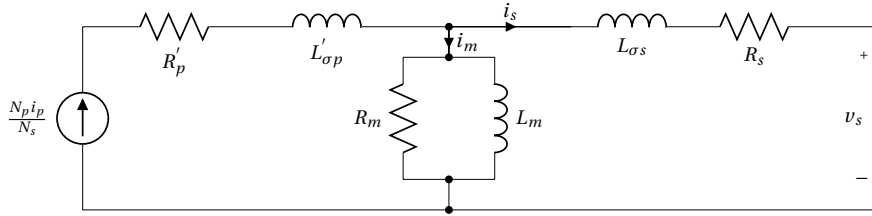


Figure 2.4: Secondary transposed transformer equivalent circuit

$$L'_{\sigma p} = \left(\frac{N_s}{N_p}\right)^2 L_{\sigma p} \quad R'_p = \left(\frac{N_s}{N_p}\right)^2 R_p$$

$L_{\sigma p}$  and  $R_p$  are cable and application dependable and therefore unknown. With respect to the secondary side parameters the value is very small. In this analysis the primary side parameters are therefore neglected. The core losses are, in the linear region, negligible as well and therefore the circuit of figure 2.4 is simplified into the circuit given in figure 2.5.

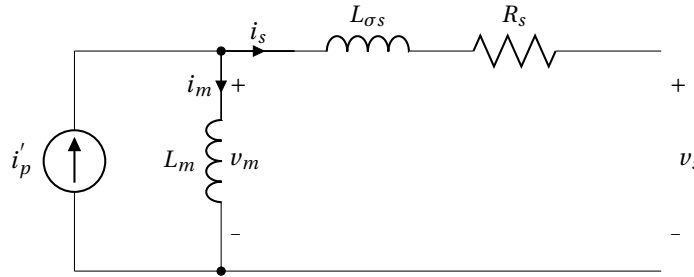


Figure 2.5: Simplification of current transformer equivalent circuit

In figure 2.5 the equivalent circuit of a current transformer is given. In this circuit the inductance  $L_m$  is the magnetizing inductance and  $L_s$  is the leakage inductance of the secondary winding. The resistance  $R_s$  is the resistance of the secondary winding.

The magnetizing inductance  $L_m$  in figure 2.5 is calculate using the dimensions of the CT as well as the core characteristics and the number of turns of secondary winding. The magnetizing inductance is calculated using equation 2.3. In equation 2.3  $\mu_0$  is the permeability in free space,  $\mu_r$  the relative permeability of the core material,  $A_e$  the cross-sectional area,  $N_s$  the number of secondary turns and  $l_c$  the magnetic core path length.

$$L_m = \frac{\mu_0 \mu_r A_e N_s^2}{l_c} \quad (2.3)$$

The circuit of figure 2.6 is another commonly used equivalent circuit in literature [3, 10, 12, 25, 26, 29, 30, 37] and the Thevenin equivalent of the current source based circuit. This circuit uses a AC voltage source as source instead of an AC current source. The inductance  $L_s$  is the given by  $L_s = L_m + L_{\sigma s}$ . The voltage is induced by the flux flowing through the core of the current transformer (equation 2.4).

In case of a CT there is a core around the current carrying conductor and using Ampere's law (equation 2.5) the magnetic field strength in the core is calculated. If equation 2.5 and 2.6 are combined expression

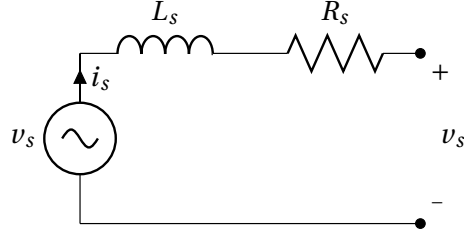


Figure 2.6: Simplification of current transformer equivalent circuit

2.7 is found in case a wire carrying a current with amplitude  $I$  is considered, and the contour  $C$  of which the magnetic field is calculated is a circle with radius  $r$ .

$$v_s = -N_s \frac{d\Phi}{dt} \quad (2.4)$$

$$\oint_C \mathbf{H} \cdot d\mathbf{l} = \iint_S \mathbf{J} \cdot d\mathbf{S} \quad (2.5)$$

$$\mathbf{B} = \mu_0 \mu_r \mathbf{H} \quad (2.6)$$

$$\mathbf{B}(r) = \frac{\mu_0 \mu_r i}{2\pi r} \quad (2.7)$$

Using Faraday's law of induction and using the cross-sectional surface of the core as integrating area the relation between flux and magnetic flux density (equation 2.8) is derived.

$$\Phi = \iint_S \mathbf{B} \cdot d\mathbf{A} = \mathbf{B} A_e \quad (2.8)$$

In equation 2.9 the expression of the primary current is given.

$$i_p(t) = I_p \cos(\omega t + \varphi) \quad (2.9)$$

If now equation 2.9 is inserted into equation 2.7 and equation 2.7 is inserted into equation 2.8 equation 2.10 is derived.

$$\Phi = \frac{\mu_0 \mu_r A_e}{2\pi r} I_p \cos(\omega t + \varphi) \quad (2.10)$$

The last step to obtain the relation between primary current ( $i_p$ ) and induced voltage ( $v_s$ ) is to substitute equation 2.10 in equation 2.4.

$$v_s = N_s \frac{\mu_0 \mu_r A_e}{2\pi r} \omega I_p \sin(\omega t + \varphi) = \frac{L_m}{N_s} \omega I_p \sin(\omega t + \varphi) \quad (2.11)$$

Although the equivalent circuit, both voltage source and current source based, are represented by lumped elements with constant value, the values are in practical situations not constant. Due to magnetic saturation of the core, the magnetizing inductance  $L_m$  is not be constant. In appendix A more information about the non-linearity of the model is given. Based on the available information a non-linear magnetizing inductance is simulated in the circuit of figure 2.5.

Element	Measured
Magnetizing inductance $L_m$	1.7 H
Leakage inductance of secondary $L_{\sigma s}$	1.8 mH
Secondary inductance $L_s = L_m + L_{\sigma s}$	1.7018 H
DC resistance of secondary $R_s$	2.54 $\Omega$

Table 2.2: Parameters of lumped elements in current transformer equivalent circuit

In table 2.2 the parameters of the lumped elements of the CT equivalent circuit are given. In most transformers the magnetizing inductance in the order of henry is not observed (mostly millihenry) but since the

secondary side has a large number of turns and all elements are considered from the secondary side the magnetizing inductance has a value of 1.7 H. These values are based on a measurement taken with an OMICRON CT Analyzer. A picture of the output of the CT analyzer is given by figure 2.7. The values are obtained by connecting the output of the CT to the input terminals of the CT analyzer.

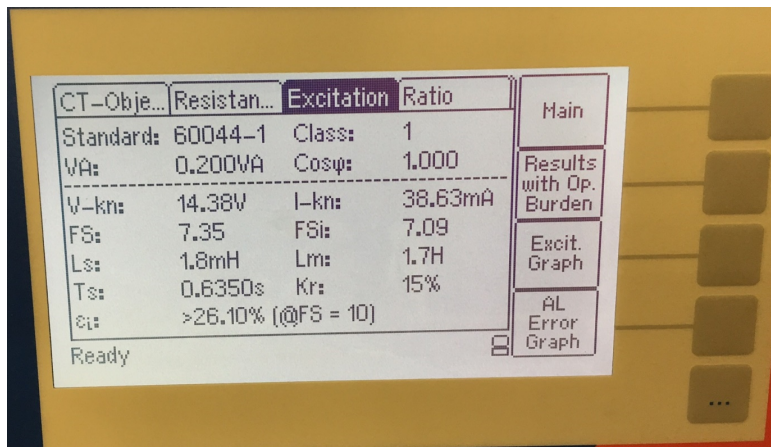


Figure 2.7: Parameter estimation of TQ40-c with OMICRON CT Analyzer

### 2.2.2. Model verification

For the verification of the equivalent circuits and the influence of the non-linearity, the results of the simulations are compared with the results of a measurement. For current measurement with a CT a burden resistance is connected to the terminals of the CT in most applications. Measuring the voltage drop across the burden resistance the current flowing through the primary conductor can be derived. The relation between burden voltage  $v_b$  and the primary current  $i_p$  is given by equation 2.12. In equation 2.12  $R_b$  is the burden resistance connected to the CT.

$$i_p = \frac{N_s v_b}{N_p R_b} \tag{2.12}$$

For the simulations and measurement a burden resistor of 1 Ω is connected to the CT. For the measurement the TQ40-c is used and for the simulations the circuits of figure 2.5 and 2.6. A non-linear magnetizing inductance in circuit of figure 2.5 is used for the simulations as well. The voltage across the burden is measured for primary currents from 1 A to 240 A. The difference between measured secondary current and the corresponding primary current, which is used as input, is used to calculate the ratio error (equation 2.1). Table 2.3 shows the results of the measurement and simulations. In figure 2.8 the simulated ratio errors are plotted in combination with the measurement and on the background the accuracy classes.

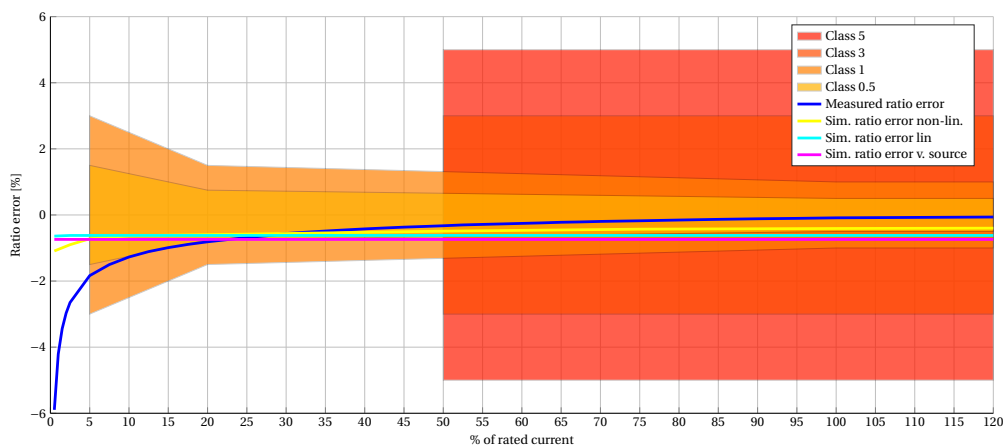


Figure 2.8: Ratio error of simulation

Ip [A]	Ip' [mA]	Measurement		Simulation					
				Current source non-linear		Current source linear		Voltage source	
		Is [mA]	ratio error	Is [mA]	ratio error	Is [mA]	ratio error	Is [mA]	ratio error
1	2,5	2,3526	-5,90%	2,4727	-1,09%	2,4839	-0,64%	2,4814	-0,74%
5	12,5	12,1688	-2,65%	12,3873	-0,90%	12,423	-0,62%	12,407	-0,74%
10	25	24,541	-1,84%	24,8194	-0,72%	24,845	-0,62%	24,814	-0,74%
20	50	49,364	-1,27%	49,6856	-0,63%	49,691	-0,62%	49,629	-0,74%
50	125	124,147	-0,68%	124,2737	-0,58%	124,23	-0,62%	124,07	-0,74%
100	250	249,183	-0,33%	248,7857	-0,49%	248,46	-0,62%	248,14	-0,74%
150	375	374,339	-0,18%	373,3692	-0,43%	372,68	-0,62%	372,22	-0,74%
200	500	499,566	-0,09%	497,9547	-0,41%	496,91	-0,62%	496,29	-0,74%
240	600	599,626	-0,06%	597,6113	-0,40%	596,29	-0,62%	595,54	-0,74%

Table 2.3: Measurement of current transformer output compared with simulation results and theoretical value

In figure 2.9 the ratio error is given for the measurement with the TQ40-c.

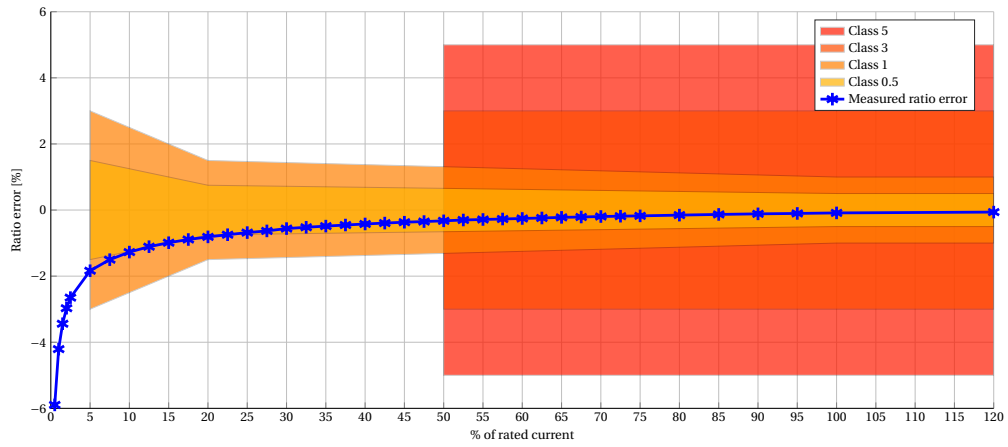


Figure 2.9: Ratio error of measurement

## 2.3. Current measurement techniques

Currents flowing through a conductor can be measured in different ways. In this section multiple current measurement techniques are discussed and they are characterized in three different groups. One group of measurement techniques is based on ohm's law. A second group is based on faraday's law of induction and a last group is based on magnetic field sensors. Within these groups several sensor exist that are used in circuits to measure currents. Each of these sensors is reviewed based on

- Accuracy
- Size
- Cost
- Losses
- Capability of measuring AC and DC

### 2.3.1. Ohm's law

Ohm's law of resistance is a law named after George Ohm which describes the relation between a current flowing through a conductor between two points and the voltage across those two points. Through time multiple forms of Ohm's law are presented and one of the simplest forms is given in equation 2.13.

$$\mathbf{J} = \sigma \mathbf{E} = \frac{1}{\rho} \mathbf{E} \quad (2.13)$$

In equation 2.13,  $J$  is the current density,  $E$  is the Electric field,  $\rho$  is the resistivity and  $\sigma$  is the materials conductivity. A more commonly used version of Ohm's law is given in equation 2.14. In this equation  $I$  is the current flowing through the conductor,  $V$  is the voltage measured across the conductor and  $R$  gives the resistance of the conductor.

$$I = \frac{V}{R} \quad (2.14)$$

The principle of relating a current to the voltage across two points and the resistance between these two points is used in many applications to measure the current. There are many sensors that imply Ohm's law and since this current measurement technique is based on the materials resistivity and the voltage drop created by the current through the resistive element every type of resistive material could be used as current sensor as long as the resistive value is known. A shunt resistor and a PCB trace are reviewed in this section based on accuracy, implementation size, cost, losses and the capability of measuring AC and DC.

#### Shunt resistor

A shunt resistor is a resistor that is placed in the path of the current needs to be measured. Shunt resistors have most of the time a small resistance value and the current is measured by measuring the voltage drop across the resistor and divide it by the resistance value of the resistor. This sensing technique is capable of measuring AC currents and DC currents. A disadvantage of a shunt resistor is the dissipated energy in the resistor. Equation 2.15 gives the loss in a shunt resistor. The power loss in a shunt resistor increases quadratic with the current flowing through the shunt resistor. The accuracy of a measurement with a shunt resistor depends on a few things. Since the voltage across the shunt is measured the shunt resistance must be chosen in such a way that at minimal current the voltage drop is still measurable. Another important parameter for the accuracy is the accuracy of the resistance value of the shunt and it's frequency dependency.

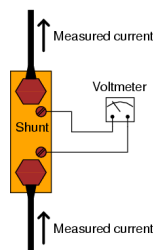


Figure 2.10: Shunt measurement

$$P_{loss} = I^2 R \quad (2.15)$$

An ideal resistor has a flat frequency response since it is not frequency dependent. In practical situations an ideal resistor does not exist and a resistor has always a small self-inductance, parasitic inductance and losses due to skin effect. The influences on the resistance value for small frequencies are negligible but for high frequencies the resistance value of the shunt is influenced in a way it is no longer negligible.

Another aspect that influence the accuracy of the measurement is temperature. The resistance of the resistor changes under influence of temperature and due to this change in resistance an error is introduced. The temperature coefficient is an indicator for the change in resistance value per change in temperature. Shunt resistors with a small thermal influence are more accurate than those with bigger thermal influence and cooling a shunt in case of high power dissipation might be required as well.

The position of the current shunt could play a role in the circuit in which the shunt is placed. If the current shunt is placed at ground level the ground level of the rest of the circuit could be lifted by the voltage drop of the current shunt. This ground offset could cause problems with parts of the electronics which require a real earth level. This problem only occurs in case of a measurement in a DC circuit.

Since a shunt is an additional component in the circuit it requires additional space. Depending on the expected power dissipated in the shunt the shunt could be very small. The cost of the shunt is low but depends on the accuracy of the shunt.

#### Copper trace

A current measurement method based on Ohm's law without the need of additional components is based on the resistance of a copper trace. The copper trace on a PCB has a certain resistance and if this resistance is

known between two points and the voltage across these points is measured the current through the trace can be calculated. By this method no additional resistance is added and therefore this method has no additional power losses.

The resistance of a copper trace is not accurately known so before this could be used a calibration measurement is needed. The resistance of a copper trace is normally small and therefore the voltage across the two points will be low as well. This small voltage across the measurement points has influence on the resolution of the measurement and inherently on the accuracy. Although the power dissipation is low changes in temperature might have bigger influence than in case of a shunt resistor. Copper traces are not designed for having low temperature dependency.

Due to the fact that no additional components are required for this method the additional cost for this type of measurement are low and the size of the measurement is small. With copper traces it is possible to sense AC and DC current.

### 2.3.2. Faraday's law of induction

Another method of current sensing is to use Faraday's law of induction. This law connects magnetic fields with electric fields. Current sensors that are based on Faraday's law of induction provide inherent electrical isolation between the current that is measured and the output signal of the sensor. For safety issues isolation between primary and secondary is an important issue in case of high and floating voltage potential. Faraday's Law of Induction (equation 2.16) describes how an electric current produces a magnetic field and, conversely, how a changing magnetic field generates an electric current in a conductor.

$$\Phi_B = \iint_S \mathbf{B} \cdot d\mathbf{A} \quad (2.16)$$

#### Rogowski coil

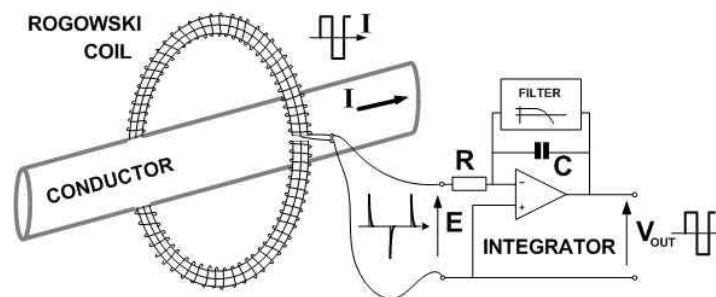


Figure 2.11: Rogowski coil

The Rogowski coil (figure 2.11) is a measurement device that uses Faraday's law of induction to measure current. The sensors consists of a non-magnetic core that is connected around the current carrying conductor. Around the non-magnetic core a coil is wound and at the end of the non-magnetic core, the return wire is sent back through the inside of the non-magnetic core.

Using Amperes law (equation 2.5) and the relation between the magnetic field strength and the magnetic flux density (equation 2.6) the relation between the magnetic flux density and the primary current can be derived.

If assumed that the cross sectional area of the Rogowski coil is much smaller than the radius between conductor and Rogowski coil and the conductor is centered inside the coil, the magnetic flux density can be simplified to equation 2.17.

$$B = \frac{\mu_0 i_C}{2\pi r} \quad (2.17)$$

Combining equation 2.17 and Faraday's law of induction (equation 2.16) the relation between the induced voltage and the primary current is found (equation 2.18)

$$v = -NA \frac{dB}{dt} = -\frac{NA\mu_0}{2\pi r} \frac{di_C}{dt} \quad (2.18)$$

In equation 2.18  $N$  is the number of turns,  $A$  is the cross sectional area,  $\mu_0$  is the permeability and  $r$  is the radius (distance from conductor to Rogowski coil). From equation 2.18 it becomes clear that the output of the Rogowski coil needs to be integrated to obtain the current  $i_C$ . It is also observed that a Rogowski coil is only able to sense a change in current  $\frac{di_C}{dt}$  and therefore constant currents can not be sensed with a Rogowski coil.

The accuracy is influenced by several factors. The first factor is the construction of the Rogowski coil. The turns needs to be evenly spaced to hold equation 2.18. Another factor is the location of the conductor with respect to the coil. Since the Rogowski coil is based on measuring a changing magnetic field the performance at low frequency is limited. The Rogowski coils thermal drift is determined by the integrator but also by the fact that due to the thermal expansion of the coil the cross-sectional area of the coil body may change.

The size is depending on the design of the Rogowski coil but due to the fact that a high number of turns is required and a certain radius  $r$  bigger than the cross sectional area the Rogowski coil has a high footprint. The Rogowski coil is commonly used in high voltage situations but in low current sensing situations where the conductor is located on a PCB this method is less likely to use. The costs of a Rogowski coil are high compared with shunt resistors and comparable with CT.

### Current transformer

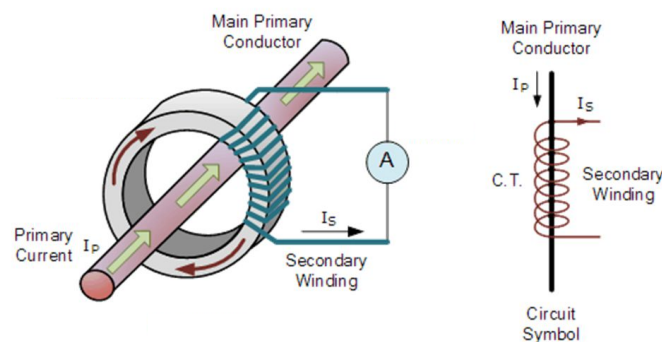


Figure 2.12: Current transformer

Current transformers are a type of instrument transformers that transform the primary current down to levels at which they can be measured [38]. Similar to the Rogowski coil, the CT is based on Faraday's law of induction to measure current as well (equation 2.16). Comparing the Rogowski coil and a CT some similarities are observed. The primary winding consists in most applications of a single turn and the secondary winding consist of multiple turns. Different from a Rogowski coil a CT uses magnetic core with a relative high permeability. In section 2.2 equations are derived for the CT.

A CT is similar to the Rogowski coil unable to measure DC current and at very low frequency the accuracy reduces. A major difference between the CT and the Rogowski coil is the fact that the output of the CT can be connected to a shunt or burden resistor which is used for the measurement of the current. The output needs no additional amplification or integration to obtain the primary current.

The errors in a measurement with a CT are mainly due to the core characteristics and the dimensioning of the secondary winding. At low primary current the measurement error is mainly caused by the magnetizing inductance. By changing the core dimensions or the burden resistor this error can be reduced but at low primary current there is always a error due to the magnetizing inductance. On the other hand if the core saturates, at the higher side of the measurement range of the CT, the CT is no longer capable of providing a linear relation between the primary and secondary current.

Power losses are usually higher than in Rogowski coil since the core and secondary winding adds additional losses. The power losses are mainly due to the winding losses since the winding resistance is not negligible and the losses increase with the square of the current ( $P_{loss} = I^2 R$ ) The size is comparable with the size of a Rogowski coil and depends mainly on the current range that is measured. The cost are comparable with the cost of a Rogowski coil.

### 2.3.3. Magnetic field sensors

In the previous section sensors based on Faraday's law of induction are discussed. Due to the nature of this law it is impossible to measure DC. Current sensors based on the magnitude of the magnetic field on the other hand are able to sense static and changing magnetic fields and are therefore able to sense AC and DC current. Examples of these sensors are Hall Effect sensors and Magneto Resistance (MR) Effect sensors.

#### Hall-effect sensor

The Hall-effect sensor (figure 2.13) is based on the Hall-effect discovered by Hall in 1879. Hall found that there is a relation between a current  $I$  flowing through a thin sheet of conductive material that is penetrated by a magnetic flux density  $B$ , and the voltage  $v$  that is generated perpendicular to both the current and the field. In equation 2.19 this relation is given and in this equation  $q$  is the charge of the current carrier,  $n$  the carrier density and  $d$  the thickness of the sheet.

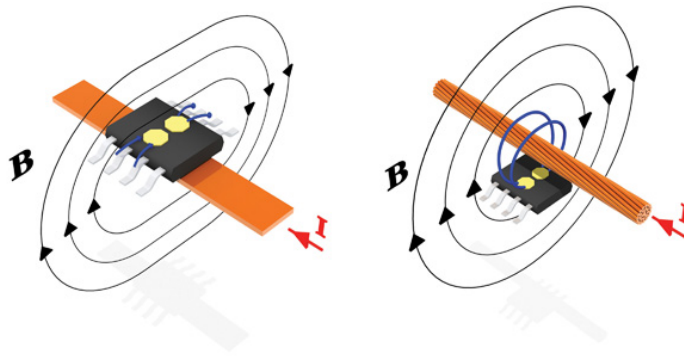


Figure 2.13: Hall-effect sensor

$$v = \frac{IB}{nqd} \quad (2.19)$$

To use the hall-effect sensor as current sensor additional circuitry is required to compensate for a misalignment voltage and thermal drift. The accuracy of hall-effect sensors when used in a closed-loop configuration is high. To sense the current additional circuitry is needed and this circuitry is the main power consumer of hall-effect sensors. They consume an almost fixed amount of energy. The size of such a sensor is small but the cost are relative high.

#### MR effect sensor

Another type of sensor based on the magnetic field effect is the magneto resistance effect sensor. This type of sensor is based on a varying resistance value at a varying magnetic field. Two examples of magneto resistance effects sensors are anisotropic MR (AMR) and giant MR (GMR).

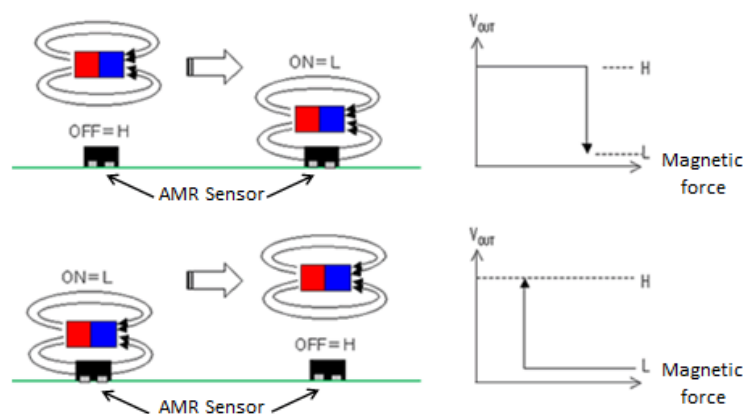


Figure 2.14: Magneto resistance effect sensor

When AMR sensors are considered the resistance of ferromagnetic materials is related to the magnitude

and direction of the applied magnetic field. Problems of AMR sensors is the high non-linearity and high thermal drift.

GMR sensors are based on another principle than AMR sensors. GMR sensors use a four layer structure that is placed in the magnetic field that needs to be measured. Based on the direction and the strength of the magnetic field the resistance of the four layer structure changes. The four layers usually used are an antiferromagnet material, a pinned (hard) ferromagnetic material, a free (soft) ferromagnetic material and a substrate. Between the pinned and free layer a thin conductor is placed. MR sensors have the disadvantages of high thermal drift and the influence of external magnetic fields. Another drawback is the influence of notable hysteresis. Apart from AMR sensor GMR sensors are not employed in closed-loop configuration which has results in typical problems like high thermal drift, poor immunity against external fields, and nonlinearity.

### 2.3.4. Conclusion

In the previous sections multiple sensors based on three different current sensing principles are reviewed based on cost, size, accuracy, losses and the ability of sensing AC and DC. The measurement techniques which will be used in this project needs to be very accurate. Linearity is an important factor in this. Table 2.4 gives an overview of the current measurement techniques described in the sections before. In the rating -- is the worst rating and ++ a very good rating. +/- is an average rating. In the analysis of the current measurement

Sensor	Accuracy	Size	Cost	Losses	AC/DC
Shunt	++	+	+	-	AC & DC
Copper trace	-	++	++	-	AC & DC
Rogowski coil	+/-	-	+/-	+	AC
CT	++	-	-	-	AC
Hall-effect	++	+	-	+/-	AC & DC
MR effect	+	+/-	-	+/-	AC & DC

Table 2.4: Current measurement sensor

sensors accuracy, AC and DC capability and size are important design consideration is this design. Losses are only important at low primary current. From this analysis it becomes clear that a shunt resistor is the best option. A shunt resistor is capable of measuring AC and DC current, if used in the right way very accurate and linear in the application of this project and the size and cost are good as well. The main drawback of a current shunt is that the losses increase quadratically with current and linear with resistor value. Because the losses are related with the current the losses are low if the current is low and that is the area where losses are most important. Therefore the current shunt will be used in this project as current sensing element.



# 3

## Energy extraction and power conversion

### 3.1. Introduction

This chapter describes the use of a CT for the extraction of energy from the magnetic field around a current carrying conductor. The energy is required for powering the electronics in the sensor that are needed for measurement, data processing and data transmission (figure 3.1). Theoretical analysis based on an equivalent circuit of a CT is used as base. Simulations and measurements are used for the verification of the analysis. Power conversion stages required for converting the CT output voltage and current into a stable DC supply for the electronics is described as well.

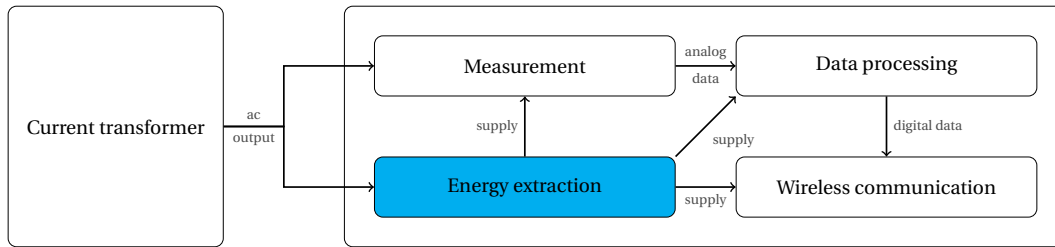


Figure 3.1: Block diagram of sensor, energy extraction block is considered in this chapter

In section 3.2 the capabilities of a CT for energy extraction is discussed. In this chapter the amount of energy that is extracted under normal condition as well as possible techniques of increased energy extraction are considered. In section 3.3 the power conversion stages are considered and the influence of the conversion on the source voltage and current waveforms are discussed.

### 3.2. Energy extraction

CTs are, like all instrument transformers, not designed for power transfer from the primary side to the secondary side of the transformer. A CT is dimensioned in a way that current is transformed to measurable quantities while the primary voltage is kept low. Typical burden resistor values and dimensions of the magnetic core keep the core out of saturation for the designed current range. If the burden resistance is too large, core saturation will be a limiting factor and the measurement error will increase.

Based on the equivalent circuit (figure 3.2) the energy extraction capabilities of a CT are discussed. In this circuit the source is a current source with magnitude which is equal to primary current multiplied with current ratio. As discussed in chapter 2 primary leakage  $L_{\sigma p}$  and primary resistance  $R_p$  are negligible. Core magnetizing inductance  $L_m$ , secondary leakage inductance  $L_{\sigma s}$  and secondary resistance  $R_s$  are included in the analysis.

For the analysis of the energy extracting capabilities of a CT a load resistance is connected to the CT. For this analysis four different resistances (1  $\Omega$ , 10  $\Omega$ , 100  $\Omega$  and 500  $\Omega$ ) are used to analyze the influence of the load on the energy extracting capabilities of a CT. These load resistances are assumed to be constant but in the application of a wireless current sensor the load will not be constant.  $Z_p$  (equation 3.1) is the equivalent

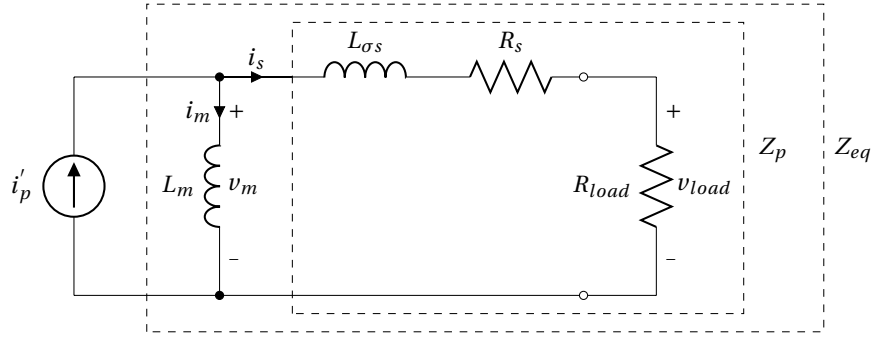


Figure 3.2: Current transformer equivalent circuit with load connected

impedance of the parallel output branch including secondary leakage inductance and secondary resistance. The circuit's total equivalent impedance (equation 3.2) is the total impedance seen by the source.

$$Z_p = R_s + R_{load} + j\omega L_{\sigma s} \quad (3.1)$$

$$Z_{eq} = j\omega L_m // Z_p \quad (3.2)$$

In equation 3.1 and 3.2  $\omega$  is given by  $\omega = 2\pi f$  in which  $f$  is the frequency of the source.

In equation 3.3 the expression representing the impedance from source perspective is given. If the core is kept constant the only variable in this equation is the load connected to the CT. Figure 3.3 is a plot of the equivalent impedance seen by the source in case the load is represented by a pure resistive load ranging from  $0\Omega$  to  $500\Omega$ . A pure resistive load is chosen because in the final design the load is a DC load which is represented by a resistive load. For the other parameters the parameters of the TQ40-c are used (table 2.2).

$$Z_{eq} = \frac{j\omega L_m (j\omega L_{\sigma s} + R_s + R_{load})}{j\omega L_{\sigma s} + R_s + R_{load} + j\omega L_m} \quad (3.3)$$

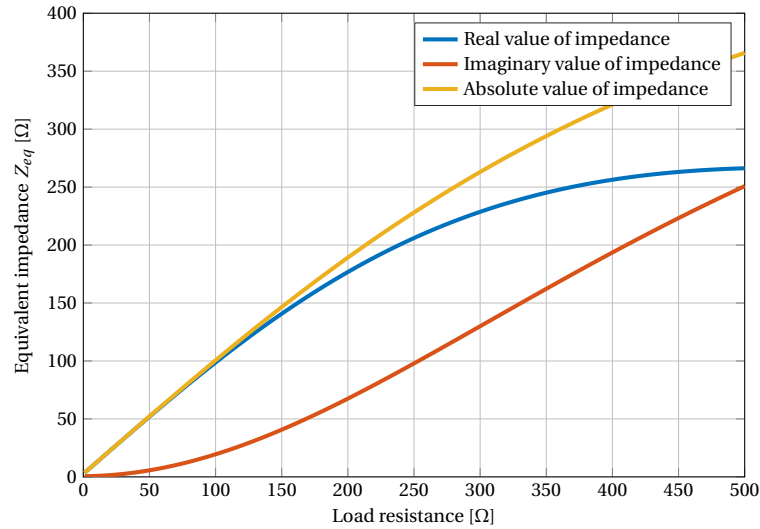


Figure 3.3: Equivalent impedance at different loads

For measurement purpose it is important that the ratio between the primary current  $i_p$  and the secondary current  $i_s$  is given by the turns ratio of the transformer. In the analysis using the equivalent circuit of figure 3.2 this means that the ratio between  $i_p' = \frac{N_p i_p}{N_s}$  and  $i_s$  must be one. The current ratio, equation 3.4, is also depending on the load resistance ( $R_{load}$ ) connected to the CT.

$$\frac{I_s}{I_p} = \frac{Z_{eq}}{Z_p} = \frac{j\omega L_m}{R_s + R_{load} + j\omega(L_{\sigma s} + L_m)} \quad (3.4)$$

The application of the wireless current sensor is within the grid and therefore the frequency is fixed at 50 Hz or 60 Hz, depending on the grid frequency at the location where the wireless current sensor is implemented. In the Dutch grid the frequency is 50 Hz. The parameters of the CT are fixed by the used CT and therefore the only variable parameters is the load connected to the CT. The influence of this is displayed in figure 3.4

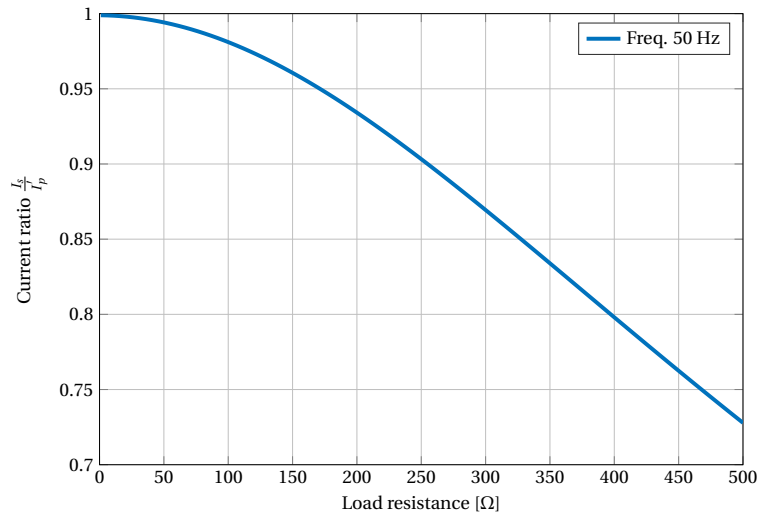
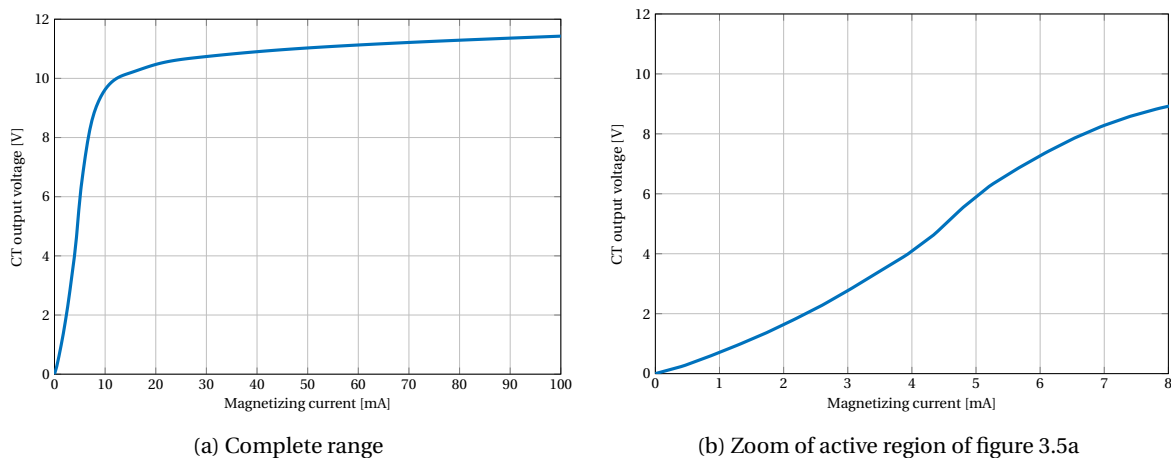


Figure 3.4: Current ratio  $\frac{I_s}{I_p}$  at different load resistance values

From the simulated current ratio (figure 3.4) it is observed that only in case of a very small load the current ratio is equal to one. A current ratio of one represents a perfect coupling between measured secondary current and expected primary current.

In the application of a wireless current sensor the load is the electronics needed for the current measurement. The electronics consumes a certain amount of power and therefore the load impedance will be different for different primary current.

The power consumed in the load depends on the impedance of the load and the current flowing through the load (equation 3.5). All electronics require DC and therefore the load is resistive. So far there is one factor not taken into account. The CT is a transformer with core and the core is not capable of carrying unlimited flux and saturates at some point. In the linear part of the saturation curve (figure 3.5) the magnetizing inductance  $L_m$  is almost constant but once the core saturates the inductance is not constant anymore. The saturation of the core has therefore influence on the equivalent circuit parameters and the power delivered to the load.



(a) Complete range

(b) Zoom of active region of figure 3.5a

Figure 3.5: Relation output voltage and magnetizing current

$$P_{load} = I_s^2 R_{load} = \left( I_p \frac{j\omega L_m}{R_s + R_{load} + j\omega(L_{\sigma s} L_m)} \right)^2 R_{load} \quad (3.5)$$

The power delivered to the load is given by equation 3.5. Based on the equation it is observed that the load is dependable on the magnetizing inductance  $L_m$ . The magnetizing inductance is more or less constant in the linear region of the CT but as soon the core saturates the magnetizing inductance changes. The influence of this inductance change is included in the simulation and therefore the results of the simulation should be equal to the measure power extraction.

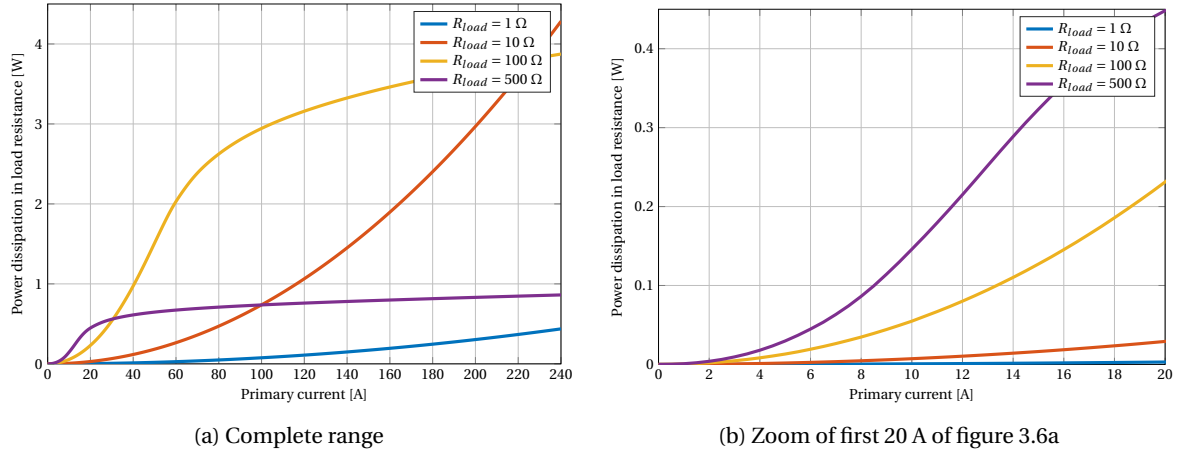


Figure 3.6: Simulated power consumed at variable load

The amount of power that can be extracted is proportional to the primary current. Therefore at low primary currents the available power is limited.

The results of figure 3.6 are compared with a measurement performed with the same setup as in figure 3.2 and with the same loads as used in the simulation. It is observed that for the current range till 20 A the simulation is more or less equal to the measurement. For higher primary current and higher load resistance the results of measurement and simulation are not equal or close to each other. The difference between simulation and measurement is due to the CT core saturation. Because there is not a good model of the CT including saturation the difference between measurement and simulation occur.

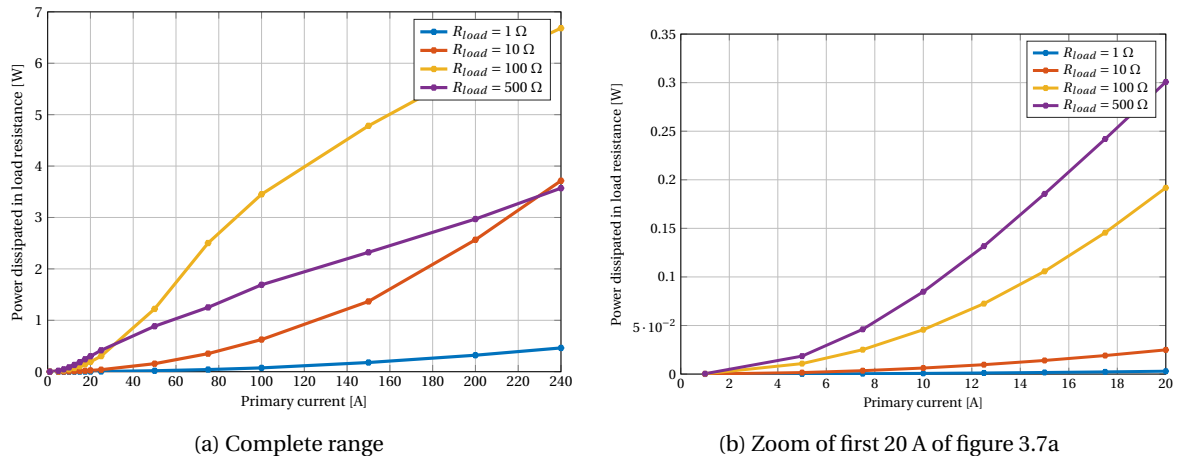


Figure 3.7: Measured power consumed at variable load

From figures 3.6 and 3.7 it is concluded that the power consumed by the load is low at low values of the primary current. The electronics used for current measurement need a certain amount of power. To obtain a larger operating range more power is required at low primary current. One of the methods to achieve higher power extraction at low primary currents is to compensate for the reactive impedance seen by the source. By compensating for reactive impedance the power extraction at low primary currents may be higher.

### 3.2.1. Series compensation for reactive currents

In air-core transformers used for Inductive Power Transfer (IPT) compensation in the form of resonance is applied in many applications. In such systems the need for reactive power compensation is accomplished by adding capacitive elements. In IPT systems compensation can be applied in both primary and secondary side and the capacitive elements can be placed in series with the inductance or parallel with the inductance. In this application it is not possible to apply compensation in the primary and therefore there are two topologies for compensation, series and parallel compensation in the secondary side.

In this section the series resonance topology is considered. Figure 3.8 gives the modified equivalent circuit of the current transformer connected to a load. A series resonance capacitor is placed at the output of the CT. The value of the capacitance is chosen such that it resonates at grid frequency and compensates for the reactive elements in the circuit.

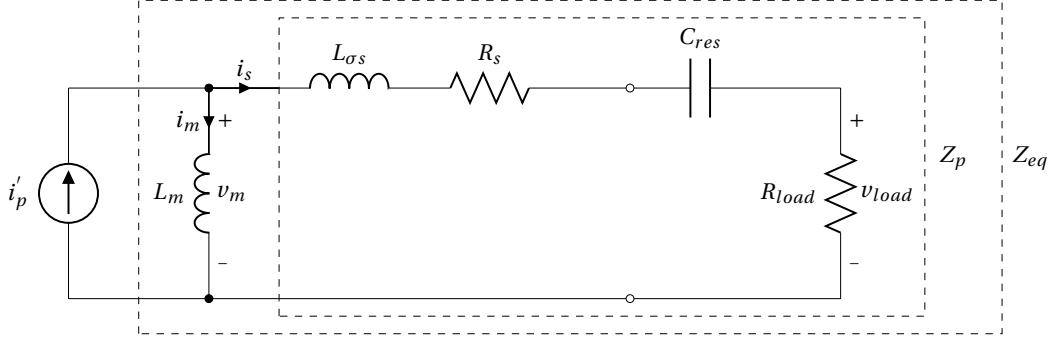


Figure 3.8: Series resonance topology

In IPT systems the secondary compensation is chosen to compensate for the secondary leakage inductance and the mutual inductance. This implies that equation 3.6 yields.

$$j\omega(L_{\sigma s} + L_m) = \frac{1}{j\omega C_{res}} \quad (3.6)$$

$\omega$  is frequency depended and therefore the value of the resonance capacitor is chosen such that it resonates at the resonant frequency  $\omega_0$  which is in this application the grid frequency.

$$C_{res} = \frac{1}{\omega_0^2(L_{\sigma s} + L_m)} \quad (3.7)$$

In most IPT systems the primary compensation is to compensate for the reactive impedance seen from the source side. In this application there is no primary compensation and therefore the resonance capacitor is chosen such that it compensates for the systems reactive impedance. For the calculation of the systems impedance first the impedance  $Z_p$  is calculated.  $Z_p$  parallel to  $Z_{eq}$  is the systems total impedance seen from source side.

$$Z_p = R_s + R_{load} + j\left(\omega L_{\sigma s} - \frac{1}{\omega C_{res}}\right) \quad (3.8)$$

The circuits total equivalent impedance  $Z_{eq}$  is given in equation 3.9.

$$Z_{eq} = \frac{j\omega L_m(R_s + R_{load}) - \omega L_m\left(\omega L_{\sigma s} - \frac{1}{\omega C_{res}}\right)}{R_s + R_{load} + j\left(\omega L_m + \omega L_{\sigma s} - \frac{1}{\omega C_{res}}\right)} \quad (3.9)$$

If equation 3.9 is reformulated in the form  $a + jb$  equation 3.10 is derived.

$$Z_{eq} = \frac{\omega^2 L_m^2 (R_s + R_{load})}{(R_s + R_{load})^2 + \left(\omega L_m + \omega L_{\sigma s} - \frac{1}{\omega C_{res}}\right)^2} + j \frac{\omega L_m (R_s + R_{load}) + \frac{\omega L_m}{C_{res}} (1 - 2L_{\sigma s}) + \omega^3 (L_m^2 L_{\sigma s} + L_m L_{\sigma s}^2)}{(R_s + R_{load})^2 + \left(\omega L_m + \omega L_{\sigma s} - \frac{1}{\omega C_{res}}\right)^2} \quad (3.10)$$

Element	Value
Magnetizing inductance $L_m$	1.7 H
Leakage inductance of secondary $L_{\sigma s}$	1.8 mH
DC resistance of secondary $R_s$	2.54 $\Omega$

Table 3.1: Parameters of CT

If the resonance frequency is chosen such that it compensates for the reactive impedance the value of the resonance capacitance is given in equation 3.11

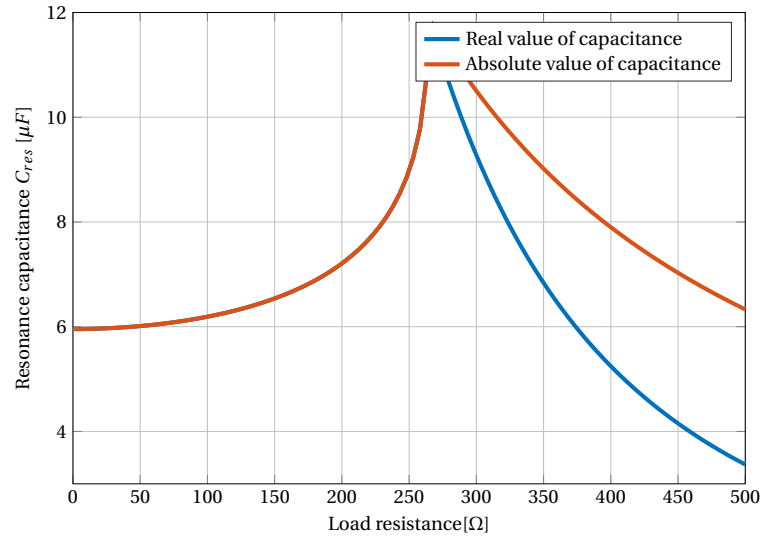
$$C_{res} = \frac{1}{2} \frac{\omega_0(L_m + 2L_{\sigma s}) - \sqrt{\omega_0^2 L_m^2 - 4R_{load}^2 - 8R_{load}R_s - 4R_s^2}}{\omega_0(\omega_0^2 L_m L_{\sigma s} + \omega_0^2 L_{\sigma s}^2 + R_{load}^2 + 2R_{load}R_s + R_s^2)} \quad (3.11)$$

If in equation 3.11 all contributions due to the resistance are ignored, equation 3.7 is found again.

The series capacitance to compensate for the reactive impedance based on equation 3.6 and the parameters of the CT from table 3.1 is

$$C_{res} = \frac{1}{4 * \pi^2 * 50^2 (1.7 + 1.8 * 10^{-3})} = 5.96 \mu\text{F}$$

The value derived above is without the influence of the resistances in the system. The influence of the resistance and the load represented by a resistance connected to the CT (equation 3.7) on the ideal value of the resonance capacitance is given in figure 3.9.

Figure 3.9: Influence of  $R_{load}$  on ideal capacitance value

From this it is concluded that unless the load is perfectly known and constant it is impossible to perfectly compensate for the reactive impedance.

If the current ratio between secondary current and primary current is observed with the influence of the series capacitance the ratio is given by the following equation.

$$\frac{I_s}{I_p} = \frac{j\omega L_m}{R_s + R_{load} + j\left(\omega L_m + \omega L_{\sigma s} - \frac{1}{\omega C_{res}}\right)} \quad (3.12)$$

If the resonance capacitor is set according to equation 3.7 the relation between primary and secondary current becomes

$$\frac{I_s}{I_p} = \frac{j\omega L_m}{R_s + R_{load}}$$

From the above relation it is observed that the ratio varies with  $\frac{1}{R_{load}}$ . In case of no reactive compensation the ratio starts at, more or less, one in case of very small load but with compensation the ratio starts at  $\frac{j\omega L_m}{R_s}$  at very small load. This means that the ratio, which should be equal to one to have a direct and good relation between primary and secondary current no longer yields. Therefore with reactive current compensation the secondary and primary current are no longer related by the turns ratio which implies more complex measurement.

One of the reasons to use resonance is to compensate for the reactive currents and extract more power from the source. The power dissipated in the load is given by equation 3.13.

$$P_{load} = I_s^2 R_{load} = \left( I_p \frac{j\omega L_m}{R_s + R_{load} + j\left(\omega L_m + \omega L_{\sigma s} - \frac{1}{\omega C_{res}}\right)} \right)^2 R_{load} \quad (3.13)$$

The power delivered to the load in the situation with resonance is given by figure 3.10.

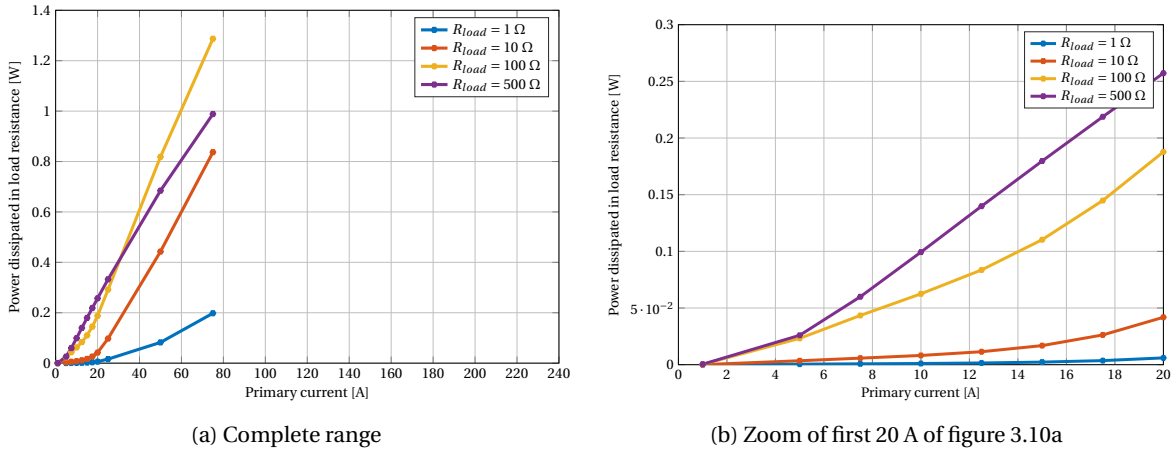


Figure 3.10: Measured power consumed at variable load with series resonance

During the measurement with series resonance the core saturated already at 5 A with almost every load. For deeper saturation the core vibrated and therefore it was decided to not exceed 75 A primary current during the measurement. The output power is for the first 20 A higher than without resonance. However, for higher values this is not true for all load resistance values. After the results of parallel compensation are discussed the results of no resonance are compared with the results of series and parallel resonance.

### 3.2.2. Parallel compensation for reactive currents

Besides series resonance it is also possible to apply parallel resonance. The circuit is given in fig 3.11. The equivalent circuit and the capacitance value for which the reactive impedance is compensated are given in the equations below.

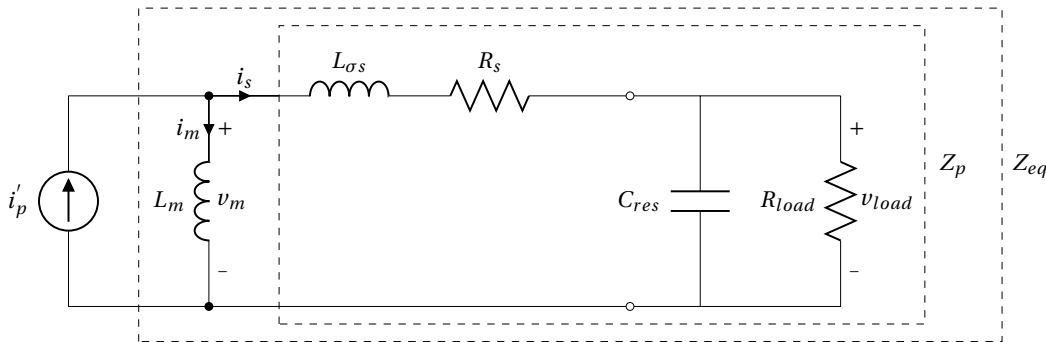


Figure 3.11: Parallel resonance topology

The parallel branch of the impedance in figure 3.11,  $Z_p$  is given in equation 3.14

$$Z_p = \frac{R_s + R_{load} + \omega^2 C_{res}^2 R_{load}^2 R_s + j\omega(L_{\sigma s} + \omega^2 C_{res}^2 R_{load}^2 L_{\sigma s} - C_{res} R_{load}^2)}{\omega^2 C_{res}^2 R_{load}^2 + 1} \quad (3.14)$$

$$Z_{eq} = \frac{Z_p j\omega L_m}{Z_p + j\omega L_m} \quad (3.15)$$

The value for reactive current compensation is given by equation 3.16

$$Z_{sqr t} = -\left(2\omega^2 L_m L_{\sigma s} + 2\omega^2 L_{\sigma}^2\right)^2 + L_m^2 R_{load}^2 \omega^2 - 8\omega^2 L_{\sigma s} R_s (L_m (R_{load} + R_s) + L_{\sigma s} (R_{load} + R_s)) - (2R_{load} R_s + 2R_s^2)^2$$

$$C_{res} = \frac{1}{2} \frac{\omega L_m R_{load} + 2\omega L_{\sigma s} R_{load} - \sqrt{Z_{sqr t}}}{(L_m L_{\sigma s} \omega^2 + L_{\sigma}^2 \omega^2 + R_s^2) \omega R_{load}} \quad (3.16)$$

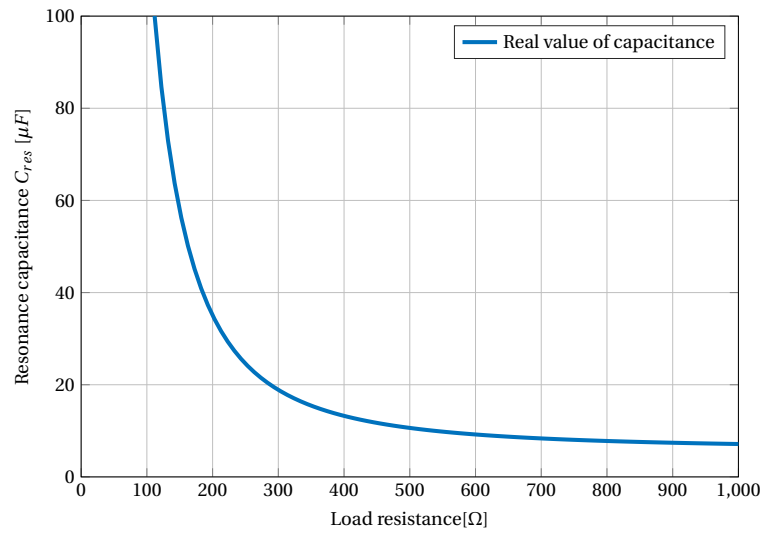


Figure 3.12: Influence of  $R_{load}$  on ideal capacitance value

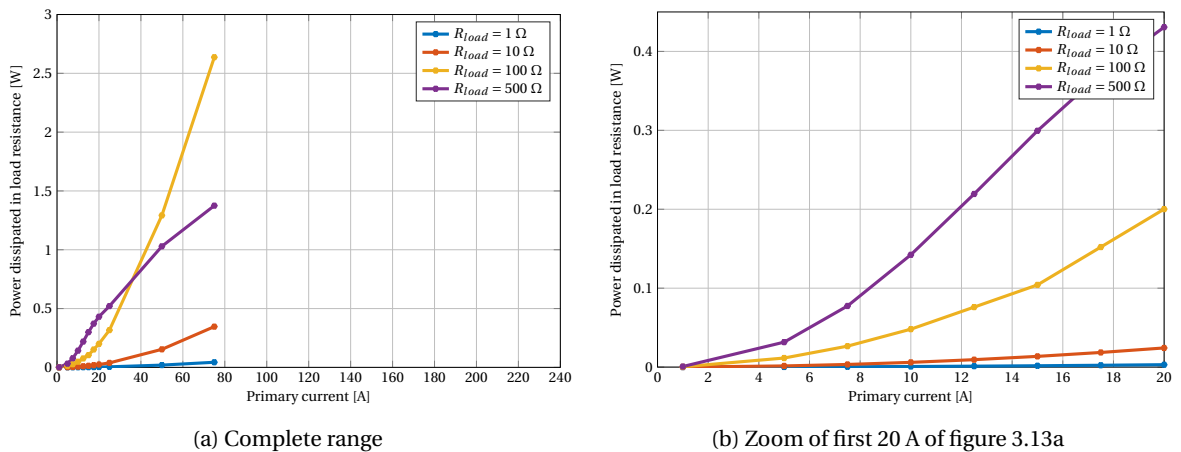


Figure 3.13: Measured power consumed at variable load with parallel resonance

In figure 3.13 the results of the measurement with parallel resonance are included. During the measurement with parallel resonance the core saturated already at 5 A with almost every load. For deeper saturation the core vibrated and therefore it was decided to not exceed 75 A primary current during the measurement.

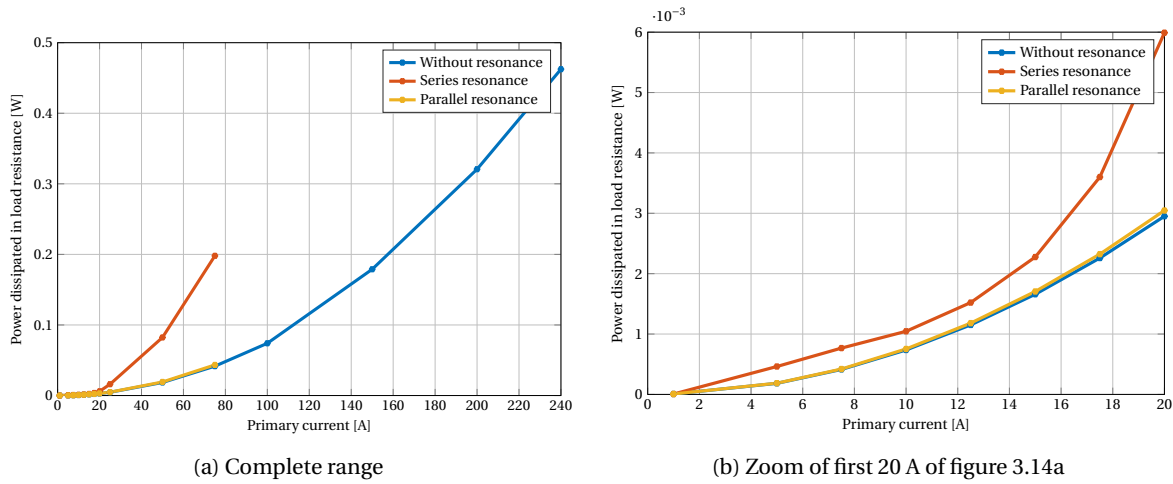


Figure 3.14: Measured power consumed at 1 Ω load resistance without resonance and with series and parallel resonance

In figure 3.14 the extracted load of the three different scenarios is compared. From this figure it is concluded that in case of parallel resonance the advantage of resonance compared with the case without resonance is almost zero. In case of series resonance the extracting capabilities of the CT increased and a clear advantage is observed. The disadvantage is the deep saturation and the influence on the secondary current. Resonance distorted the measurement and the core vibrates at higher primary current.

In figure 3.15 the same comparison is made but in case of a 100 Ω load resistance. Here it is observed that the parallel resonance still has almost no advantage over the situation without resonance. The series resonance is in this case only for the first 15 A better based on energy extraction. In this case the core vibrated as well. Therefore it is concluded that the influence of resonance can increase the energy extracting capabilities but it has the disadvantage of saturation.

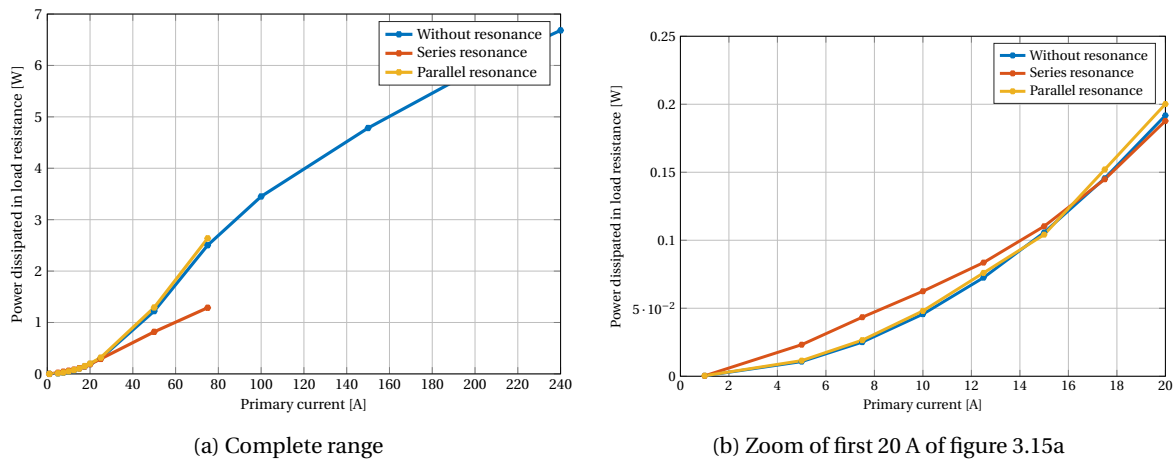


Figure 3.15: Measured power consumed at 100 Ω load resistance without resonance and with series and parallel resonance

### 3.2.3. Alternative configuration for compensation of reactive currents

In the previous simulations and measurements it is observed that the core saturates at low currents. The limiting factor is the saturation characteristic of the core. To overcome this limitation it could be an option to create an air-gap in the cores magnetic path. The results of the inclusion of an air-gap in the cores magnetic path is that the BH-curve has a knee point at higher magnetic field strength  $H$  and therefore the magnetizing current can be bigger before the core saturates.

The introduction of an air-gap has influence on the cores relative permeability and thus on the magnetizing inductance  $L_m$ . The magnetizing inductance becomes much smaller. The problem of this effect is that at the currents at which the core not saturates the output power is lower as well. Therefore it is concluded that

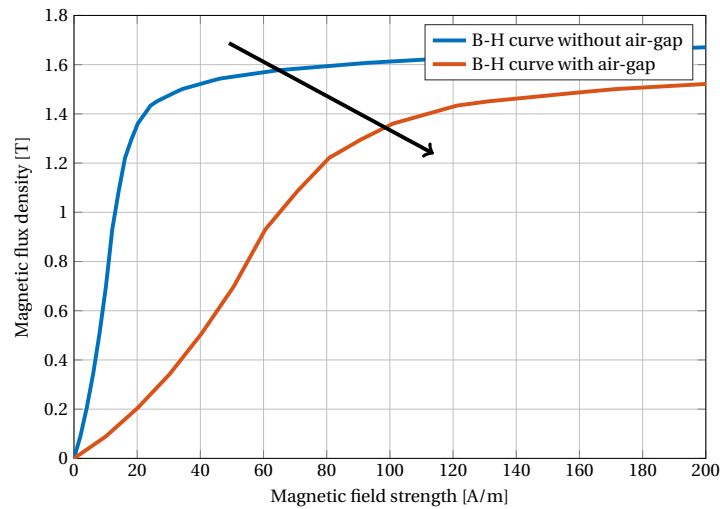


Figure 3.16: Relation output voltage and magnetizing current with and without air-gap

the introduction of an air-gap only shifts the problem of low saturation point.

Another option is to switch between resonance and non-resonance topology as illustrated in figure 3.17. The implementation of the switching strategy is out of the scope of this project and therefore not implemented and investigated. This option also implies switching and the effect of this switching is not known and unsure. In case it has influence on the primary current waveforms. For future research this could be investigated.

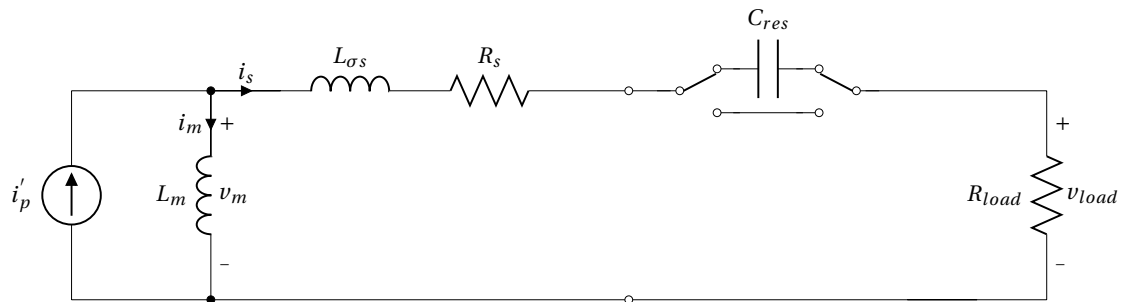


Figure 3.17: Hybrid series resonance topology

### 3.2.4. Conclusion

At low primary current the extracting capabilities of the used CT are limited. The energy extraction can be improved by means of resonance or by increasing the load connected to the CT. The disadvantage of increased energy extraction is the distortion on the measurement. The energy extraction with a series resonance capacitor is much higher but the disadvantage is the quickly saturating core. A possible solution to overcome the saturation is to introduce an air gap in the circuit. By adding the air gap the inductance value decreases and the core refuses to saturate. The energy extraction becomes however less effective with an air gap and therefore this method is not very useful.

Another option is to use a hybrid solution, with other words, switching between a circuit with resonance and without resonance will solve the problem of saturation. There is however a problem in this solution since more components are required and at the starting point it is not known which current is flowing and therefore which part of the circuit should be active. The switching effect is not included as well and the measurement is still distorted by the application of resonance.

Therefore there are possibilities to increase the energy extraction of a CT but they all influence the measurement. Within this project the electronics are selected such that the needed power is reduced but methods of increased energy extraction are left for future projects.

### 3.3. Power conversion

To power the electronics in the self-powered wireless current sensor a power conversion stage is needed. The input of this power conversion stage is the voltage and current coming from the current transformer. The AC source needs to be transformed to a stable DC signal. The power conversion stage is divided into two stages. The first stage of this conversion is the AC/DC conversion. The second stage is to go from uncontrolled DC voltage to a controlled DC voltage.

#### 3.3.1. AC/DC conversion

For the conversion of a AC voltage with a line-frequency of 50 or 60 Hz to a DC voltage rectification of the source is needed. A commonly used method for the rectification is the use of rectifiers with diodes. Rectifiers with diodes convert the input AC voltage into DC in an uncontrolled manner. Due to the characteristics of diodes the power flow is from the input AC to the output DC. The diode rectifier (figure 3.18) rectifies the AC voltage in a successful manner but the output is far from stable/constant DC voltage. In most applications a stable DC voltage with a small ripple is required and to obtain a stable DC voltage a filter capacitor is placed at the output of the rectifier. The unregulated DC voltage will now increase to almost AC peak voltage. The diodes in the rectifier only conduct when the AC voltage is higher than the DC voltage and the forward voltage of the diode (equation 3.17).

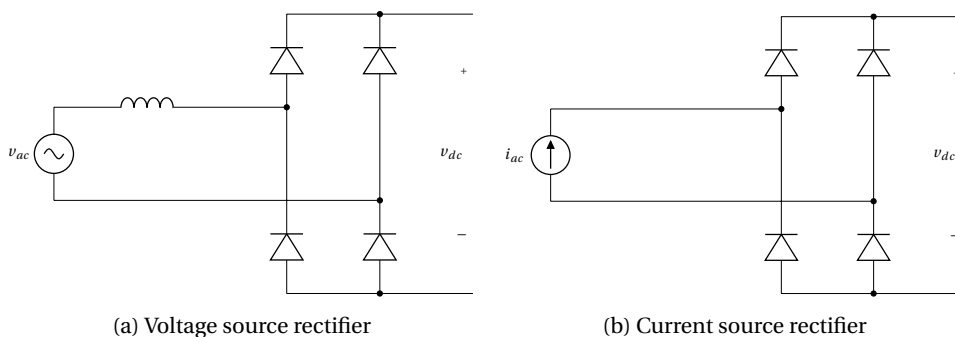


Figure 3.18: Voltage source and current source based rectifiers

$$v_{ac} > v_{dc} + V_f \quad (3.17)$$

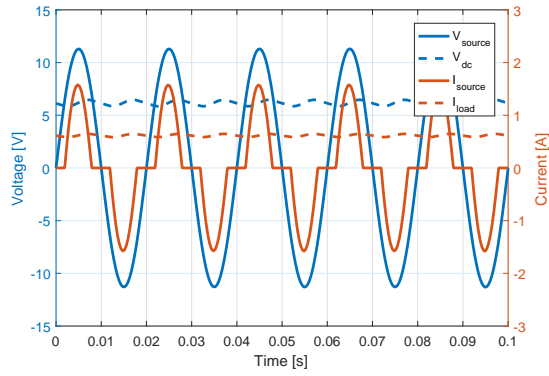
If the DC voltage increases the conduction time becomes shorter and the consumed power is supplied in the period that the diodes conduct. Since the conduction time decreases current peaks occur at the moments the diodes conduct while no current flows when the AC voltage is lower than the DC voltage plus forward voltage of the diodes. These current peaks and zero current moments cause distorted current flow at the AC side.

The distorted current has great influence on the Power Factor (PF) and in the application of a current sensor a distorted current is not acceptable since it influences the measurement. The distortion in the AC current and voltage can have different sources [19]. One of the source of distorted current flow is the filter capacitor at the output of the rectifier. The DC load could play a role as well. In the case of inductive load or in the case of a load with internal DC voltage the AC current is distorted [19]. At the AC side of the rectifier there can also be distortion. Most AC supply source have an internal impedance which is in practice primarily inductive. The effect of this inductive element in the source is called commutation [19] and causes distortion in the supply voltage.

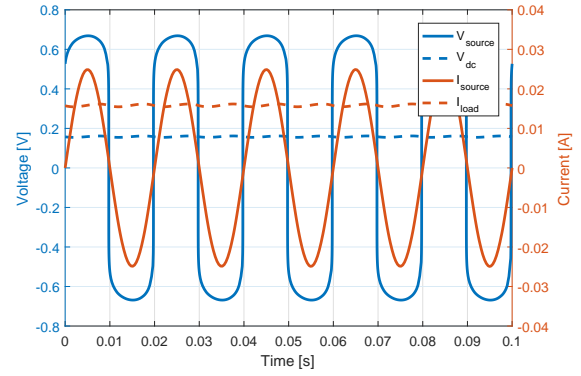
In most studies where rectifiers are considered a AC voltage source is used with a small inductive series impedance. In case of a current transformer (chapter 2 section 2.2.1) the type of source is different. The source has a current character which is equal to a voltage source with a very large series inductive impedance.

In case of rectification there is a big difference between a source with voltage character (figure 3.19a) and the rectification of a source with current character (figure 3.19b). The difference can be explained by the current limiting effect of the rectification in case of a voltage source.

An experiment of the setup used in the above simulation is used in a measurement as well. The same signals are measured and the results is given in figure 3.20. As observed the results of the current source rectification are almost identical to the simulated rectification of the current source.



(a) Waveforms voltage source rectification



(b) Waveforms current source rectification

Figure 3.19: Waveforms of current source and voltage source rectification

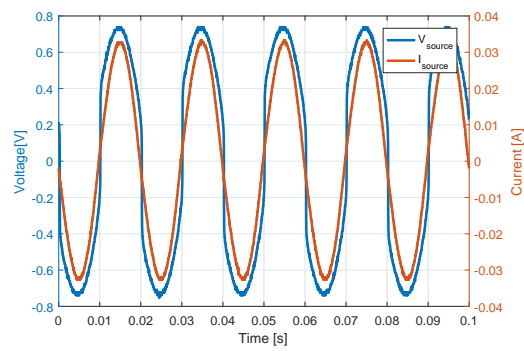


Figure 3.20: Rectification of the output of a CT

One of the key elements is that the current transformer used in this project has a relative low output voltage (0 - 12 volts). The voltage can be higher than 12 volt but the knee-point of the saturation curve is at about 12 volt. If voltages higher than 12 volt are measured the core is saturating which has negative influence on the measurement. If normal diodes are used for rectification there is a significant loss due to the forward voltage drop of the diodes. Diodes with zero forward voltage drop don't exist but Schottky diodes have significant lower forward voltage drop. By using Schottky diodes the AC to DC conversion becomes more efficient.

Even if Schottky diodes are used there is a significant voltage drop due to the diodes. A method to overcome this issue is to use active rectification. Using MOSFETS as switches instead of using diodes has the advantages that the voltage drop is very low if the current is low and that they start conducting in an early stage. The disadvantage is that at some point the voltage drop across the MOSFET becomes higher than the voltage drop of a (Schottky) diode.

The voltage drop across the different elements is given in figure 3.21.

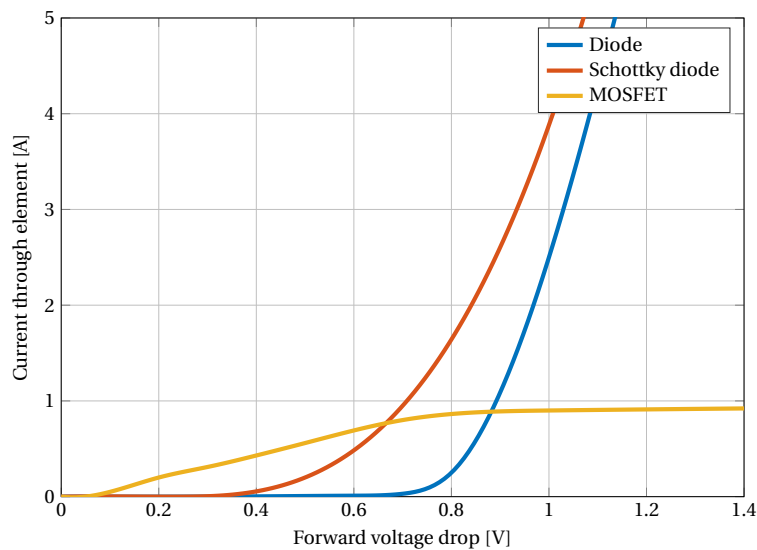


Figure 3.21: Voltage-source character of diode, schottky diode and MosFET

Overcoming the problem of significant voltage drop due to (Schottky) diodes another option is to increase the voltage. If the rectified voltage is too low the voltage could be doubled by a voltage doubler or a Walton-Craft circuit. This is a sort of series rectifier which doubles the voltage with each additional step. Some examples of energy harvester based on current transformers use this principle to increase the voltage at the output of the rectifier (figure 3.22)[22, 26].

There is a big difference in the rectification of a voltage source (normal situation) and the rectification of a current source (case if CT is used). For the current waveform it has positive influence but the ac voltage is distorted in the case of rectification of a current source. The distortion of the current waveform is due to the forward voltage and the unregulated DC voltage behind the rectifier. The diodes start conducting as soon as the AC voltage becomes higher than the unregulated DC voltage plus the forward voltage of the diodes. The voltage is build-up by the magnetizing current. The higher the magnetizing current is the sooner this threshold is reached. Therefore at lower primary currents this phenomena is observed while at higher primary currents this effect is almost not visible.

### 3.3.2. DC/DC conversion

In the previous section about AC to DC conversion the output of the rectifier was unregulated DC voltage. Most electronics however require a stable DC voltage with a maximum allowed voltage ripple. Commonly used DC to DC conversion techniques are linear converters and switching mode converters[19]. Depending on the size and costs and the required efficiency the decision for a linear or switch mode converter is made. The size and efficiency of switch-mode converters are usually higher but these converters use more components, introduce more Electromagnetic interference (EMI) and are complex. Therefore it is application dependant which type converter is used.

#### Linear mode converter

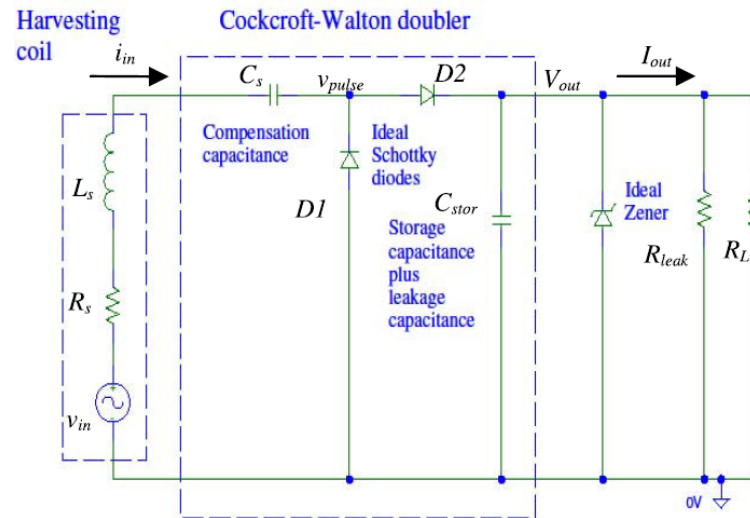


Figure 3.22: Walton-Craft voltage doubler circuit[26]

A linear mode converter is a converter used to maintain a steady output voltage. The input voltage of such a converter needs to be higher than the output voltage. The linear converter changes its internal voltage drop in such a way that the output voltage is at the required level. The difference between input and output voltage is consumed in the linear converter. The voltage drop of such converter is usually in between 0.1 mV and 1 V. The advantage of this type of converters is that it doesn't have switching elements and therefore can obtain a very low output voltage ripple. The main disadvantage is that the voltage difference is consumed in the converter which leads to low efficiencies when input voltage increases. Low-dropout (LDO) regulator can regulate the output voltage even when the input voltage is close to the output voltage. The low voltage drop is usually ranging from in the order of millivolt up to about 300 mV.

$$P_{loss} = (V_{in} - V_{out})I_{out} + (V_{in}I_Q) \quad (3.18)$$

The power dissipated in the voltage regulator is given in equation 3.18. In this equation  $I_Q$  is the current required for the regulation process. Since the minimum input voltage needs to be above the output voltage it is sometimes needed to place a transformer in front of the regulator in order to have the good input voltage.

### Switch mode regulator

Switch-mode regulators are different than linear regulators since they use switching devices like MOSFET or IGBT's for the regulation of the DC voltage. Since these switches are fully on or fully off the losses inside these converters are much lower in comparison with linear regulators. Using storage elements input voltages lower, equal or higher than the output voltage can be converted to a stable output voltage. Depending on the ratio between input and output voltage different types of converters are identified. Up/boost converters, down/buck converters or up-down/buck-boost converters are the three types of converters. Within these three type of converters there are many topologies. A disadvantage of switch-mode regulators over linear regulators are the complexity and the induced EMI due to switching actions. Since they require more components the costs are usually higher of this type of converters. Switch mode converters can be divided into isolated and non-isolated converters. In [19] non-isolated converters like buck, buck-boost, boost, Ćuk and Full-bridge converters are discussed. Isolated converters are derived from these type of converters and in [19] fly-back, forward, push-pull and full-bridge converters are discussed.

In this application the input voltage level can vary between 0 and approximate 12 volts. The required output voltage level is around 3 volts and therefore a buck-boost type topology seems to be the most suitable topology. There are multiple topologies that can convert lower input and higher input to a regulated 3.3 V output. A basic schematic circuit of those converters is given in the following figures. The following topologies are discussed based on their advantages and disadvantages.

By standard DC/DC converters it could happen that the AC waveforms are distorted. Since the AC waveform is used for the measurement it is important that the waveform remains as undistorted as possible. An option to do this is to apply PFC techniques to reduce the harmonic distortion and keep the AC sine wave

undistorted. PFC are there in many different forms and types but most are partly based on the earlier mentioned DC/DC converters. Therefore by choosing the right topology an acceptable converter can be created.

### 3.3.3. PFC techniques

As mentioned AC/DC power converters have a negative influence on the PF at the input of these converters. The influence on the PF is in the application of wireless current sensor with measurement and extraction combined disastrous since a pulsating current wave gives no correct information about the current flowing in the primary side circuit. The problem of low PF of AC/DC power converters is also a problem in power supplies [14]. In [14] different compensating techniques are discussed. In a paper by Singh et al. many of these PFC techniques are discussed [27]. Based on [14] PFC can be classified in active and passive correcting techniques.

Passive power factor correction can be achieved by inserting an LC filter between the AC source and the input of the diode rectifier. This technique is simple but is bulky in size and weight due to the big inductors and capacitors needed for the filter and the power factor cannot be very high [19]. Active power factor correcting approach uses active shaping of the input current to get up to unity power factor. For this a Switch Mode Power Supply (SMPS) techniques is used. These active PFC techniques can be classified as:

1. Pulse Width Modulation (PWM)
2. Resonant
3. Soft switching

Examples of PWM converters are buck, flyback, boost, buck-boost and Ćuk. These converters, if switched at the right moment, all have their own advantages and disadvantages if applied for power factor correcting [14]. The Ćuk converter has the advantage of continuous input current even if converter operates in discontinuous conduction mode and the output voltage can be higher or lower than the instantaneous input voltage. Disadvantages are requirement of an extra inductor and capacitor, the lack of isolation and the increased stress on power devices [14].

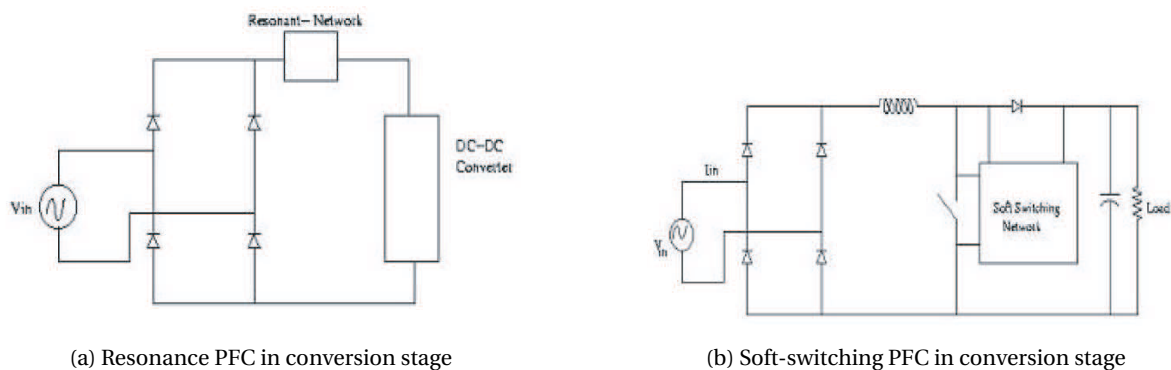


Figure 3.23: Two schematic circuits of PFC techniques

In the resonant converter, the voltage across a switch or the current through a switch is shaped by the resonance of inductor and capacitor to become zero at the time of turned on or off. Thus the switching loss is greatly reduced. The high power factor is achieved by the natural gain-boosting characteristic of the resonant converter. The major drawbacks are higher voltage and current stress on the power switch with respect to PWM mode and variable switching frequency employed [14]. Although the higher stress on the switches this method is used in some applications to improve the PF. A charge-pump PFC converter is described in [23]. A schematic picture of such a converter is provided in figure 3.23a.

The soft-switching PFC technique combines the advantages of PWM mode and resonant mode techniques with an additional resonant network consisting of a resonant inductor, a resonant capacitor and an auxiliary switch. The AC/DC converter operates in PWM mode during most portion of a switching cycle but operates in resonant mode during the switch turn-on and turn-off intervals. As a result, the PFC circuit works at constant switching frequency and the power switch turns on and off at zero current or zero voltage conditions. Thus efficiency and power factor both improved by this technique [14]. In figure 3.23b a basic schematic of the soft-switching circuit is provided. By applying zero-current-switching or zero-voltage-

switching the stress at the switching elements is reduced and PF can be improved. A soft-switching converter with inherent PF improvement is presented in [13].

PFC techniques are currently only available in situations where the power output is in the range of tens of watts and higher. The reason why PFC is not applied in (ultra) lower power converters is the effect of these converters on line currents and their surrounding equipment. PFC techniques and papers about this technique are mostly designed for shaping the current. According to the measurements and simulations on CT rectification the current waveform is only distorted by the forward voltage of the rectifier and the voltage waveform is distorted. In this application the voltage waveform isn't that important and therefore PFC is not applied in this application.

#### **3.3.4. Conclusion**

AC/DC conversion based on a current source is different than a voltage source. A CT has a current character and this has for the rectification in this application a positive influence. In AC/DC conversion with a current source the voltage waveform is distorted while the current waveform is almost not influence. This is also measured with a CT to verify.

For the DC/DC conversion a SMPS is used. The advantage is that the power losses are lower than LDO regulators and depending on the topology the input voltage can be lower, equal or higher than the output voltage. The disadvantage of SMPS is the ripple in the output. The ripple is however adjustable by changing the components of the DC/DC converter.

If the DC/DC conversion stage introduces distortion in the AC current it might be required to use PFC techniques to reduce the influence of the DC/DC converter. In the simulations of this application almost no distortion is noticed so PFC are not used in this application.

# 4

## Network structure

### 4.1. Introduction

At the start of this project no other parts or components exist for a network of self-powered wireless current sensors. To prove that a network of sensors could work together and provided detailed information about the currents in the network, the network topology and the wireless communication protocol are important as well. In this chapter the network topology and the wireless communication protocol are discussed. They have influence on for example the required power extraction level and the ability of providing time synchronization.

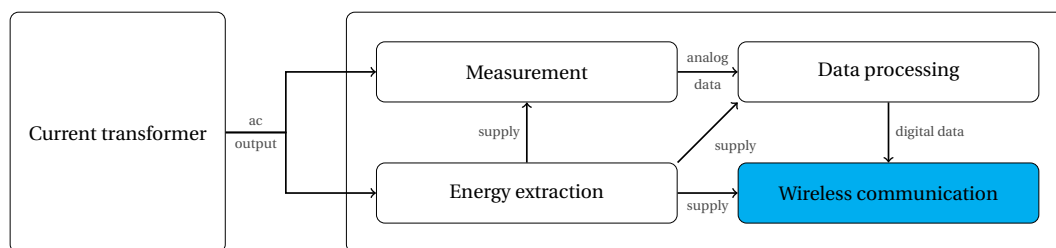


Figure 4.1: Block diagram of sensor, wireless communication and network structure is considered in this chapter

All sensors need to share the same time in order to provide a reference for phase calculations. Power consumption is important because at low primary current the output power of the CT is limited. The network topology is considered in section 4.2. Based on the network topology some communication protocols are discussed in section 4.3. With the selected communication protocol and the topology of the network the synchronization of the nodes is considered and two concepts are tested to proof decent synchronization (section 4.4).

### 4.2. Network topology

Wireless Sensor Network (WSN) can be structured in many ways. Some structures are better for low power consumptions while other structures are cheaper to implement. The network structure can have large impact on required power level and the amount of data that could be send. Since both factors are important for the design of the wireless current sensor, different network structures are reviewed based on power level, implementation cost, and the amount of data that could be send. In this section the location of the gateway and the structure of the nodes with respect to the gateway are discussed. The communication between the different nodes of the network is discussed in section 4.3. There are three structures considered in this section based on the location of the gateway.

#### 4.2.1. Existing gateway far away

A first location one could think of in case of WSN is an existing location at a distance up to a few kilometers away from the sensor nodes. Existing networks in which the wireless sensor nodes could be integrated are the telecom networks (3G, 4G, etc.) or special designed networks for wireless sensors such as LoRaWAN [28].

Since telecom networks are not designed for WSN there is no platform within the network for WSN. The WSN need a telecom chip with a unique number according to the rules of the telecom networks. Those networks are designed for very high data rates and the amount of data that could be transferred is almost unlimited. The cost for this advantage is the high power requirement of this type of network. The frequency at which is communicated is high and since the distance is also large the power requirement is high as well.

To overcome the problem of high power requirement but keep the advantage of large distances that could be covered, recently networks are rolled out specially designed for WSN. These networks, depending on location LoRaWAN [28], are low-power long range networks. Due to the lower radio frequency, the protocol with less overhead and the allowed data rates (1 % of the time may be used for data transmission [28]) the power sensors based on this network require is much lower.

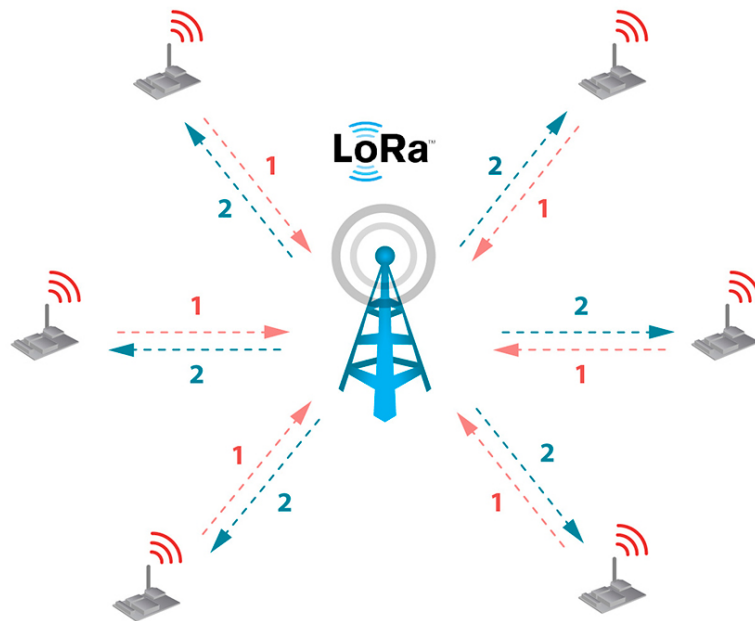


Figure 4.2: Network structure of LoRa network

Since an existing network is used it is in this type of networks not possible to locally connect sensors with each other for local synchronization and data exchange. In case of local synchronization and data exchange a separate network must be implemented.

The main disadvantage of LoRaWAN and Sigfox is however the limited possibility for data transmission. LoRaWAN and Sigfox is designed for sensors nodes that transmit at low update frequency data and the maximum allowable update frequency is once every minute. Therefore this is ideal for sensor nodes that send updates once every hour or a few times a day.

#### 4.2.2. Existing gateway nearby

To overcome the disadvantage of the relative high energy requirement due to distance between sensor node and gateway a structure using an existing gateway close to the sensor nodes. A well known, and widely integrated, network is WiFi. Wireless sensors nodes with a WiFi transceiver connect directly to the Internet via the routers which are in almost every building. This technique has the advantage that it could be installed in every building with WiFi connection available. The drawbacks of WiFi are the relative high power consumption. The main reason for high energy consumption is the network overhead and the frequency which requires more power. Communication between sensor nodes and the synchronization of sensor nodes is limited by the network technology.

Another advantage of this structure over the structure of LoRaWAN, SigFox or telecom network is that it becomes easier to include a concentrator in which information is combined and calculations could be performed.

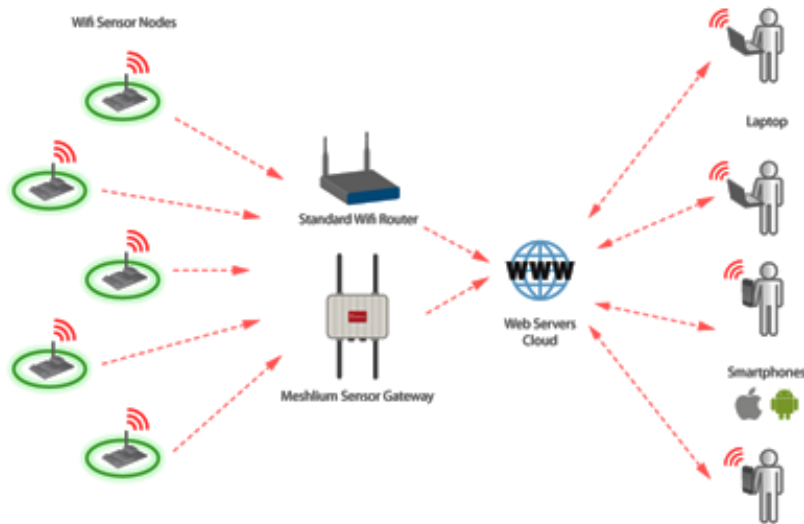


Figure 4.3: Network structure with IP router

### 4.2.3. Custom gateway

Based on the previous to structures using existing gateways a third structure is using a custom gateway. The use of a custom gateway that is specifically designed for wireless current and voltage sensors. Since it is a application specific gateway the implementation of this gateway requires more effort than using an existing gateway. On the other hand, since it is a application specific gateway, they can be placed at the application best position. The distance between gateway and sensor nodes is also free to choose. Based on the type of communication between sensor and gateway and between gateway and Internet of Things (IoT) the location of the gateway is bounded. Since the power requirement of a link increases if the link is longer it is a tradeoff in cost which type of communication is used and where the gateway is placed.

The link between gateway and sensor is free to implement and therefore data rate and amount of data is free to choose. The freedom in the implementation is an advantage for the amount of data that needs to be transmitted and the required power level for the communication. Some example of low power communication are sub 1 GHz communication [20], 6LoWPAN [21] and Zigbee [1].

With this type of gateway it is possible to combine measurements at the gateway. For example, if current sensors, as considered in this thesis, or voltage sensor are combined, information about the power flow is known.

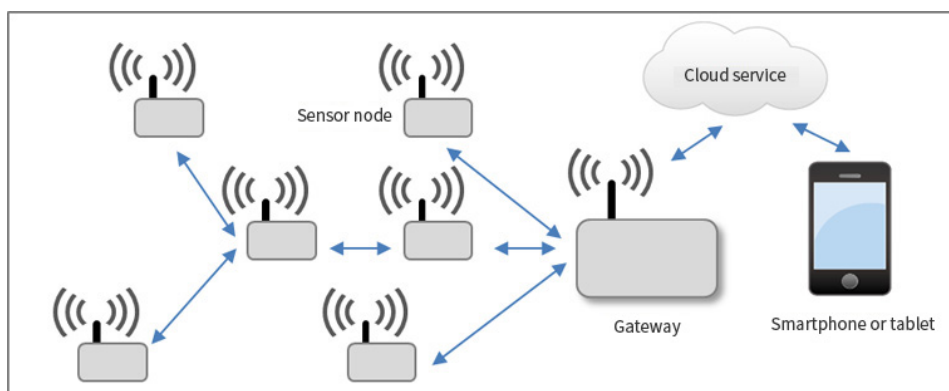


Figure 4.4: Network structure with custom gateway

### 4.2.4. Conclusion

Based on the analysis in this section the discussed network structures are rated. In the analysis different points are considered and based on the analysis a decision is made for a network structure. The required

power level, implementation cost and data rate are important factors for the used network. In table 4.1 a rating is placed based on these factors. In the rating -- is the worst rating and ++ a very good rating. +/- is an average rating.

Network structure	Power	Cost	Data rate
Existing gateway far away	-	+	-
Existing gateway nearby	+/-	++	++
Custom gateway far away	+/-	+/-	+
Custom gateway nearby	++	-	++

Table 4.1: Network structure rating

Within this project the power consumption is a very important parameter. The required power level determines the lower boundary at which the current sensor starts working. The data rate and cost are less important in this application. Another important factor is the flexibility of the solution. The custom gateway nearby is therefore the best solution within this application. This solution gives flexibility and due to this flexibility it is possible to choose the lowest power link and therefore the operating range of the sensor will be biggest.

### 4.3. Communication protocol

In this section the communication protocol in the network is discussed. From the discussion on network topology it was concluded that a gateway nearby and using a custom gateway was best. Therefore the communication protocol is free to choose. Based on power consumption, protocol overhead and data rate some likely candidates are discussed. Based on literature there are three protocols which are commonly used within WSN. As addition these protocols are supported by the same (set of) microcontrollers that is used for this project [33]. The reason for this microcontrollers is mainly based on the power consumption of these chips and the support of all other functions required for this project.

#### 4.3.1. Bluetooth

Bluetooth is already many years a communication protocol used for nearby data transfer. Since bluetooth was started there were some updates on the protocol and the more recent version of bluetooth become more and more feasible for WSN. The newest versions of bluetooth, Bluetooth Low Energy, require less and less power for the communication and therefore this protocol might be used as communication protocol in the WSN of current sensors. The range is limited to a couple of tens of meters and the power level required for the protocol is about 50 mW for sending and receiving messages. The overhead of the protocol is relative high so transceiver needs to be active most of the time. The advantage of BLE is that high data rates are possible with this protocol.

#### 4.3.2. Zigbee

A second protocol that is feasible for a network of wireless current sensors is Zigbee [1]. Zigbee works at 2.4 GHz and has some Zigbee communication stacks for different types of data transfer. The overhead of these communication stacks is rather high but the power requirement for transmitting and receiving data is rather low. Within the platform chosen for this sensor network it is however difficult to implement Zigbee communication. Parts of the source were not available and the program required for the programming is not open source. The range is, same as Bluetooth LE limited to a couple of tens of meters. Data rates are well within the required data rate requirements of this application.

#### 4.3.3. 6LoWPAN

The last communication protocol considered in this thesis is 6LoWPAN [21]. This protocol is, same as with BLE and Zigbee, available at many low power platforms of Texas Instruments. Within 6LoWPAN it is tried to combine the networking strengths of wireless internet protocols like WiFi but at a much lower power level and with less network overhead. 6LoWPAN is a commonly used solution in WSN and combined with an operating system that is also designed to run with small overhead this is a strong competitor with the more well known communication protocols. Contiki, the operating system in which 6LoWPAN is embedded, runs with a very small overhead and has many functions that are useful for wireless sensor networks. Due to the

design concerns at the design of this communication protocol the overhead of this type of communication is low and many methods of communication can be easily implemented. The source code is open source and this has the advantage of being maintained by a large group of people. The biggest disadvantage of 6LoWPAN in combination with Contiki OS is that it is not free of bugs. It is relative new and therefore it still takes some time to run very stable. The advantage is that this communication stack uses the least power and that the data rate is still good. Also the advantage of the type of network structure (IPv6) is an important advantage.

**4.3.4. Conclusion**

Based on the analysis in this section the discussed communication protocols are rated. In the analysis different points are considered and based on the analysis a decision is made for a communication protocol. The required power level, data rate and ease of implementation are important parameters in the decision for a suitable communication protocol. In table 4.2 a rating is placed based on these parameters. In the rating -- is the worst rating and ++ a very good rating. +/- is an average rating.

Communication protocol	Power	Implementation	Data rate
Bluetooth LE	+	+/-	++
Zigbee	+	-	++
6LoWPAN	++	+	++

Table 4.2: Communication protocols rating

Based on the above table the power level and the ease of implementation are the most important parameters in this rating. Based on the rating the decision is made to use 6LoWPAN as communication protocol in this design. The combination of the chosen network topology and the communication structure gives a network that has the structure as given in figure 4.5.

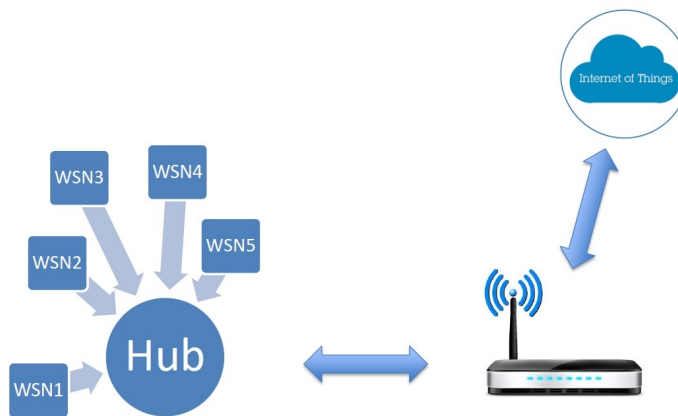


Figure 4.5: Proposed network topology

**4.4. Synchronization of sensor nodes**

There are multiple reasons for sensor nodes to be synchronized. Synchronization of sensor nodes means that all sensors share the same time. The reason for this time sharing is on one hand to be able to timestamp measurements and on the other hand it is possible to reduce radio on-time. Radio transceivers in sensor nodes are often the most energy consuming parts. By synchronizing sensor nodes the on time of the radio can be scheduled which will lead to reduced power requirement.

Synchronization can be, depending on the application, internal or external. With internal time synchronization it is meant that nodes synchronize with each other based on the time of a reference node. External time synchronization means that sensor nodes are not only synchronized with each other but also share the same global time used in the outside world.

With the accuracy of the time synchronization it is meant the time offset between the reference node and any other sensor node. For the wireless current sensor it is important to provide information about the phase

offset with respect to other current sensors of the phase offset or with respect to voltage sensors. The grid frequency is 50 Hz which corresponds with a period of 20 ms. To provide phase information within  $1^\circ$  it is required to have a offset between any of the nodes of maximum 55.5  $\mu\text{s}$ .

To form a clear understanding of synchronization within WSN it is important to have the terminology clear. In the following list some important terms are explained.

- **Clock skew** describes the difference in time shown by the clocks at the different nodes on the network.
- **Clock drift** is the term used for the error in time which occurs due to difference in oscillator frequency. The drift of a clock is a flexible error which depends on temperature [24]. If two sources are perfectly synchronized at the same point they will eventually drift away from each other. For example small differences in oscillator frequency due to temperature lead to this drifting of the clock.

For the transmission of the time in a WSN there are also several delays which contribute to the error between nodes. In the list below these terms are explained.

- **Send time** is the time required at the sender of a message to construct a message.
- **Access time** is the time it takes for the controller to process the message and get access to the wireless channel.
- **Propagation time** is the time it takes for the message to travel from sender to receiver.
- **Receive time** is the time the receiver needs to process the message and to notify the controller a message is received.

Due to the nature of clocks in controllers there is always a some drift in the nodes time. Due to this drift it is required to send a new synchronization message over time. The higher the frequency of this resynchronization beacon the higher the accuracy of the time could be but it takes more overhead in the wireless communication and therefore more power.

For internet connected wireless sensor networks in an early stage Network Time Protocol (NTP) was used. In case of NTP nodes synchronize with NTP servers with accuracy in the order of milliseconds by statistical analysis of the round-trip time. The time servers are synchronized by external time sources such as GPS [24]. With both NTP and GPS the sensor node obtains global time. Since global time is not always a requirement and it is many applications enough to have a local time many techniques and protocols are designed in the past few years. In a survey of time synchronization techniques by Ranganathan and Nygard many different methods such as Timing-sync Protocol for Sensor Networks [11], Lightweight Tree-based Synchronization [36], Flooded Time Sync protocol [18] and Reference Broadcast Scheme are discussed [24]. Other surveys focus more on the problem [9] of time synchronization. Table 4.6 provides the results of a survey on many time synchronization protocols including some common used protocols.

Another type of synchronization is based on schedule based protocols. In these protocols at one of the lowest layers the time is divided into slots. An algorithm is used to synchronize the slots. An example of such a synchronization protocol is TSCH [5]. In the network there is an initiator which divides the channel into slots and each sensor node that is connected to the initiator get its own time-slot. Based on an algorithm the slots are synchronized. An additional advantage is that the sensor nodes only activate their radio during the assigned time-slot. Networks based on TSCH achieve synchronization within 55  $\mu\text{s}$  [5].

#### 4.4.1. Implemented synchronization

As part of the prototype synchronization is implemented on a basic level. There were two methods implemented. One method of synchronization is based on sending a time beacon to all sensor nodes. Time information is added to the message at the operating system level. In the paragraph below the results of this measurement is included. Due to the variable send time, access time and receive time this method is not so accurate. Another method in which the time is slotted and each linked sensor node has its own time-slot (TSCH) is implemented in a very basic way. With this method much better results are obtained.

In a first test IP based communication is used. Two sensors communicate based on UDP with each other. The sender sends a synchronization beacon and just before the operating systems gives the command that something must be send a pin is toggled at the microcontroller. The receiver node toggles a pin once the operating system received the message. Therefore this method of synchronization has a delay which include send time, access time, propagation time and receive time. About 40 samples are taken and the delay between

Time Sync methods	Accuracy	Energy Efficiency	Complexity	Scalability	Fault Tolerance	Byte Alignment
1. RBS	Low, 29.1 $\mu$ s is the average error per hop	High	High	Good	No	Note Handled
2. TPSN	16.9 $\mu$ s per hop	High	Low	Poor	No	Not Handled
3. FTSP	1.48 $\mu$ s per hop	High	High	Average	No	Handled
4. GTSP	Average network wide error, 14 $\mu$ s, Avg. neighbor sync error is 4 $\mu$ s	High	Average	Good	Yes	Not Handled
5. PulseSync	4.4 $\mu$ s (compared to 23.96 $\mu$ s for FTSP between any two nodes)	High	High	Good	No	Unknown
6.All-node	Low	Low	Low	No	No	No
7.Diffusion techniques	Average	Average	High	Good	No	No
8. Mock et.al	High	Low	Low	NA	Yes	Unknown
9 .Ganeriwal [4, 5]	High	Average	Low	Good	Yes	No
10 .Ping	High	High	Low	Good	Yes	Unknown
11.SLTP	High	High	Average	High	No	NA

Figure 4.6: Overview of survey [24]

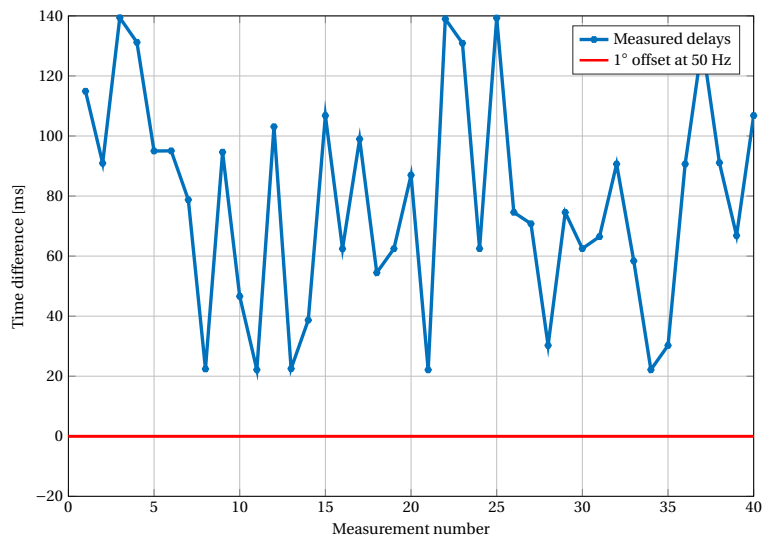


Figure 4.7: Measured delays between initiated beacon transmission and beacon reception

sending and receiving pin toggle was measured using an oscilloscope. Figure 4.7 gives the delays between sender and receiver for the measured samples.

As observed in the figure the delay is rather high and unpredictable. With a mean delay of 78.2 ms and a standard deviation of 35.9 ms this synchronization method is not suitable for time synchronization of the sensor nodes considered in this thesis. The problem with this protocol is not the delay but the high standard deviation. If the delay was more or less constant and had a fixed offset, this method could have worked by compensating for the fixed delay. The delays are long and unpredictable because the send, access and receive time are not fixed and cause unpredictable delays. To minimize the influence of these errors a second implementation is used.

An option to overcome this uncertainty in timing and the large delay that could occur is to add timestamp at lowest possible level in the send and receive process. Therefore the send time and receive time are no longer part of the measured delay. Depending on the implementation of the MAC layer the influence of the access time can be removed as well. The only delay which remains is the propagation delay and since this delay is very small it contributes to the error but the influence is relative small. As discussed, with TSCH it is possible to achieve much smaller offsets between the times of nodes [5].

Within the used OS (contiki) this is recently added but not officially released. With the unreleased code a measurement is performed using time stamping in the MAC layer. To have low power consumption the time is divided into slots based on TSCH.

Figure 4.8 gives the results of a measurement on the delays in case TSCH is used for the synchronization of a node to a initiator. The average delay is 6.2256  $\mu\text{s}$  and the standard deviation is 22.203  $\mu\text{s}$ . Both are within the 1° phase offset or 55.5  $\mu\text{s}$  and therefore TSCH is a suitable option of the synchronization of sender and receiver.

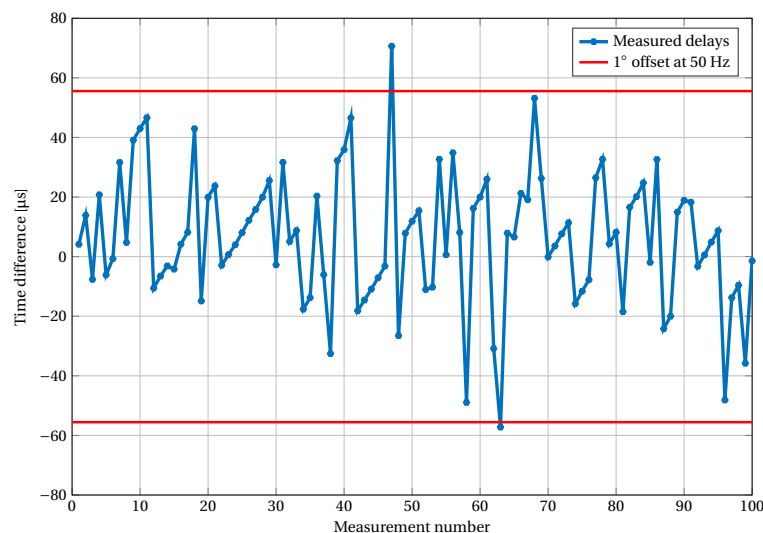


Figure 4.8: Measured delays between time slot initiator and sensor node

From the results of this second measurement one important difference can be noticed. Although it is unlikely, and it looks wrong, it is possible to have negative delays. The main reason for this is the difference in measurement. Since the time is divided into time-slots and the edge toggles at the start of the time-slot it could happen that the sensor node thinks a slots starts before it is actually started. The time difference between sender and receiver is now much smaller. Based on the measurement it is concluded that TSCH, in combination with timestamping at the lowest level, could be used to synchronize the sensor nodes with a initiator of the time-slots. An additional advantage is that it is possible to resynchronize. Since the time is divided into numbered times-slots a sensor node regains synchronism once it regains a time-slot and therefore is synchronized with the initiator.

In figure 4.9 the current wave form and the zero-crossing signal is given. In the bottom half of the figure the time divided into time-slots is given. Based on the time offset between the zero-crossing and the start of the time-slot a measure of the phase is created. The offset between positive and/or negative crossing and the start of a timeslot gives an offset  $t_{zc}$ . This information, if combined with other sensor nodes, could lead to information of the phase difference between signals or the power flow through the conductor.

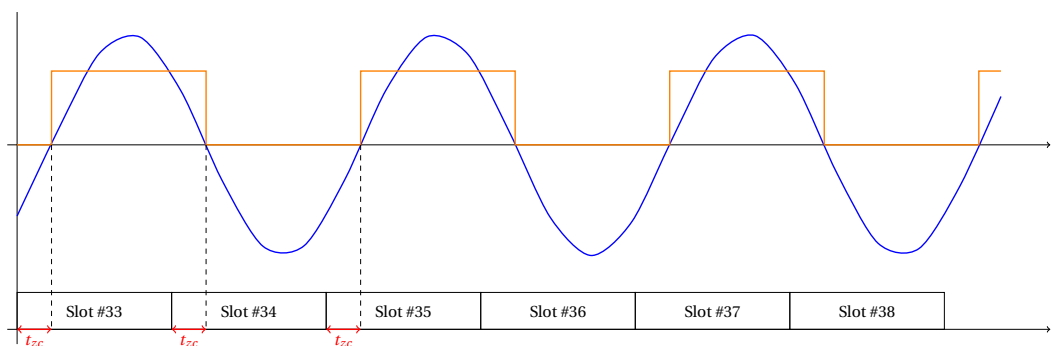


Figure 4.9: TSCH based time slots with current and zero-crossing signals

#### 4.4.2. Conclusion

From measurement in many other papers it can be concluded that it is possible to use TSCH to share a local time among all nodes. The advantage is that this protocol is commonly used for sensor networks cause it reduces the RF on-time. Supported by the measurement with the used platform TSCH can be implemented as synchronization technique. Further research needs to be done to optimize the synchronization of the sensor nodes.

Unlike the synchronization based on a beacon it is with TSCH easier to regain synchronism. Since the synchronization is based on numbered time-slots and the time-slot of the imitator is send to all receivers the sensor node will resynchronize with the initiator as soon as the communication is re-established.

	Mean	Standard deviation
Beaconing	78.2 ms	35.9 ms
TSCH	6.2256 $\mu$ s	22.203 $\mu$ s

Table 4.3: Synchronization results of beaconing and TSCH



# 5

## System integration and model of system

### 5.1. Introduction

With all parts discussed in chapters 2 till 4 the integration of these parts will lead to a final design of the self-powered wireless current sensor. In the combination stage there are some new topics or topics which need some more discussion. These topics, integration of current measurement and the consumption of excess energy, are discussed before the complete system configuration is created. Based on the system configuration a simulation model of the system is created and the results of these simulations are included in this chapter as well.

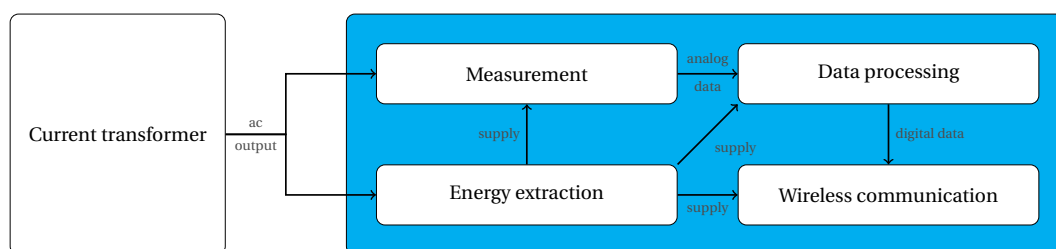


Figure 5.1: Block diagram of sensor, in this chapter the integration of all blocks into a system are considered

The setup of the wireless current sensor which is considered in this chapter is the same as in chapter 1 and given in figure 5.1. The location of each block with respect with each other is considered and finally result in a complete system configuration which is simulated and in the next chapter a prototype design is realized.

### 5.2. Integration

In this section the integration of the measurement and the energy extraction is considered and based on the configuration of the measurement part excess energy consumption is required. Finally this will result in a complete configuration of the sensor.

#### 5.2.1. Measurement

Based on the analysis in chapter 2 a shunt is used to measure the current. In this application it is important to notice that the primary current needs to be measured. The primary conductor however may not be interrupted by the measurement. An additional CT for the measurement, is as already mentioned in chapter 1, not a possibility for this configuration. Therefore the shunt is embedded in the energy extraction circuit. There are two places where the shunt can be placed. Both positions are given by figure 5.2. The shunt and additional circuitry can be placed in the AC path (figure 5.2a) or in the DC path (figure 5.2b).

The advantage of measurement in the DC path is that the voltage across the shunt is only positive which is an advantage for the ADC stage needed for the data processing. Placing a shunt in the AC path has the disadvantage of negative voltages across the shunt and inherent problems by the ADC stage. The disadvantage of a measurement in the DC path is however that there is important information lost about the primary

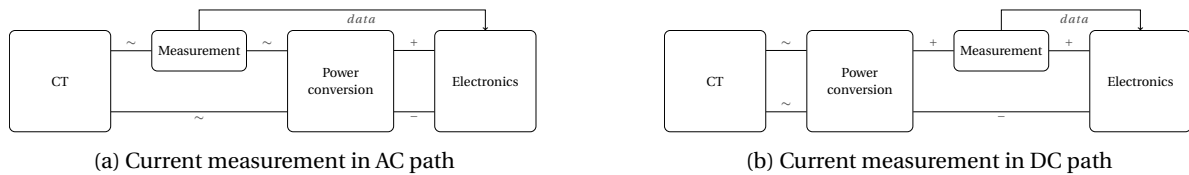


Figure 5.2: Location of current shunt, both in AC and DC path are considered

current. The amplitude can still be measured but it is not possible to measure information about the phase of the signal. Information of the phase of the signal is available if the shunt is placed in the AC path and since information about the phase is a requirement of the measurement the shunt is placed in the AC signal.

AC current measurement in combination with a shunt without additional circuitry is done by lifting one of the sides of the resistor to a certain potential. In figure 5.3 an example of such a circuit is given. In this example one of the sides of the resistor is set to a defined voltage level while the other side floats around this potential based on the current flowing through the resistor. This technique only works if the shunt resistor is isolated from the actual current (in the configuration of figure 5.3 by means of a CT). The DC reference voltage (3.3 V in figure 5.3) used for lifting the potential needs to be isolated from the AC current as well to successfully lift the potential.

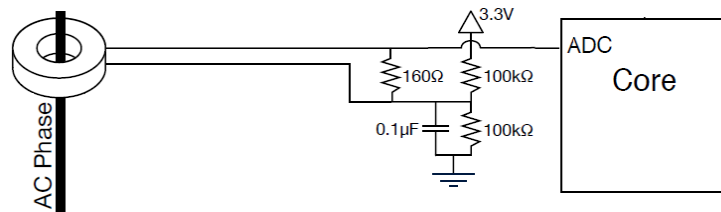


Figure 5.3: Lifting potential for ADC measurement of AC current

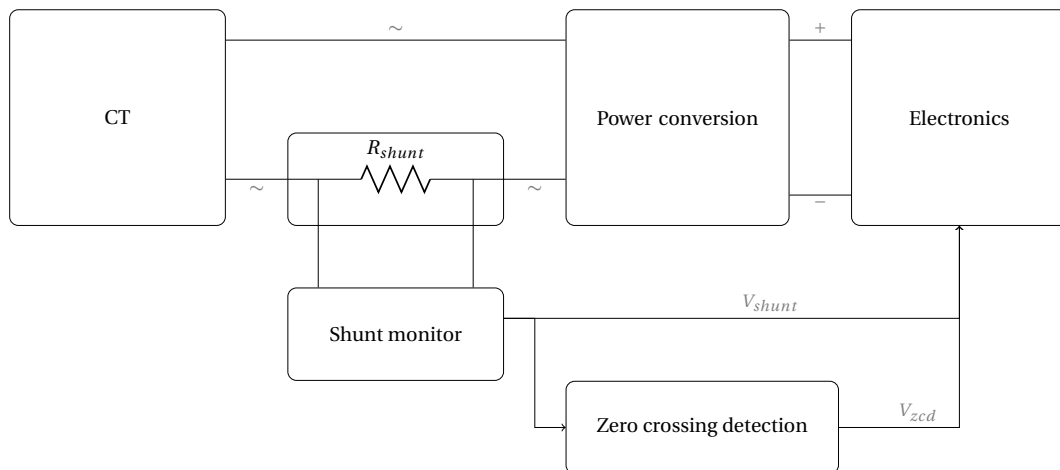


Figure 5.4: Block diagram of sensor with more details on measurement subsystem

During this project three methods that could solve the isolation problem are identified.

- Isolation of shunt by means of a transformer
- Isolation of DC voltage
- Use an isolated differential amplifier

In case of isolation of the shunt my means of a transformer in the AC path a transformer is placed and on the secondary side the shunt is placed. The situation is similar to the case in which a CT is connected to the

primary conductor. Although the dimensions of the transformer are smaller the measurement is less accurate than the case in which a second CT is used. This method is not further considered because the disadvantages of inserting a transformer are too big.

Providing isolation in the DC/DC conversion stage can also provide the isolation between the AC and DC domain. This isolation could make it possible to use the potential lifting principle of figure 5.3 again. The isolation by means of an isolated DC/DC converter is not considered in the rest of this project because it is most likely that it adds costs and increases the size. This method is not tested by means of simulation and measurement and therefore it is not sure if this method works.

The last method of isolation is to use a differential amplifier with isolation. Differential amplifiers are commonly used for current measurement applications with a shunt. An isolation stage for the two shunt signals is placed between the shunt and the differential amplifier. The differential amplifier (figure 5.5) has an output voltage given by equation 5.1.

$$V_{out} = \frac{R_2}{R_1} (V_2 - V_1) + V_{ref} \tag{5.1}$$

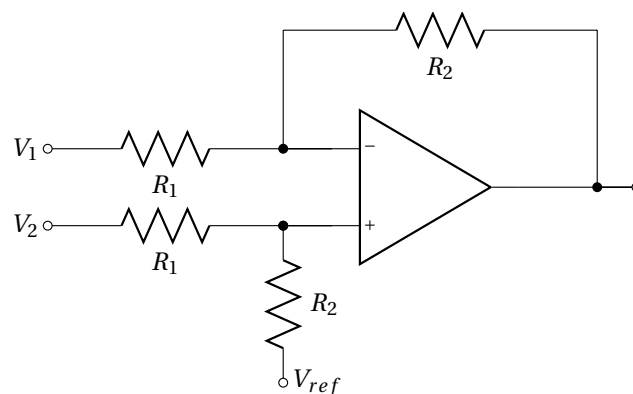


Figure 5.5: Differential amplifier with reference voltage

There are differential amplifiers with input isolation available on the market and such a device is used in this project to monitor the shunt and provide input for the ADC stage. The INA282 [31] of Texas Instruments (schematic of device in figure 5.6) uses a series of laser trimmed capacitors to provide isolation between the shunt and the differential amplifier.

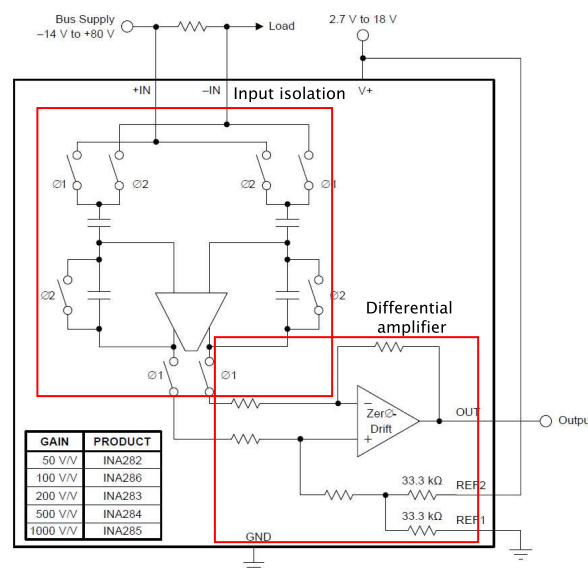


Figure 5.6: Schematic picture of INA282 which is used for monitoring the shunt

For the current sensor the amplitude and the phase information are important. The output of the shunt monitor provides information for the ADC and is used to obtain amplitude information. Phase information can be obtained in software or using a piece of hardware.

In this application the phase information is retrieved from the shunt monitors output. A comparator is used to detect whether the current is above or below a threshold. The threshold for this detection is based on the reference voltage of the shunt monitor. The output of this zero-crossing detection is a square wave signal which is high if the current is above the threshold. If the output of the shunt monitor is below the threshold, the output of the zero-crossing detection is low.

### 5.2.2. Excess energy consumption

In the system configuration considered in this project the shunt for the current measurement is placed in the AC path. In order to related the measured voltage drop across the shunt to the primary current, the measured current multiplied by the turns ratio of the CT should be equal to the primary current. The electronics need a relative constant amount of current. If the available current exceeds the current requirement of the electronics not all current will flow through the shunt.

If the power requirement of the electronics is considered to be constant, the filter capacitor at the DC side of the rectifier will be charged to an increased level as long as the demand is lower than the available current. The current transformer has to produce a increased voltage and this requires a higher magnetizing current. At some point the current transformer saturates and the CT is not able to charge the capacitor anymore. At this point only the current needed for the electronics is flowing through the shunt.

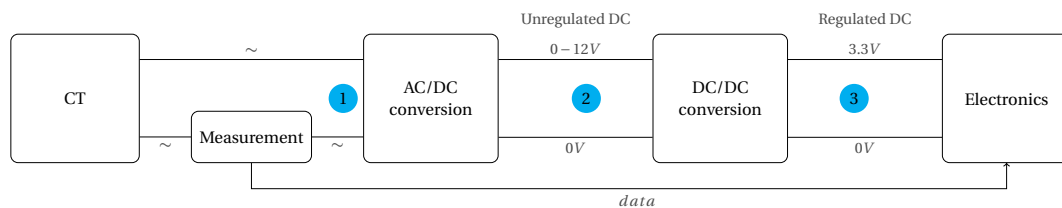


Figure 5.7: Block diagram of sensor with more details on energy extraction and subsystem and the location of excess energy consumption

To prevent an increased voltage of the unregulated DC voltage adaptive power consumption is required. Adaptive power consumption means that the excess energy is consumed. The electronics placed behind the shunt ask for the amount of current that is available from the CT. In figure 5.7 the block diagram of the sensor is given and in the diagram three locations are marked. At the different location the excess energy can be consumed.

1. Between shunt and AC/DC conversion
2. At the unregulated DC level
3. At the regulated DC level

In this project the excess energy is consumed in for example a resistor but the energy can be used for other purposes as well. The excess energy can for example be used to charge a battery or to light the room the sensor is placed in. It must be noted that this is not a stable and fixed supply. Therefore it is only possible to use this source for loads that don't require a stable supply.

The first location identified in figure 5.7 is between the shunt and the AC/DC conversion. At this point the current and voltages are AC. Both other locations are DC. A second location of excess energy consumption is to place the variable load between the AC/DC conversion stage and the DC/DC conversion stage. By consuming energy at the unregulated DC level the voltage is bounded. The last method is based on consumption on the 3.3V level.

The advantage of position 1 over positions 2 and 3 is that the AC/DC conversion and DC/DC conversion can be rated on the current requirement of the electronics. The reason for this is that the excess energy is consumed before these conversion stages and therefore the current will not flow through these stages. The disadvantage of position 1 over positions 2 and 3 is that the excess energy consumption is close to the shunt and therefore it is more likely that the measurement is distorted by the consumption of the excess energy. Based on disturbance reduction location 3 is the best.

Based on the advantages and disadvantages location 2 is used for the excess energy consumption. The most important reason is the lower rating of the DC/DC conversion stage which is possible using this location and the AC/DC conversion stage is between the excess energy consumption and the location of the shunt.

The excess energy can be consumed in a passive and an active way. The passive method uses, for example, a zener diode to consume the excess energy in case the unregulated DC voltage becomes higher than the threshold value of the zener diode. The advantage of this method of excess energy consumption is that it is passive and therefore better less likely to fail than active consumption. A second method of excess energy consumption is to use active components. A switch in series with a resistor could be used to consume the excess energy in that case.

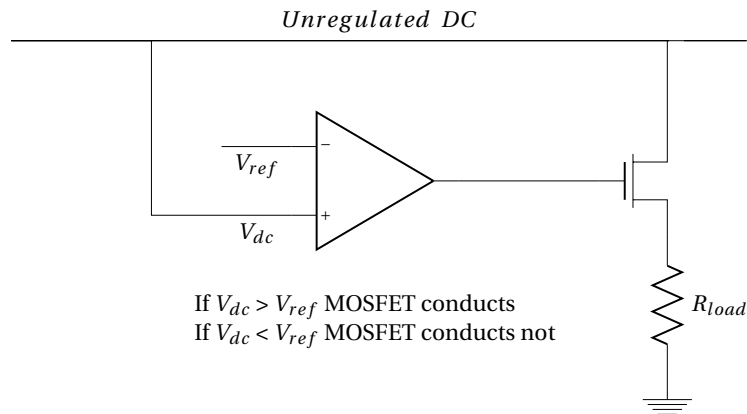


Figure 5.8: Circuit used for the excess energy consumption

As excess energy consumption system a voltage monitor is implemented. A comparator with hysteresis monitors the voltage level of the unregulated DC. If the unregulated DC voltage goes above a the upper threshold the MOSFET of figure 5.8 start conducting and the dump resistor is connected to the unregulated DC voltage. Once the voltage level is below the threshold the MOSFET stops conducting and the dump resistor is disconnected from the DC bus. In figure 5.8 a simplified circuit is given. The excess energy consumption system is designed in a way that it is almost continuous consuming excess energy if the maximum primary current is flowing. This control circuit controls the dump of excess energy. Therefore the unregulated DC voltage is kept at an acceptable level. Since the capacitor is never fully charged and the CT is capable of generating the unregulated DC voltage, the current flow through the shunt is almost the full available current from the CT

### 5.2.3. Complete configuration of sensor

If the current measurement, the power conversion and the excess energy consumption are combined the configuration is given by figure 5.9. This block diagram gives the location of each part and the link with the other parts. If this figure is compared with the block diagram at the beginning of this chapter (figure 5.1) the measurement stage is implemented by a shunt in combination with a shunt monitor and for the phase information a zero-crossing detection circuit. The energy extraction is implemented using the AC/DC conversion and the DC/DC conversion as well as the excess energy consumption. The data processing and the wireless communications is covered by the block electronics in figure 5.9.

The electronics that cover the data process and the wireless communication is done by a processor of Texas Instrument. The CC2630 [32] is a ultra-low power microcontroller with internal radio transceiver. This microcontroller uses ultra-low energy levels and only the addition of an antenna is needed to implement the wireless communication stage. Based on these components a simulation model is created to model the behavior of the sensor. This model is explained in more detail in section 5.3.

## 5.3. Simulation model of current sensor

The system model is created in LT Spice. LT Spice is a program for circuit simulation and consists of detailed libraries of components. The model is based on the different parts which can be identified from the detailed block diagram (figure 5.9). In appendix B the complete model is given. In this section the different parts that can be identified are described shortly.

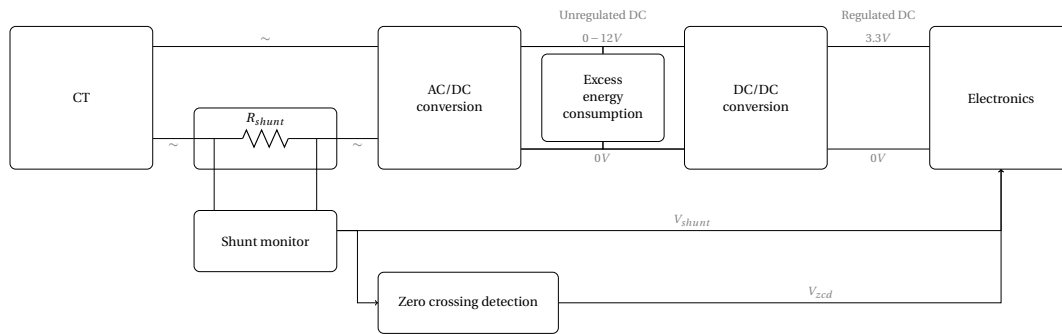


Figure 5.9: Detailed block diagram of the self-powered wireless current sensor

- The CT is simulated using the equivalent circuit derived in chapter 2 (figure 2.5). The used equivalent circuit is only accurate if the core does not saturate. However, saturation will never occur within the specified operating range. The excess energy consumption circuit works as a variable load. The output voltage will not be higher than about 5 V. Since the saturation knee-point is at about 12 V, saturation will not occur. Only in case of a failing excess energy consumption the voltage can be higher than 5 V.
- The power conversion stage is simulated using an energy harvesting chip (LTC3588 [17]) of which a detailed model was available in LT Spice. The LTC3588 integrates a low-loss full-wave rectifier. The chip also has an internal, high efficiency, buck converter with selectable output voltage. The advantage of this chip is the minimum amount of additional components needed for integration in the system. The chip forms a complete energy extraction solution. The chip has also the ability to connect a filter capacitor between the rectifier and the buck converter. This unregulated DC output is used in this setup as buffer and to consume the excess energy.
- The electronics used for the data processing and wireless transmission of data is modeled as a constant load. The magnitude of the load is defined based on the expected current consumption of the electronics. The expected current consumption is only in the microcontroller since the rest of the components are separately included in the model. If the microcontroller is active, uses radio transceiver and some other modules the current requirement is about 16.5 mA. Since the voltage is 3.3 V the load is modeled by a 200  $\Omega$  resistance.
- A spice model of the INA282 [31] is used for the current measurement. The shunt used in the simulation model is a 39 m $\Omega$  resistor. The two terminals of the resistor are connected to the input of the shunt monitor. The supply and ground are connected supply pins and reference pins to get a measurement around half supply voltage (1.65 V).
- For the zero-crossing detection a comparator is used. The LTC1540 [16] is a ultra low power comparator with internal reference. The resistor needed for scaling input are selected to detect a level of 1.65 V. This is the zero current output level of the shunt monitor. The output of the zero-crossing detecting is high in case of current levels above zero, and low in case of current levels below zero. In the electronics a pin is triggered on the rising and falling edges of this signal to detect the zero-crossings.
- The excess energy consumption is implemented by a comparator which is used to turn on a MOSFET. The MOSFET is in series with a power resistor used to consume the excess energy. A hysteresis band is set to prevent excessive switching. The comparator used in this application is the LTC1540 [16].

In the model a few signals are observed. The output of the shunt monitor, the output of the zero-crossing detection and the input current which is set are observed. The simulation results are discussed in the next section (section 5.4).

## 5.4. Simulation results

Based on the model described in section 5.3 multiple simulations are executed to simulated the behavior of the system at different primary current value. The primary current is used as input variable and with these varying input multiple signals are measured and captured. The measured and captured signals are listed below.

- ADC signal to input of microcontroller
- Zero-crossing detection signal to input of microcontroller
- Unregulated DC voltage level
- Regulated DC voltage level
- Source current

The simulated source current is set at 5 %, 10 %, 20 %, 100 % and 120 % of the rated current (200 A). Based on the Root Mean Square (RMS) value of the source current, the output of the shunt monitor, and the relation between shunt monitor output and secondary current, the ratio error is calculated. In table 5.1 the results of the measurement and the calculations is given. In figure 5.10 the plot of ratio error and percentage rated current is given.

% rated current [%]	Theoretical current [A]	Simulated current [A]	Measured current [A]	ratio error [%]
5	10	9.997	9.230	-7.67
10	20	20.004	19.876	-0.64
20	40	39.995	39.915	-0.20
100	200	199.874	200.830	0.48
120	240	239.637	240.554	0.38

Table 5.1: Ratio error based on complete system simulation

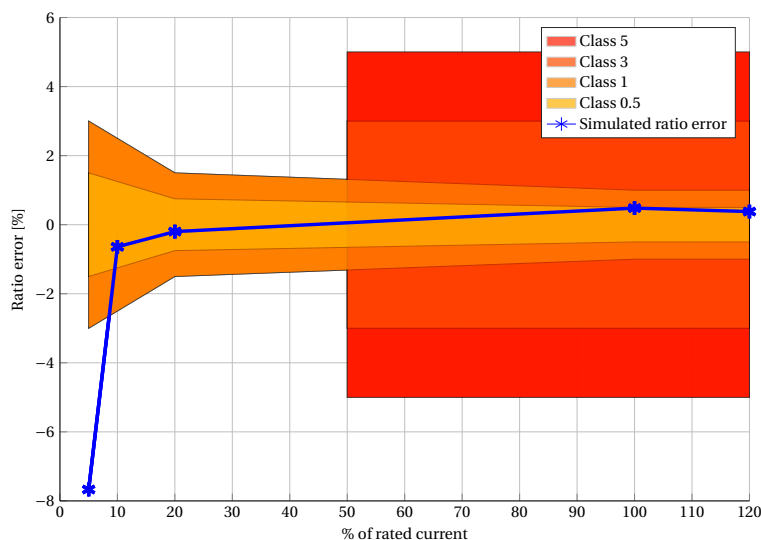


Figure 5.10: Ratio error based on simulation results

In figure 5.11 the signals from the simulation at 100 % rated current are given. The unregulated DC voltage varies with a certain ripple. This ripple is due to the hysteresis band set to the voltage level comparator of the excess energy consumption implementation. The output of the buck-converter gives a much more stable DC voltage which is used to power all electronic components in the system. From figure 5.11 it is also observed that the zero-crossing detection system provides a square wave output used to detect the zero-crossings of the primary current.

Based on the simulation results it is concluded that for almost the complete targeted range the system is within the targeted class 1 accuracy class. Only for the lower boundary the measurement is not accurate enough to meet the requirement of the accuracy class 1. The measurement is within class 3 of the IEC61869-2 standard. The main reason that at 5 % the measurement is not accurate enough is that the CT is not able to supply the electronics without influencing the measurement. Increasing the core size of the CT might solve this problem.

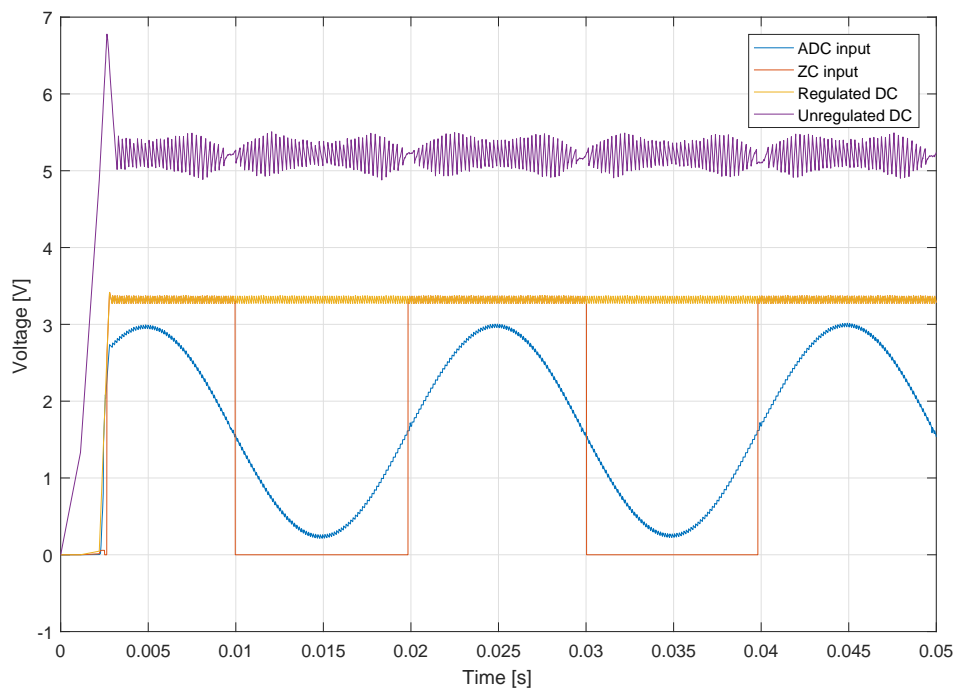


Figure 5.11: Simulated ADC input, zero-crossing input and DC voltage levels at 100% rated current

# 6

## Design and measurement results

### 6.1. Introduction

Based on the model of the system (chapter 5) a prototype is designed. Before the start of this project no sensor node as well as a concentrator node exist. Therefore a minimalistic implementation of a concentrator node is included in this chapter. Based on the design of the sensor node and the concentrator node, measurements are taken in order to check if the sensor node is working correctly.

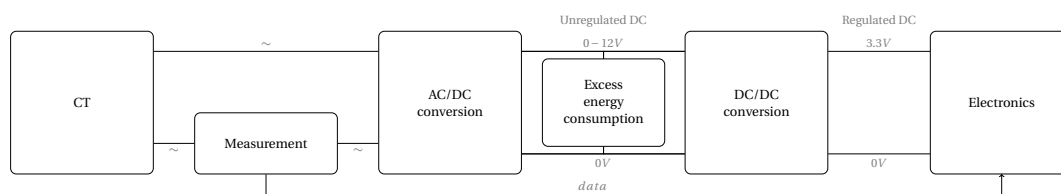


Figure 6.1: Detailed block diagram of the self-powered wireless current sensor

Section 6.2 starts with the design of the sensor node based on the block diagram of figure 6.1. Section 6.3 describes the basic implementation of the concentrator followed by the results of the measurements in section 6.4.

### 6.2. Sensor node

In this section the prototype design of the self-powered wireless current sensor is discussed. This section is divided into the hardware design and the software design. The prototype is based on the block diagram of figure 6.1. In chapter 5 this block diagram is discussed in more detail and based on the simulation model created in that chapter, the prototype is designed.

#### 6.2.1. Hardware design

For the design of the prototype a PCB is designed. One of the requirements of the sensor node was to minimize the additional space required for the PCBs. The electronics can be placed most easily on the bottom of the transformer. The bottom side of the TQ40-c is about 40 mm squared and to fit the PCB inside the existing housing the size of the PCB is chosen to be squared 35 mm. Using this dimensions it is possible to place the PCB on the bottom side of the existing housing and the final adjustment to the housing is bounded to a small increase in depth of the TQ40-c.

With this PCB area it is not possible to make a design in which all parts fit on the PCB area. It is therefore decided to split the design into two parts. The first PCB contains the power conversion stage. This PCB has three connectors on it. The first connector is used to connect the current transformer AC output to the PCB. The second connector connects to the second board and is used to place the shunt near the shunt monitor, which is on the other PCB. The third connector is used for the power supply connection of the second board (0V and 3.3V).

The second PCB contains a PCB antenna, the microcontroller, the current shunt monitor, the shunt and the electronics needed for the zero-crossing-detection. The main reason to split the design was the size constraint. Splitting the power conversion from the measurement and data processing has the advantage of splitting the sensitive parts (microcontroller and measurement) from the possible noise sources (power conversions and excess energy consumption).

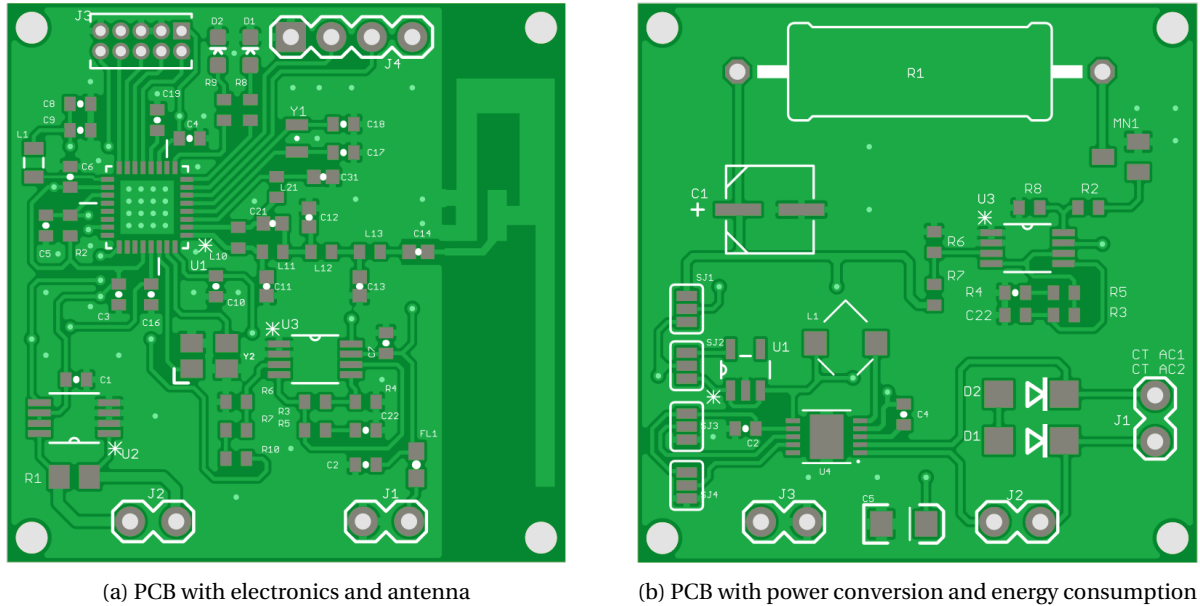


Figure 6.2: Designed PCBs for the sensor node

The designs of both PCBs are given in figure 6.2. On the left side (figure 6.2a) the PCB with measurement components as well as the microcontroller and the PCB antenna. The other PCB (figure 6.2b) includes the AC/DC conversion stage, the DC/DC conversion and the consumption of the excess energy. The boards are connected by each other via 4 connections at the bottom of the figures. The full design including schematic, board layout and Bill of material (BOM) is included in appendix C.

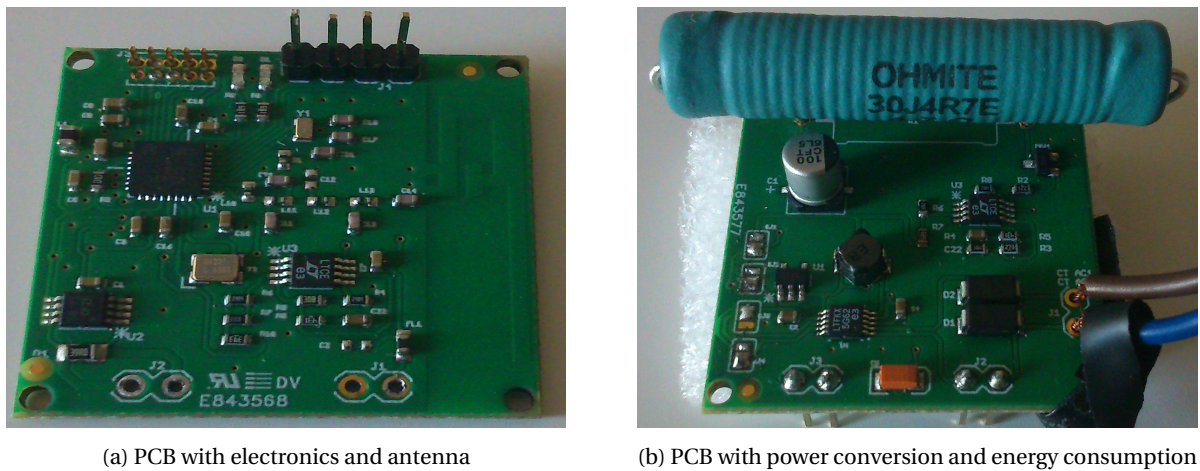


Figure 6.3: PCBs for the sensor node

In figure 6.3 a picture of the PCBs is given. The design of this first PCB contained a minor problem. According to the simulations all selected components had the correct rating but during the test and verification of the PCB it was found that the energy harvesting chip was not able to rectify all the current. For the measurement an external rectifier was connected to have full and correct functionality of the power conversion PCB.

On the other board a wrong component is placed by the company that manufactured the PCB. The shunt value soldered on the board is a thousand times bigger than it should be ( $39\ \Omega$  instead of  $39\ \text{m}\Omega$ ).

A last issue with the electronics board is with the JTAG debugger. The used debugger does not recognize the microcontroller. Help from the manufacturer did not solve the problem so far.

### 6.2.2. Software design

The software running on the concentrator node is divided into a few tasks running with the Contiki OS as operating system. Although certain parts are within the source of the operating system the tasks as below can be identified. Some of these tasks are combined in the source.

- ADC sampling
- Minimum, maximum and average RMS value calculated
- Zero-crossing time offset calculation
- Synchronization with concentrator (TSCH slave operation)
- Data transmission (sending to concentrator)

The ADC sampling task converts the signal from the shunt monitor into digital values. The 50 Hz signal is sampled with a frequency of 800 Hz. The 800 samples that are taken are divided into blocks of 40 samples and the RMS value is calculated. From the 20 RMS values per second the minimum, maximum and average value is send to the concentrator.

The process of taken the analog samples and the calculation of the RMS values is divided into two tasks to minimize the effect of computational delays on the sampling and calculation.

For the zero-crossing detection the difference between the start of a time-slot and a zero-crossing is measured and this time is send to the concentrator as well. Based on the differences of this time the phase of the current can be compared with other sensor nodes and phase information is derived. The zero-crossing detection is based on a interrupt routine which is trigger at both rising and falling edges in order to detect if the current is in the positive part of the sine wave or in the negative part of the sine wave.

For the transmission of data a task is defined and this task sends every second the minimum, maximum and average RMS value of that second to the concentrator. The transmission of data is started as soon as the sensor node is coupled with the concentrator and the TSCH is initialized.

## 6.3. Concentrator

For the concentrator a minimalistic implementation is created within this project. For the concentrator node no PCB is designed. The concentrator node is used as an interface between the sensor nodes and the IoT. In this section the hardware design and the software design are discussed.

The communication between the sensor nodes is based on 6LoWPAN and the concentrator receives average, minimum and maximum values of each sensor node and information of the zero-crossing with respect to a reference time send from the concentrator. Every sensor node sends every second measured data to the concentrator. The concentrator, in this basic implementation, averages the current value and send an update to thingspeak.com every minute. The same yields for minimum, maximum and phase information.

### 6.3.1. Hardware design

The minimalistic implementation of the concentrator node consists of a CC2650 launchpad which has the same radio as the sensor nodes. The connection of the concentrator with the internet is done by a ESP8266 WiFi module. The availability and the functionality of these components resulted in a concentrator that can be used to connect the sensor nodes with the IoT.

In figure 6.4 the concentrator node is given. This minimalistic implementation of the concentrator consist of a CC2650 launchpad. A WiFi module is connected to the board to get a connection with the IoT.

### 6.3.2. Software design

The software running on the concentrator node is divided into a few tasks running with the Contiki OS as operating system. Although certain parts are within the source of the operating system the tasks as below can be identified.



Figure 6.4: Concentrator node with CC2650 launchpad and ESP8266 WiFi module

- Data receiving from sensor nodes
- Synchronization of nodes (TSCH initiator)
- Data processing of sensor nodes data
- Data transfer to IoT

The concentrator has a task to interact with other nodes. This task configures the TSCH scheduling. Once the synchronization of a node with the concentrator is established, the sensor node send a connection request to check if the communication link is ready to use. Theoretically the communication link should work but from some tests it became clear that the first few packages were lost.

Once the communication link is checked the sensor node will start sending data and the concentrator receives the data and after the first reception it will trigger a task every minute to send the received data to the IoT. In this first prototype and minimalistic implementation of the concentrator it is not implemented to support multiple current and/or voltage sensors. The platform supports the link with multiple nodes and therefore it is advised for future project to expand the functionalities of the concentrator to support multiple nodes.

## 6.4. Results of measurement

With the designed prototype some measurement were taken to check the operation of the sensor. The most important measurement was to relate the output of the sensor with the actual current in order to give an indication of the accuracy. Also the spreading on the measurement results, in this case a minimum and maximum value during the sampled period were used.

Unfortunately it was not possible to use the designed PCB for the measurement. The production of the PCB took longer than expected and due to some minor errors (subsection 6.2.1) the designed PCB could not be used. Since the small mistakes were identified it was possible to make some small modifications on the concept demonstrator on breadboard to do the measurement. With the small modifications it was possible to measure the complete targeted range of currents (10 A to 240 A).

Also the software as described in section 6.2 was slightly modified. Due to time constraints it is so far not possible to integrate all developed parts together. Therefore it was decided to use a version of the software only processing the measurement instead of including the wireless transmission.

For the measurement on the accuracy the sensor node is not connected wireless to a concentrator but all calculations are performed on the sensor node. The data is sent to a PC with a UART connection. The sensor samples the current with 800 samples per second to calculate the RMS value and sends an average, minimum and maximum value every minute. The wireless link is removed from the setup due to software issues which

were not completely solved in time. Since all separate parts work, the decision was made to take the sensor readings out of the sensor using a UART connection.

The CT was connected to a cable that carries an adjustable current. The current value is adjustable and the current flowing through the conductor is measured by a CT with digital display as reference. The CT with digital display has a resolution of 2 A and therefore the reference current is not very accurate. In the lower current region it was possible to do the measurement with an adjustable current source and these readings had a much more accurate current reading.

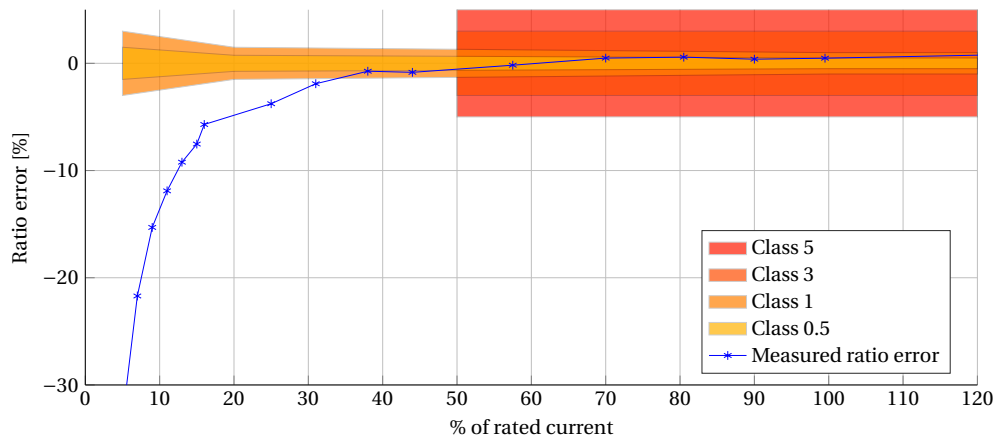


Figure 6.5: Measured sensor node accuracy based on ratio error

The sensor output readings were not current values but voltage readings. The voltage readings were multiplied by a calibration value to get the current readings. Based on these current readings and the reference current the ratio error is calculated and given in figure 6.5.

Current [A]	10	18	30	50	88	115	140	180	199	242
% Rated current	5%	9%	15%	25%	44%	58%	70%	90%	100%	121%
Spreading [A]	0,92	0.68	0.62	0.57	0.53	0.98	0.88	1.01	3.61	1.06
% influence on measurement	9.19%	3.79%	2.06%	1.14%	0.60%	0.85%	0.63%	0.56%	1.82%	0.44%

Table 6.1: Spreading of measurement and influence on measurement

From the readings it is observed that from about 35 % rated current the sensor gives an output with accuracy class 1. Below 35 % the accuracy of the measurement drops quickly and below 5 % the sensor can not extract enough power to power the electronics. As mentioned this measurement is not taken with a perfectly designed setup and the reference current was not measured very accurately. Therefore it is expected that the results might improve if small modifications in the prototype are made as well as in the measurement setup. The measurement is within the boundaries of IEC 61869-2 class 3.

During the measurement not only the average value over a minute was taken but also the minimum and maximum RMS value were measured. Based on that data and the constant current during that period, the spreading of the measurement is calculated.

Table 6.1 gives the results that are calculated. In this table the % influence on measurement is the contribution of the spreading to the measurement. In case of a primary current of 10 A and a difference between minimum measured current and maximum measured current of 0.92 A this means an influence of 9.2 % on the measurement. The influence on the measurement is relative large at low primary current but the influence at higher current levels becomes small.

In figure 6.6 the output signal of the shunt monitor and zero-crossing detection are given. The DC voltage levels, both regulated and unregulated, are in the same figure. If the waveforms are compared with the figures obtained from the simulations (chapter 5 figure 5.11) the waveforms look more or less similar. The amplitude of the shunt monitor output in the measurement is slightly different if compared with the simulation. The reason for this difference in amplitude is due to a difference in shunt value. For the measurement a smaller shunt is used than in the simulation were the one of the simulation gives the best resolution.

Based on the results of the measurement it can be concluded that for currents above 35 % of the rated current the sensor meets the specifications of a class 1 current transformer but below 35 % the error increases

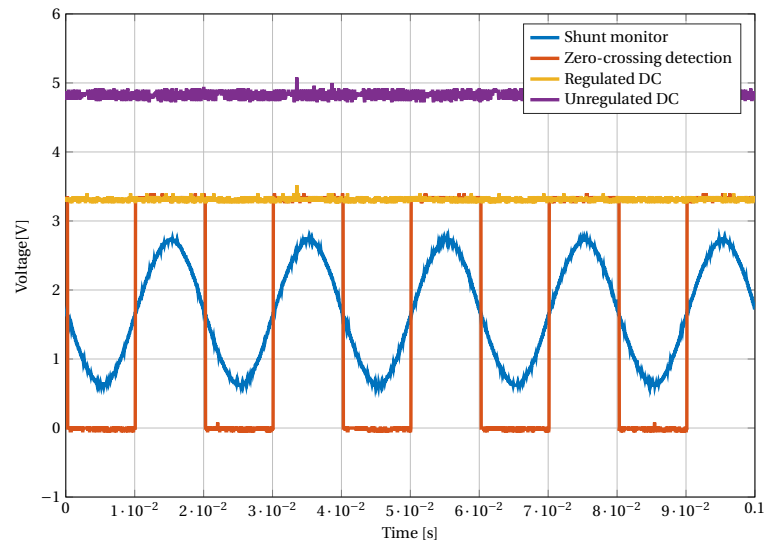


Figure 6.6: Measured ADC input, zero-crossing input and DC voltage levels at 100% rated current

and also the fault in the measurement (% influence on measurement) increases. A possible improvement to get the measurement more accurate is to increase the resolution of the ADC. Especially at low primary current the amplitude of the ADC input becomes too low to do a reliable measurement and calculate the primary current.

# 7

## Conclusions and recommendations

In this chapter the conclusions of this research project are presented. In the first chapter of this thesis the objective is defined and related research questions are used to cover the objective.

The main goal of this thesis was to combine continuous current measurement with energy extraction using one CT as link between sensor and current carrying conductor. To achieve this goal the project was divided into a few questions.

1. What type of current measurement techniques are currently available and could be implemented in the application of self-powered wireless current sensor?
2. What amount of energy can be extracted with a CT and what influence has the extraction of energy on the normal operation of a CT?
3. How can continuous current measurement be combined with energy extraction?
4. Which network topologies could be used for wireless current sensors and how can accurate time synchronization be achieved?

In section 7.1 the conclusions are presented based on the above repeated question. In section 7.2 the recommendations for further research projects or for ELEQ to continue and improve this proof of concept.

### 7.1. Conclusions

In this study the configuration of combining continuous current measurement with energy extraction was studied. The configuration which was tested, used one CT to couple the primary conductor to the electronics needed for the current measurement. The power supply for the electronics used the same CT output as used for the measurement. To determine the measurement method, the type of power supply and the interconnection of the power supply with the measurement, the thesis is divided into several chapters to answer the questions of this research project.

To simulate the system, and for analysis regarding energy extraction, an equivalent circuit is derived. This circuit is verified with a CT. Based on the verification of the circuit it is concluded that the linear behavior of the circuit gives an accurate representation of the CT. The non-linear behavior of the CT at low primary current, and if the iron core of the CT saturates, was not accurately covered by the circuit.

Three different current sensing principles and multiple current sensors were rated based on accuracy, size, cost, power loss and the ability of sensing AC and DC. Accuracy and low power loss at low current were most important. Although the losses of a shunt increase with the square of current, a shunt was selected as best measurement method because the accuracy is good, the cost are low and the required size is small. The losses are acceptable at small current and at higher current power loss is not an issue.

Based on simulation and measurement the energy extracting capabilities of a CT were studied. The power dissipated in a load resistance increased with the square of the current as it was expected. Therefore at low current the amount of energy is limited. To increase the energy extraction at low current the effect of resonance is studied. Based on the measurements, the effect of resonance increased the power dissipation in a load resistance but the drawback of the resonance is that the core saturates at low currents. The problem

with resonance is that the secondary current is no longer linear proportional with the primary current and combined with the saturation this gives problems for the current measurement.

For the realization of a self-powering current sensor based on a single CT, the measurement needs to be combined with the energy extraction. To successfully combine measurement and energy extraction two important problems are solved. The first problem is to successfully measure an AC current with a ADC that only supports positive voltages. The second problem is to ensure all CTs output current is passing through the shunt.

For the measurement of AC with an ADC the shunt and the ADC must be isolated from each other. In this project the isolation is implemented using a shunt monitor with internal isolation of AC from the differential amplifier used for the measurement. The output of the shunt monitor is directly connected to the ADC.

To ensure all CTs output current is passing through the shunt the excess current, the current which is not needed for supplying the electronics, is dissipated behind the shunt. Different locations and implementations of this consumption are possible. In this thesis the excess energy is dissipated in a resistor which is switched into the unregulated DC voltage bus.

Using these two solutions, the measurement of current and the extraction of energy for supplying the electronics, can be combined. To classify the measurement the accuracy classes from IEC 61869-2 standard are used to specify the accuracy of this measurement. Based on the simulation of the system the realized setup meets accuracy class 1. Accuracy class 1 was selected at the start of this project. Based on the measurement the sensor is not accurate if the current is low. From about 35 % rated current the sensor meets accuracy class 1. The current sensor is within the boundaries of a class 3 CT.

A last part of this project is to specify the configuration of the network and the communication protocol to ensure low power consumption and accurate synchronization of sensor nodes. Using a local concentrator node as hub between the IoT and the sensor nodes provides combination of readings from multiple sensors. Using the concentrator as initiator of time synchronization resulted in a non-optimized time deviation of maximum 55  $\mu$ s.

Based on the conclusions on the questions it is concluded that it is possible to combine continuous current measurement with energy extraction supplying the electronics of the sensor. Based on the simulation results the achievable accuracy class is class 1 as specified in IEC 61869-2. The realized concept demonstrator does not meet this accuracy. The accuracy of the concept demonstrator is within the boundaries of class 3. Based on the recommendations in section 7.2 it is expected that the accuracy of the concept demonstrator can be improved and within the boundaries of class 1.

## 7.2. Recommendation for further research

For the further improvement of the realized concept demonstrator some recommendations are mentioned below. Other improvements or topics for further research based on this project are specified as well.

For the application of energy management detailed information of voltage and current is needed. Not only amplitude of voltage and current is needed but information about the phase is required to calculate actual power flow. For the measurement current sensors and voltage sensors are required. To prevent high installation cost, the sensors need to be non-invasive. In this thesis the design of a non-invasive, self-powering, current sensor is discussed.

The designed self-powered wireless current sensor can be used for current measurement from 10 A to 240 A. The used concept based on a single CT and continuous measurement is new. The developed setup is able to measure current but it is suggested to further improve the design.

- To improve the accuracy of the measurement an ADC with higher resolution is suggested. In this proof of concept the limited range of the ADC resulted in less accurate readings for small currents. Therefore it is suggested to change the ADC used in this concept demonstrator by an ADC with higher resolution.
- In this thesis a basic implementation of TSCH is used to synchronize sensor nodes with a concentrator. Based on literature it is expected that the time synchronization of the sensor nodes can be improved. It is therefore recommended to optimize the configuration of the TSCH. Besides a more accurate synchronization between sensors the software for the phase measurement needs to be implemented in future project.
- The designed concept demonstrator is able to sense currents from 10 A to 240 A. However, the principle may work for other current ranges as well and therefore it is recommended to study the effect of a

different CT and a different range of currents on the operation of the sensor.

- Based on the measurement with the concept demonstrator as well as the simulated system, a ripple in the regulated DC voltage was present. This ripple is also visible in the output of the shunt monitor and contributes to the measurement error. To minimize the contribution of the DC ripple to the measurement it is recommended to optimize the power conversion stage. Using an active rectifier or a PFC DC/DC converter may reduce the ripple in the electronics supply voltage as well as the small influence of the power conversion on the AC current passing the shunt.
- In this concept demonstrator the excess energy is transformed into heat by a dump resistor. To prevent unnecessary heat production and use the extracted energy in a useful way it is recommended to replace the excess energy dumping circuit in the concept demonstrator by a load that uses the excess energy in a more useful way.

Besides the current sensor a voltage sensor is required to provide information of the voltage. For integration in the sensor network for energy management it is recommended to do research for the possibilities of a non-invasive self-powered voltage sensor.

For the implementation of multiple sensor in a network a concentrator is required. Also the combination of current and voltage readings requires a concentrator. In this project a very basic concentrator is realized for time synchronization between sensor node and concentrator. A new project to realize a concentrator supporting multiple sensors and providing a user-friendly interface for the configuration of the network is suggested.

During this project the CT was only used within the linear region. If it is expected to pass the boundaries of the linear region, with for example resonance, it is suggested to realize a non-linear circuit that describes the full behavior of the CT.

For increased energy extraction with a CT based on resonance the suggested solutions for preventing the iron core to saturate can be research in more detail. Implementation of an air-gapped core or a hybrid solution in which is switch between resonance and non-resonance are two suggestion that may solve the problem of saturation due to resonance.



# Bibliography

- [1] Zigbee Alliance. Zigbee enables smart buildings of the future today. *Zigbee Whitepaper*, 2007.
- [2] Domenico Balsamo, Gianluca Gallo, Davide Brunelli, and Luca Benini. Non-intrusive zigbee power meter for load monitoring in smart buildings. In *Sensors Applications Symposium (SAS), 2015 IEEE*, pages 1–6. IEEE, 2015.
- [3] Rashed H Bhuiyan, Roger Dougal, Mohammad Ali, et al. A miniature energy harvesting device for wireless sensors in electric power system. *Sensors Journal, IEEE*, 10(7):1249–1258, 2010.
- [4] Bradford Campbell and Pranab Dutta. Gemini: A non-invasive, energy-harvesting true power meter. In *Real-Time Systems Symposium (RTSS), 2014 IEEE*, pages 324–333. IEEE, 2014.
- [5] Tengfei Chang and Qin Wang. Adaptive compensation for time-slotted synchronization in wireless sensor network. *International Journal of Distributed Sensor Networks*, 2014, 2014.
- [6] Shih-Hsien Cheng and Sheng-Fuu Lin. A self-powered current monitoring module with zigbee communication for industrial applications. *Journal of the Chinese Institute of Engineers*, 38(3):304–316, 2015.
- [7] Samuel DeBruin, Bradford Campbell, and Prabal Dutta. Monjolo: An energy-harvesting energy meter architecture. In *Proceedings of the 11th ACM Conference on Embedded Networked Sensor Systems*, page 18. ACM, 2013.
- [8] ECN. *Energietrends 2014*. ECN, 2014.
- [9] Jeremy Elson and Deborah Estrin. Time synchronization for wireless sensor networks. In *IPDPS*, volume 1, page 186, 2001.
- [10] LA Feler, M Rigoni, HF Santos, RA Elias, N Sadowski, P Kuo-Peng, NJ Batistela, and JPA Bastos. A system for harvesting energy from stray magnetic fields. *Sensing and Imaging*, 16(1):1–13, 2015.
- [11] Saurabh Ganeriwal, Ram Kumar, and Mani B Srivastava. Timing-sync protocol for sensor networks. In *Proceedings of the 1st international conference on Embedded networked sensor systems*, pages 138–149. ACM, 2003.
- [12] Vikram Gupta, Arvind Kandhalu, and Ragunathan Raj Rajkumar. Energy harvesting from electromagnetic energy radiating from ac power lines. In *Proceedings of the 6th Workshop on Hot Topics in Embedded Networked Sensors*, page 17. ACM, 2010.
- [13] Masoud Jabbari and Hosein Farzanehfard. A new soft switching step-down/up converter with inherent pfc performance. *Journal of Power Electronics*, 9(6):835–844, 2009.
- [14] Aman Kumar Jha, BG Fernandes, and Avinash Kishore. A single phase single stage ac/dc converter with high input power factor and tight output voltage regulation. In *Progress In Electromagnetics Research Symposium*, pages 26–29, 2006.
- [15] Ping Li, Yumei Wen, Ziqiang Zhang, and Shiqiang Pan. A high-efficiency management circuit using multi-winding up-conversion current transformer for power-line energy harvesting. *Industrial Electronics, IEEE Transactions on*, 62(10):6327–6335, 2015.
- [16] *LTC1540 Nanopower Comparator with Reference*. Linear Technology, 4 2003. Rev. A.
- [17] *LTC3588-1 Nanopower Energy Harvesting Power Supply*. Linear Technology, 8 2015. Rev. C.
- [18] Miklós Maróti, Branislav Kusy, Gyula Simon, and Ákos Lédeczi. The flooding time synchronization protocol. In *Proceedings of the 2nd international conference on Embedded networked sensor systems*, pages 39–49. ACM, 2004.

- [19] Ned Mohan and Tore M Undeland. *Power electronics: converters, applications, and design*. John Wiley & Sons, 2007.
- [20] Olivier Monnier. A smarter grid with the internet of things. *Texas Instruments White Paper*, 2013.
- [21] Jonas Olsson. 6lowpan demystified. *Texas Instruments. Saatavissa: <http://www.ti.com/lit/wp/swry013/swry013.pdf>*, 29:2015, 2014.
- [22] Danilo Porcarelli, Davide Brunelli, and Luca Benini. Clamp-and-forget: A self-sustainable non-invasive wireless sensor node for smart metering applications. *Microelectronics Journal*, 45(12):1671–1678, 2014.
- [23] Jinrong Qian and Fred C Lee. Charge pump power-factor-correction technologies. i. concept and principle. *Power Electronics, IEEE Transactions on*, 15(1):121–129, 2000.
- [24] Prakash Ranganathan and Kendall Nygard. Time synchronization in wireless sensor networks: a survey. *International journal of UbiComp (IJU)*, 1(2):92–102, 2010.
- [25] Nina M Roscoe and Martin D Judd. Harvesting energy from magnetic fields to power condition monitoring sensors. *Sensors Journal, IEEE*, 13(6):2263–2270, 2013.
- [26] Nina M Roscoe and Martin D Judd. Optimization of voltage doublers for energy harvesting applications. *Sensors Journal, IEEE*, 13(12):4904–4911, 2013.
- [27] Bhim Singh, Brij N Singh, Ambrish Chandra, Kamal Al-Haddad, Ashish Pandey, and Dwarka P Kothari. A review of single-phase improved power quality ac-dc converters. *Industrial Electronics, IEEE Transactions on*, 50(5):962–981, 2003.
- [28] N. Sornin, M. Luis, T. Eirich, T. Kramp, and O. Hersent. LoRawan specification. *LoRa Alliance technical specification*, 2015.
- [29] Keiji Tashiro, Hiroyuki Wakiwaka, Shingo Inoue, and Yusuke Uchiyama. Energy harvesting of magnetic power-line noise. *Magnetics, IEEE Transactions on*, 47(10):4441–4444, 2011.
- [30] Kunihisa Tashiro, Gen-ya Hattori, and Hiroyuki Wakiwaka. Magnetic flux concentration methods for magnetic energy harvesting module. In *EPJ Web of Conferences*, volume 40, page 06011. EDP Sciences, 2013.
- [31] *INA28x High-Accuracy, Wide Common-Mode Range, Bidirectional Current Shunt Monitors, Zero-Drift Series*. Texas Instruments, 11 2009. SBOS485C, REVISED MAY 2015.
- [32] *CC2630 SimpleLink™ 6LoWPAN, ZigBee® Wireless MCU*. Texas Instruments, 2 2015. SWRS177B, REVISED JULY 2016.
- [33] *Wireless Connectivity Solutions*. Texas Instruments, 2015. URL: <http://www.ti.com/lit/ml/swrb035/swrb035.pdf>.
- [34] Instrument Transformers—Part. 2: Additional requirements for current transformers. *IEC Standard 61869–2*, 2012.
- [35] Ministerie van Economische Zaken. *Energierapport 2015: Transitie naar Duurzaam*. Ministerie van Economische Zaken, 2015.
- [36] Jana Van Greunen and Jan Rabaey. Lightweight time synchronization for sensor networks. In *Proceedings of the 2nd ACM international conference on Wireless sensor networks and applications*, pages 11–19. ACM, 2003.
- [37] Sheng Yuan, Yi Huang, Jiafeng Zhou, Qian Xu, Chaoyun Song, and P. Thompson. Magnetic field energy harvesting under overhead power lines. *Power Electronics, IEEE Transactions on*, 30(11):6191–6202, 2015.
- [38] Stanley E Zocholl and DW Smaha. Current transformer concepts. In *Proceedings of the 46th Annual Georgia Tech Protective Relay Conference, Atlanta, GA*, pages 7–9, 1992.